2015

Using multi-resolution remote sensing to monitor disturbance and climate change impacts on Northern forests

BOSTON UNIVERSITY

GRADUATE SCHOOL OF ARTS AND SCIENCES

Dissertation

USING MULTI-RESOLUTION REMOTE SENSING TO MONITOR DISTURBANCE AND CLIMATE CHANGE IMPACTS ON NORTHERN FORESTS

by

DAMIEN SULLA-MENASHE

B.A., Boston University, 2006
M.A., Boston University, 2006

Submitted in partial fulfillment of the

requirements for the degree of

Doctor of Philosophy

2015

Approved by

First Reader

Mark Friedl, PhD
Professor of Earth and Environment

Second Reader

Curtis Woodcock, PhD
Professor of Earth and Environment

Third Reader

Lucy Hutyra, PhD
Professor of Earth and Environment

Acknowledgments

I would first like to thank all the faculty, staff, and graduate students in the Department of Earth and Environment for making my stay as a graduate student at Boston University so meaningful and full of wonderful memories. There is no way I can convey enough gratitude to my advisor Mark Friedl, who has patiently helped me along towards this final goal and has always been there for me when I have struggled. I would not be where I am without his guidance and generous financial support. I would also like to give special thanks to the other members of my Dissertation Committee, including Curtis Woodcock, Lucy Hutyra, Robert Kennedy, and Adrien Finzi, for giving me so much time for meaningful discussion, ensuring this work would go as smoothly as possible. Many other people have given me essential professional guidance and advice during my Ph.D. research, in particular Nathan Philips, Olga Krankina, Alessandro Baccini, Scott Goetz, Pieter Beck, Suchi Gopal, Ian Sue Wing, Luis Carvalho, Mike Wulder, and Nicholas Coops. I am grateful to all my colleagues of the Land Cover and Surface Climate Group, both past and present, who have given me years of free ideas and support, these include Josh Gray, Eli Melaas, Jon Wang, Leah Cheek, Radost Stanimirova, Xiaoman Huang, Manish Verma, Meghan Salmon, Parker Abercrombie, Koen Hufkens, Mary Farina, Sangram Ganguly, Le Li, Mary Farina, and Adam Sibley. Final thanks go to my family and to all my close friends who make living in Boston so enjoyable.

USING MULTI-RESOLUTION REMOTE SENSING TO MONITOR DISTURBANCE AND CLIMATE CHANGE IMPACTS ON NORTHERN FORESTS

(Order No.)

DAMIEN SULLA-MENASHE

Boston University Graduate School of Arts and Sciences, 2015

Major Professor: Mark Friedl, Professor of Earth and Environment

ABSTRACT

Global forests are experiencing a variety of stresses in response to climate change and human activities. The broad objective of this dissertation is to improve understanding of how temperate and boreal forests are changing by using remote sensing to develop new techniques for detecting change in forest ecosystems and to use these techniques to investigate patterns of change in North American forests.

First, I developed and applied a temporal segmentation algorithm to an 11-year time series of MODIS data for a region in the Pacific Northwest of the USA. Through comparison with an existing forest disturbance map, I characterized how the severity and spatial scale of disturbances affect the ability of MODIS to detect these events. Results from these analyses showed that most disturbances occupying more than one-third of a MODIS pixel can be detected but that prior disturbance history and gridding artifacts complicate the signature of forest disturbance events in MODIS data.

Second, I focused on boreal forests of Canada, where recent studies have used remote sensing to infer decreases in forest productivity. To investigate these trends, I collected 28 years of Landsat TM and ETM+ data for 11 sites spanning Canada's boreal forests. Using these data, I analyzed how sensor geometry and intra- and inter-sensor calibration influence detection of trends from Landsat time series. Results showed systematic patterns in Landsat time series that reflect sensor geometry and subtle issues related to inter-sensor calibration, including consistently higher red band reflectance values from TM data relative to ETM+ data.

In the final chapter, I extended the analyses from my second chapter to explore patterns of change in Landsat time series at an expanded set of 46 sites. Trends in peak-summer values of vegetation indices from Landsat were summarized at the scale of MODIS pixels. Results showed that the magnitude and slope of observed trends reflect patterns in disturbance and land cover and that undisturbed forests in eastern sites showed subtle, but detectable, differences from patterns observed in western sites. Drier forests in western Canada show declining trends, while mostly increasing trends are observed for wetter eastern forests.

Contents

List of Tables

List of Figures

List of Abbreviations

AVHRR	Advanced Very High Resolution Radiometer
BRDF	Bidirectional Reflectance Distribution Function
CCDC	Continuous Change Detection and Classification
CMI	Climate moisture index
EOSD	Earth Observation for Sustainable Development of Forests
ETM+	Enhanced Thematic Mapper Plus
EVI	Enhanced Vegetation Index
FMask	Function of Mask
GIMMS	Global Inventory Modeling and Mapping Studies
L1T	Level-one Terrain-corrected
LandTrendr	Landsat-based detection of Trends in Disturbance and Recovery
LEDAPS	Landsat Ecosystem Disturbance Adaptive Processing System
LFDB	Canadian Large Fire Database
MERIS	Medium Resolution Imaging Spectroradiometer
MODIS	Moderate Resolution Imaging Spectroradiometer
MODTrendr	MODIS-based detection of Trends in Disturbance and Recovery
NBAR	Normalized BRDF-Adjusted
NBR	Normalized Burn Ratio
NDVI	Normalized Difference Vegetation Index
NIR	Near Infrared

NWFP	Northwest Forest Plan
OLI	Operational Land Imager
PDF	Probability density function
PET	Potential evapotranspiration
PLM	Panel Linear Model
SeaWiFS	Sea-Viewing Wide Field-of-View Sensor
SLC	Scan Line Corrector
SPOT-VGT	Vegetation sensor aboard the Satellite Pour l'Observation de la Terre platform
SWIR	Shortwave Infrared
TM	Thematic Mapper
USGS	United States Geological Survey
VI	Vegetation Index
VIIRS	Visible Infrared Imaging Suite
WRS2	Worldwide Reference System-2

Chapter 1

Introduction

1.1 Research Statement

Forests are key components of the global radiation budget, water balance, and carbon cycle (Bonan, 2008). Losses to forest cover from human activities and natural disturbances represent major threats to biodiversity and ecosystem services (Ojima et al., 1994; Hansen et al., 2010b, 2013), and produce both positive and negative feedbacks to the warming of the climate system (Brovkin et al., 1997). Recent reports of widespread forest mortality events suggests that climate change is already impacting the structure and function of forested ecosystems (Allen et al., 2010; Michaelian et al., 2011; Schwalm et al., 2012). While little is known about the mechanisms by which recent climate changes have caused these mortality events (Anderegg et al., 2012), observations and models suggest an increasing threat to forested ecosystems in the high latitudes of the Northern Hemisphere (Hansen et al., 2006; Wang et al., 2006; Piao et al., 2009).

Northern temperate and boreal forests are already experiencing changes in productivity and structure caused by climate warming (Soja et al., 2007; Piao et al., 2008; Beck et al., 2011b). Because the photosynthetic capacity of trees is directly tied to the seasonal co-occurrence of moisture and light, changes to these quantities from longer growing seasons and increased frequency of drought events will affect the

growth rate and productivity of these forests (Xu et al., 2013). In addition, warmer and drier summers will amplify disturbance regimes in these regions including the intensity and extent of forest fires (Kasischke and Turetsky, 2006; Westerling et al., 2006) and increase the reproductive success of forest-damaging insects (Hicke et al., 2006, 2011). These changes are important because temperate and boreal forests provide a large sink of atmospheric carbon dioxide at annual time scales and store large amounts of carbon in their biomass and soils that are released into the atmosphere following disturbance (Bonan and Shugart, 1989; Hicke et al., 2011; Kasischke et al., 2013). Further, the feedbacks between the biosphere and the atmosphere are not well-understood, especially the future strength of the terrestrial carbon sink (Friedlingstein et al., 2006). Because of the inaccessibility of these remote regions, information about the spatial extent of disturbed and stressed forests is incomplete.

Remote sensing has allowed new research about the response of the biosphere to changes to the climate system, but only a few satellite sensors provide consistent observations of the surface for more than a decade. Of these, the Advanced Very High Resolution Radiometer (AVHRR) provides over 30 years of information on global change at coarse (8-km) spatial resolution. Several studies have used these time series to relate climate warming with trends in the Normalized Difference Vegetation Index (NDVI), which is correlated with net primary production (Myneni et al., 1997; Nemani et al., 2003; Bunn and Goetz, 2006; Pouliot et al., 2009; Beck and Goetz, 2011; Xu et al., 2013). Many of these studies suggest a lengthening of the growing season at high latitudes but some also show decreasing primary productivity across much of the North American boreal forest zone. However, the coarse spatial and radiometric resolutions and poor calibration of AVHRR limit the inferences that can be made from these results.

Two general classes of space-borne sensors have the potential to improve understanding of the spatial and temporal patterns in forest cover and link recent productivity changes to climate warming. First, the Landsat Thematic Mapper (TM) and Enhanced Thematic Mapper (ETM) now provide over 30-years of fine (30-m) spatial resolution data but are limited by uneven spatial and temporal acquisitions. Second, the Moderate Resolution Imaging Spectroradiometer (MODIS) and the Visible Infrared Imaging Suite (VIIRS), provide shorter time series (15 years) of moderate (500-m and 750-m, respectively) spatial resolutions, but provide near-daily repeat observations of the entire globe. The radiometric similarities and temporal continuity between these two classes of sensors have enabled novel approaches for data fusion (Gao et al., 2006; Hilker et al., 2009b). The main goal of this dissertation is to exploit the strengths of each data source to better understand changes in North American forest cover and productivity and to explore how these properties and processes translate across spatial scales using co-located remote sensing data sets. In addition, my research helps to clarify the role of climate variability in observed trends in peak-summer vegetation "greenness" across boreal forests in North America.

1.2 Remote sensing of forest disturbance

Accurate information regarding spatial and temporal patterns in forest disturbance and better understanding of the human and climate drivers of these patterns are needed to reduce uncertainties in Earth system models (Friedlingstein et al., 2006). International policies aimed at mitigating climate change impacts are being influenced by the capabilities of remote sensing datasets to capture and quantify these changes (Turner et al., 2004; Gibbs et al., 2007; Baccini et al., 2012). As the volume of remote sensing data continues to increase, more complex methods for detecting

and characterizing forest disturbance are being developed (Lu et al., 2004). Despite these advances, there are relatively few sensors with the temporal continuity and spatial coverage to monitor these processes at regional to global scales (Frolking et al., 2009).

The most effective approaches to characterize disturbance from space-borne sensors use dense time series of such observations (Hilker et al., 2009a; Huang et al., 2010; Kennedy et al., 2010; Verbesselt et al., 2010a; Gómez et al., 2011; Zhu et al., 2012; Zhu and Woodcock, 2014). Some strengths of these approaches include: (1) the ability to capture subtle, long-term trends as well as abrupt changes (e.g., Kennedy et al., 2010); (2) low reliance on *a priori* information of the surface that may introduce errors (e.g., Zhu and Woodcock, 2014); and (3) the possibility to generalize across different spectral indices and sensors (e.g., Verbesselt et al., 2010a). Of particular focus here are the radiometric similarities and overlapping time series of Landsat and both MODIS and the newly launched VIIRS instrument. Indeed, multi-resolution approaches to disturbance detection have received new life with the opening of the Landsat archive (Wulder et al., 2012) and the launch of Landsat 8 (Irons et al., 2012).

1.3 Conflicting observations of forest productivity changes in boreal North America

The effects of climate warming are already being observed at high latitudes (Serreze et al., 2000; Sturm et al., 2001; Smith et al., 2005; Kim et al., 2012; Ma et al., 2012; Xu et al., 2013; Jeganathan et al., 2014), where climate models predict further increases in warming and drying in the future (Barnett et al., 2005; Sitch et al., 2007; Dai, 2012; Sillmann et al., 2013). Remote sensing observations from the AVHRR sensor provide compelling evidence of greening in the Arctic tundra (Myneni et al., 1997;

Pouliot et al., 2009), but suggest a different story of forest decline or "browning" for much of the boreal region of North America (Tateishi and Ebata, 2004; Goetz et al., 2005; Beck and Goetz, 2011; Bi et al., 2013; Guay et al., 2014). Most of these studies are based on the Global Inventory Modeling and Mapping Studies (GIMMS) data set (newly released as version 3G), which provides 30 years of NDVI observations from the Advanced Very High Resolution Radiometer (AVHRR) at 8-km spatial resolution (Tucker et al., 2005; Pinzon et al., 2007; Pinzon and Tucker, 2014). However, AVHRR NDVI time series include substantial uncertainty because of the sensors' low spatial and radiometric resolution, challenges involved in cloud screening and atmospheric correction (Fontana et al., 2012), the use of data from different AVHRR sensors (Tucker et al., 2005; Pinzon and Tucker, 2014), and geolocation uncertainty(Alcaraz-Segura et al., 2010). Indeed, the geographically extensive decreasing NDVI trends ("browning") observed across boreal North America in the GIMMS 3G dataset were not detected in previously available AVHRR NDVI data sets (Slayback et al., 2003; Olthof and Latifovic, 2007; Pouliot et al., 2009; Alcaraz-Segura et al., 2010; Beck et al., 2011a).

To clarify the debate between "browning" and "greening" of the boreal forest of North America, it is necessary to look more closely using a time series from a sensor with higher radiometric quality and spatial resolution such as MODIS or Landsat. Beck and Goetz (2011) showed similar browning trends from 8-year MODIS time series in many areas of dense boreal tree cover but suggested that more work was needed to clarify whether deciduous or evergreen tree types were most affected. Guay et al. (2014) showed substantial correspondence in NDVI trends in this region across several sensors including AVHRR, MODIS, SeaWiFS, and SPOT-VGT but only for the period between 2002 and 2008. Studies that have used Landsat data have either

focused largely on greening trends (Neigh et al., 2008; Pouliot et al., 2009; Fraser et al., 2011; McManus et al., 2012) or have analyzed time series at single locations in the temperate forest zone (Neigh et al., 2012). These studies have found complex interactions between climate, disturbance, and forest cover, but use small sets of Landsat images that may not be representative of the entire boreal forest zone.

1.4 Dissertation Structure and Objectives

My dissertation research has two major goals. First, to demonstrate how information about forest health and disturbance can be obtained from remote sensing data sets and to characterize the sources of bias and variability that affect these observations. Second, to improve our knowledge of the patterns of greening and browning trends in the boreal forests of North America. To achieve these goals I address the following three research questions, each of which corresponds to a separate chapter in my dissertation:

1. What is the signature of forest disturbance in moderate resolution remote sensing and how is this signature affected by the size, severity, and timing of these processes?

2. What factors influence the detection of trends in vegetation indices in boreal Canada based on Landsat data?

3. How do spatial patterns in disturbance, land cover, and climate influence VI trends from Landsat time series in Canadian boreal forests?

To do this, I leverage new methods to process and interpret dense time series of satellite imagery at the spatial resolutions of MODIS and Landsat. To address the first question I explore the strengths and weaknesses of MODIS time series to detect

forest disturbance. To address the second, I used over 30 years of Landsat imagery for 11 sites across the Canadian boreal forest zone to investigate sources of bias and variability in these data sets that are related to artifacts in the time series. For the third chapter, I expanded the original set of 11 Landsat sites to 46 and examined how disturbance events, land cover, and climate variability influence the direction and magnitude of vegetation index trends in these regions.

Taken together, I demonstrate the myriad challenges in drawing inferences on the response of forests to recent climate changes using coarse spatial resolution remote sensing data sets. To overcome these challenges I describe guidelines on the use of remote sensing data with higher radiometric quality and spatial resolution for these purposes. Furthermore, I provide a more nuanced perspective on the magnitude of recent changes to the biosphere at high latitudes that will help reduce uncertainties in global climate models.

Chapter 2

Detecting Forest Disturbance in the Pacific Northwest from MODIS Time Series Using Temporal Segmentation

2.1 Introduction

Forest disturbance and succession processes influence land surface water, carbon, and radiation budgets, and therefore affect feedbacks between forest ecosystems and climate (Bonan, 2008). Recent evidence suggests that processes related to climate change are negatively affecting forests in many parts of the world (Bunn and Goetz, 2006; Fensham et al., 2009; Allen et al., 2010), and that fire and insect disturbance regimes are likely to change in the coming decades (Flannigan et al., 2005; Westerling et al., 2006; Hicke et al., 2011). Anthropogenic disturbances, including forest harvest, forest removal for agriculture, and urban development are also widespread (Ojima et al., 1994; DeFries et al., 2004; Ellis and Ramankutty, 2008). Poor understanding of disturbance regimes is a key source of uncertainty in global carbon models (Turner et al., 2004; Bond-Lamberty et al., 2007; Anderegg et al., 2012) and improved information regarding spatial and temporal patterns in forest disturbance is needed to reduce uncertainties in modeled feedbacks between the atmosphere and

the biosphere (Kasischke et al., 1995; Friedlingstein et al., 2006). From a policy perspective, national carbon stock inventories need to account for both deforestation and degradation to meet the requirements of international agreements such as the United Nations program on Reducing Emissions from Deforestation and Degradation (UN-REDD; Gibbs et al. 2007; Baccini et al. 2012).

Remotely sensed data from space-borne sensors provide the most efficient and cost-effective tool for monitoring forest health and associated carbon stocks over large areas (Lepers et al., 2005; Masek et al., 2008; Frolking et al., 2009). Although the availability of satellite imagery has increased over the last decade, relatively few sensors are available to support these tasks at regional to global scales. These sensors include the Advanced Very High Resolution Radiometer (AVHRR), the Moderate Resolution Imaging Spectroradiomater (MODIS), the Medium Resolution Imaging Spectroradiometer (MERIS[1]), and the Visible Infrared Imaging Radiometer Suite (VIIRS). Of these, the AVHRR time series is the longest, but has the lowest spatial resolution and radiometric quality. The MODIS instrument onboard the Aqua and Terra satellite platforms has now acquired over 12 years of near-daily data (2000 to present; Justice et al. 2002. The launch of VIIRS onboard the Suomi National Polar-orbiting Partnership mission in October of 2011 is designed (in part) to provide continuity with MODIS until at least 2015, and will support the need for long-term coarse-spatial resolution Climate Data Records (Townshend and Justice, 2002).

The spatial coverage and temporal continuity provided by instruments such as MODIS and VIIRS make them well-suited for monitoring forest dynamics at inter-annual to decadal time scales. Leveraging this, a number of studies have developed algorithms to detect ecosystem changes from time series of MODIS observations

[1]Note that because of the failure of Envisat, MERIS data are no longer being collected.

(Zhan et al., 2002; Roy et al., 2005; Potapov et al., 2008; Hilker et al., 2009a; Mildrexler et al., 2009; Verbesselt et al., 2010b; Spruce et al., 2011). Many of these algorithms focus on specific disturbance agents such as fire (Roy et al., 2005) or insects (Spruce et al., 2011) while others are designed for more general applications. Most importantly, the utility of coarse spatial resolution data (∼500-m) for monitoring forest disturbance remains an open question (Frolking et al., 2009). The objective of this research is to characterize the major strengths and weaknesses of MODIS time series for forest change monitoring at the regional-to-continental scales required for large-scale carbon monitoring. Specifically, we addressed two main questions:

1. How do the size and severity of forest disturbance events affect the signature of these events in MODIS time series?

2. How does disturbance history, including coincident sub-pixel disturbance and regrowth, affect disturbance detection?

Stated another way, we wanted to assess the factors that determine the strength of the forest disturbance signatures in MODIS time series, and identify sources of background noise that complicate these signatures.

To achieve these goals we adapted an algorithm that has been developed from Landsat imagery for use with MODIS data, and applied this algorithm over an area that encompases a wide range of forest types, disturbance regimes, and management practices. To address the first question we evaluated if and how the use of of coarse-resolution MODIS data limits the accuracy achievable by our MODIS-based algorithm, a phenomenon known as the "low-resolution bias" (e.g., Boschetti et al. 2004). As part of this analysis we also evaluated how gridding artifacts inherent to MODIS data affect disturbance detection (e.g., Tan et al. 2006). To address the

second question, we explored sources of error (both omission and commission) in disturbances detected from MODIS, and examined how disturbance history, including regrowth processes that occur during the time series, introduce these errors (e.g., Loboda et al. 2012).

2.2 Data and Methods

2.2.1 Study Area and Reference Data

The Northwest Forest Plan (NWFP) area contains approximately 18 million hectares of forest along the west coast of Washington, Oregon, and California and is bordered by the Cascade Mountains in the east. This region is characterized by a moderate climate with warm, wet winters followed by dry summers that favor highly productive and diverse conifer forests (Waring and Franklin, 1979). The NWFP was enacted by the U.S. federal government in 1994 to conserve habitat for two endangered bird species – the northern spotted owl and the marbled murrelet – while at the same time preserving timber interests in the region (Haynes et al., 2006). As a result, land ownership strongly influences forest management and disturbance regimes (Turner et al., 2011). To assess the effectiveness of this conservation plan and describe long-term trends in biomass and productivity across the management zone, Kennedy et al. (2012) produced a NWFP forest disturbance database using 22 Landsat scenes. To do this, an algorithm called LandTrendr was applied to a 25-year time series (1984-2008) of Landsat Thematic Mapper and Enhanced Thematic Mapper (TM and ETM) images. The disturbance database provides detailed information related to the type, size, timing, and severity of disturbance processes occurring in the NWFP area between 1985 (the first year a disturbance could be detected) and 2008, and is therefore well-suited to serve as a reference data set for this study. Hereafter,

we refer to this database as the NWFP-DB.

The LandTrendr (Landsat-based detection of Trends in Disturbance and Recovery) algorithm uses temporal segmentation of remotely sensed time series to characterize long-term dynamics in forest properties, including abrupt disturbance events (e.g., fire, harvest), gradual disturbance processes (e.g., insect outbreaks), and vegetation growth and recovery (Kennedy et al., 2010). To perform the segmentation, linear regressions are applied across time series of spectral observations at each pixel. Potential vertices are identified by the residual error at each time step. Each identified vertex defines the start and end points for new regression segments. This process is recursively repeated until a measure of statistical fit is satisfied (*pval*, see Section 2.2.3). A particular strength of this strategy is that it does not require *a priori* information and it does not require a specific spectral quantity or index.

To create the NWFP-DB, LandTrendr was applied to annual late-summer Landsat images of the Normalized Burn Ratio (NBR). The NBR is calculated using near infrared (NIR; Landsat band 4 or MODIS band 2) and short-wave infrared (SWIR; Landsat band 7 or MODIS band 7) channels: NBR = (NIR − SWIR) / (NIR + SWIR) (García and Caselles, 1991). Also known as the Normalized Difference Infrared Index (NDII; Hardisky et al. 1983), the NBR has been used to estimate canopy water content (Roberts et al., 2006) and above-ground biomass (Baccini et al., 2012; Ji et al., 2012), and to detect changes in forest cover caused by fire (Key and Benson, 1999; van Wagtendonk et al., 2004; Loboda et al., 2007; French et al., 2008; Beck et al., 2011b), insect damage (DeBeurs and Townsend, 2008; Cohen et al., 2010), hurricane disturbance (Wang et al., 2010), and logging (Cohen et al., 2010).

To identify disturbance events LandTrendr estimates a set of vertices that connect distinct segments in NBR time series at each pixel (Figure 2.1). A segment

corresponds to a disturbance event if the slope of the segment (in time) is negative. Note that hereafter we use the term "event" to refer to any disturbance segment, including gradual trends that may persist for several years. The first year of a disturbance segment identifies the event onset, the length of the segment (in years) defines its duration, and the magnitude of change in NBR (dNBR) is used to characterize the disturbance severity. By defining disturbance severity in this way, we avoid confusion caused by assigning specific changes in forest properties (e.g., changes in above-ground biomass, forest cover, or soil carbon) to information provided by remote sensing indices (Ryan, 2002; Jain, 2004; Keeley, 2009).

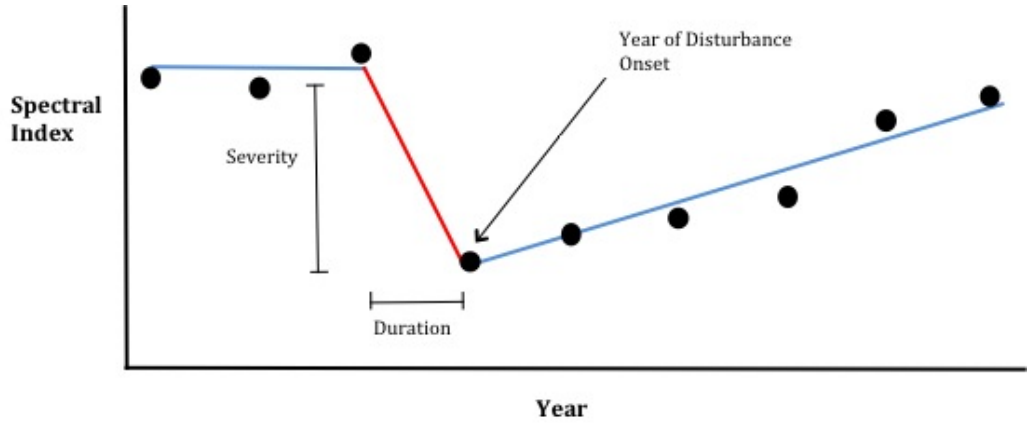

Figure 2.1: Example of a segmentation result from LandTrendr. In a sequence of some spectral index for a single Landsat pixel through time, a disturbance segment (highlighted in red) can be summarized by its timing, severity, and duration.

To compare results from MODIS data against the NWFP-DB, we chose a study area that encompasses the northern half of the NWFP area and intersects with MODIS tile h09v04 (Figure 2.2). Within this study area, the 30-m NWFP-DB was aggregated to the 463-m spatial resolution of MODIS. To do this we first reprojected the NWFP-DB to the MODIS sinusoidal projection. Then, for each MODIS pixel

and for each year from 1985-2008, we calculated the area of disturbed Landsat pixels (A_p, the proportion affected within each MODIS pixel) with disturbance onset of that year, the average severity of disturbed Landsat pixels (S_p, in units of dNBR), and the duration (in years) of those events. To evaluate how disturbance events that occurred before the launch of Terra affect results from MODIS, we used the NWFP-DB to stratify the onset of disturbance events into two periods: 1985-2000 and 2001-2008. For MODIS pixels affected by more than one disturbance event in either of these periods, a single value for A_p, S_p, and the duration of disturbance was assigned using the largest event in the series. To explore how disturbance type affected our results, we created a map from the NWFP-DB that classifies each disturbance segment into three broad classes: harvest, fire, or insect/other (Figure 2.2). Disturbance segments with duration greater than 3 years were distinguished from abrupt disturbances and labeled as insect/other; this class includes disturbance caused by insect pests such as defoliators and bark beetles, and mortality from long-term drought. For abrupt disturbances, fire events were distinguished from harvest removals using the USGS Monitoring Trends in Burn Severity (`http://www.mtbs.gov`) database derived from Landsat data. The harvest class includes abrupt deforestation from a variety of causes that range from clearcut logging to storm damage.

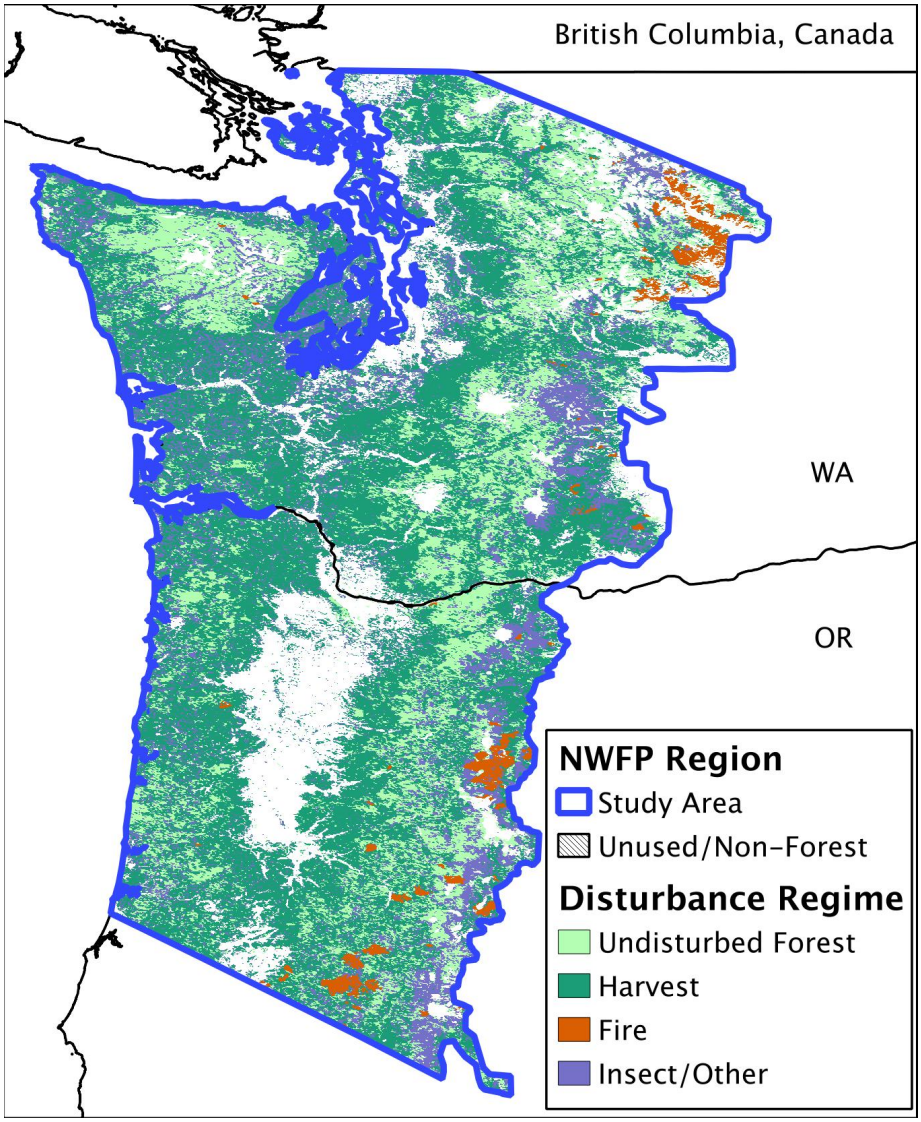

Figure 2.2: The study area is the region of the Northwest Forest Plan (NWFP) that intersects with MODIS tile h09v04. The region of the NWFP is shown in black hatches and the study area is highlighted in blue. For each MODIS pixel the most likely disturbance agent (if present) has been colored according to the disturbance type layer of the NWFP-DB.

2.2.2 MODIS Surface Reflectance Data

LandTrendr was designed to detect disturbance events using a single high quality observation per year (Kennedy et al., 2010). Therefore, the first step in our analysis was to produce an 11-year time series (2000-2010) of late-summer surface reflectance data from MODIS. To compile a set of reflectance inputs to LandTrendr in a time frame that is consistent with the NWFP-DB, we extracted all available observations between July and mid-August (day of year: 180-220, corresponding to five 8-day MODIS periods) for the Normalized BRDF-Adjusted Reflectance (NBAR) product (MCD43A4). The NBAR product has been screened for clouds and snow, is atmospherically corrected, and provides modeled reflectances adjusted to a nadir-viewing angle at local solar noon, thereby minimizing variation in surface reflectance caused by surface anisotropy (Schaaf et al., 2002). The availability of NBAR data substantially reduces the time required to pre-process MODIS data relative to an analogous stack of Landsat imagery.

Mid-summer surface reflectances were derived by computing quality-weighted arithmetic means of available observations using quality flags from the MODIS NBAR Quality Assurance product (MCD43A2), where high-quality reflectance values were weighted more heavily than lower quality values. The resulting late-summer reflectances were then converted into NBR. To constrain our analyses to forest-dominated areas we used a forest mask included in the NWFP-DB, which was developed using a linear regression model to predict forest cover as a function of Landsat NBR (Kennedy et al., 2010). To aggregate these data to the resolution of MODIS data, we first counted the number of forested Landsat pixels within each MODIS pixel. MODIS pixels with less than 60% forest based on the NWFP-DB were labeled as non-forest and excluded from further analyses. The purpose of this threshold was

to avoid mixtures of different land cover types that could interfere with the disturbance signal we are trying to characterize. Note that because forests in the study area are quite dynamic and our mask is based on maximum forest cover between 1984 and 2008, a small number of pixels identified as forest may have been disturbed prior to 2000 and incorrectly classified as forest during the MODIS era.

2.2.3 Adapting LandTrendr to use MODIS Data: MODTrendr

LandTrendr was originally developed for use with Landsat TM/ETM data and is calibrated using a set of parameters designed to maximize detection of disturbances and minimize over-fitting to noise in Landsat NBR time series. For the NWFP-DB, the parameters were calibrated using a set of known disturbance sites (Kennedy et al., 2010). To adapt the algorithm to MODIS NBR time series, we used the same basic approach, using a small set of sites from the NWFP-DB to tune the algorithm to MODIS data. This procedure involved two steps: (1) identification of parameter values, and (2) identification of a threshold in MODIS dNBR below which MODIS pixels are considered undisturbed. Hereafter, we refer to the version of LandTrendr calibrated to MODIS data as "MODTrendr." While the MODTrendr segmentation framework is not fundamentally different from that of LandTrendr, the use of MODIS requires a different set of pre- and post-processing steps. We therefore refer to this algorithm as being distinct from LandTrendr to help avoid confusion between MODIS- and Landsat-scale LandTrendr results.

To calibrate MODTrendr we sampled from two subsets of MODIS pixels. The first subset included pixels with stable forest between 1985 and 2000 that had been disturbed once between 2001 and 2008 (hereafter, disturbed pixels), and the second subset included pixels that were undisturbed across the entire 1985-2008 period

(hereafter, undisturbed pixels). By excluding MODIS pixels affected by more than one disturbance event, we avoided locations where disturbance and regrowth occurred simultaneously. To ensure that the calibration sample captured the full range of disturbance phenomena, we stratified the disturbed pixels into 18 strata according to the timing, size, and severity of disturbance events. To do this we grouped the onset of disturbance segments into three eras: 2001-2003, 2004-2005, and 2006-2008. We then sub-divided the disturbed pixels for each era into six strata defined by the intersection of three classes of disturbance size and two classes of disturbance severity. The disturbance size classes corresponded to disturbances that occupied 0.05-0.3, 0.3-0.7, and 0.7-1.0 MODIS pixels (those occupying less than 0.05 MODIS pixels were excluded as undisturbed), and the disturbance severity classes were defined based on a threshold in Landsat dNBR of S_p=0.6 (the range of dNBR for disturbed segments is 0-1).

For the first calibration step we selected a random sample of 144 pixels, including an equal number of undisturbed and disturbed pixels (4 from each of the 18 strata described above). Using this sample, we tested 48 unique combinations of the five input parameters for MODTrendr (Table 2.1). The segmentation results were then manually interpreted, using the NWFP-DB disturbance information and the original MODIS NBR time series as references. For each pixel, each of the 48 results was ranked according to whether or not it correctly captured a disturbance event. The optimal set of parameters were selected based on the pooled rankings across all 144 calibration pixels.

While these rankings helped to identify those parameter values that produced the best temporal segmentation results, the effect of one parameter (*pval*) was more difficult to objectively interpret. This parameter is used to test the significance of

each segmentation model's F-statistic (Kennedy et al., 2010). As such, it controls the degree to which the model fits to noise in the time series. To select an appropriate value for this parameter and to identify a threshold in MODIS dNBR that distinguishes noise from actual disturbance signals we used a larger sample that contained a higher fraction of disturbed pixels. Specifically, we randomly sampled 630 pixels, including 90 pixels from the undisturbed stratum and 30 pixels from each of the 18 strata for disturbed pixels, thereby capturing combinations of disturbance timing, size, and severity. Using this sample we plotted omission and commission error rates from MODTrendr as a function of both *pval* and the threshold in MODIS dNBR used to identify disturbance segments.

Table 2.1: Selection of parameters for MODTrendr segmentation.

Parameter	This work	Values tested	Kennedy et al. (2012)	Definition
Maximum number of trajectory segments	4	3, 4	6	The maximum number of segments allowed in fitting.
Despiking parameter	1	0.75, 1	0.9	Removes an outlier if it varies from its neighbors more than a certain threshold. Lower values filter spikes more aggressively; a value of 1 turns off de-spiking.
Recovery threshold	1	0.5, 1	0.25	Rejects segments with positive slopes greater than 1/recovery threshold (in years).
Best model proportion	0.75	0.75, 1	0.75	The proportion of the best model's F-statistic that needs to be exceeded by a simpler model for it to be chosen.
Maximum p-value for fitting	0.1	0.05, 0.1, 0.15	0.05	Defines the statistical significance (p-value) required for a model fit based on the F-statistic for the entire trajectory. If the p-value of the F-statistic exceeds this threshold, the entire trajectory is considered no change.

2.2.4 Assessment of Results from MODTrendr

To assess results from MODTrendr using the NWFP-DB, we computed three metrics at each MODIS pixel using disturbance information within the NWFP-DB. The first metric quantifies the disturbance magnitude for a given MODIS pixel (p): $DM_p = S_p \times A_p$, where S_p and A_p are the disturbance severity (dNBR) and area from the NWFP-DB, as defined in Section 2.2.1. The second metric provides a measure of the disturbance magnitude in a 3 × 3 window surrounding the MODIS pixel of interest: $DM_{NB} = S_p \times (A_p + A_{NB})$, where A_{NB} is the total area of disturbed pixels in the NWFP-DB across neighboring MODIS pixels in the window (i.e., the range of A_{NB} is 0-8). The third metric is the cumulative disturbance magnitude: $DM_c = S_p \times A_c$, where S_p is the disturbance severity from the NWFP-DB for the largest disturbance and A_c is the total disturbed area within a MODIS pixel accumulated over the entire time series. This latter metric accounts for the effect of multiple disturbance events occurring within the MODIS time series. If only one disturbance event occurred, it is equal to DM_p.

Our assessment included three elements. The first element evaluated how well MODTrendr was able to detect both the location and timing of disturbance events using the sample of 630 MODIS pixels we previously used to estimate the minimum dNBR noise threshold (Section 2.2.3). Omission errors were identified within the size and severity disturbance strata identified in Section 2.2.3, commission errors were evaluated for pixels identified as undisturbed, and the estimated timing was treated as correct if the year of disturbance onset identified by MODIS was within ±1 year of the disturbance onset from the reference data.

In the second element of this assessment, we evaluated how disturbance severity and spatial gridding artifacts in MODIS data affected results from MODTrendr. To

perform this analysis, we randomly sampled 2,000 disturbed MODIS pixels with sub-pixel disturbed areas (A_p) greater than 0.05 MODIS pixels. MODIS dNBR values associated with disturbance events were then compared with corresponding DM_p and DM_{NB} from the NWFP-DB using linear models to measure the relationship between MODIS dNBR and each of these metrics; differences between the two models were used to assess whether dNBR disturbance signatures originated outside the MODIS pixel of interest.

In the third and final element of this assessment, we explored how disturbance history and other factors were related to rates of omission and commission errors in MODTrendr results. To do this, we computed the cumulative disturbance magnitude (DM_c) for every forested pixel during two periods: 1985-2000 and 2001-2008. Rates of omission and commission errors were calculated relative to all forested MODIS pixels in the study area that were disturbed in the same time period (i.e., any disturbance with $A_p > 0.05$ MODIS pixels). We then calculated statistics characterizing how the timing, frequency, and duration of disturbances for both the pre-MODIS and post-launch eras influenced these results.

2.3 Results

2.3.1 Calibration of MODTrendr

Calibration of MODTrendr included two main elements: (1) selection of parameter values, and (2) identification of the dNBR threshold below which MODIS pixels were considered undisturbed. Most of the parameters were selected based on interpretation of results from the sample of 144 pixels described in Section 2.2.3 and are given in Table 2.1. However, we found that tuning the *pval* parameter required further examination. Figure 2.3 shows how errors of omission and commission depend both

on this parameter and the threshold of MODIS dNBR used to distinguish noise from disturbance events. As the MODIS dNBR "noise" threshold varied from 0 to 0.2, the rates of omission and commission errors diverged. The effect of the *pval* parameter was strongest for MODIS dNBR values between 0 and 0.05, which reflects a tradeoff between detecting small disturbances and over-fitting to noise; when *pval* was set to 0.15 more disturbances were detected and commission errors tended to be higher than when *pval* was set to 0.05. Figure 2.3 shows that results from MOD-Trendr depend quite strongly on the values selected for the noise threshold and the *pval* parameter. For all the analyses presented in following sections we used a *pval* parameter of 0.10 and set a noise threshold at 0.08 dNBR, which are designed to minimize both commission and omission error rates.

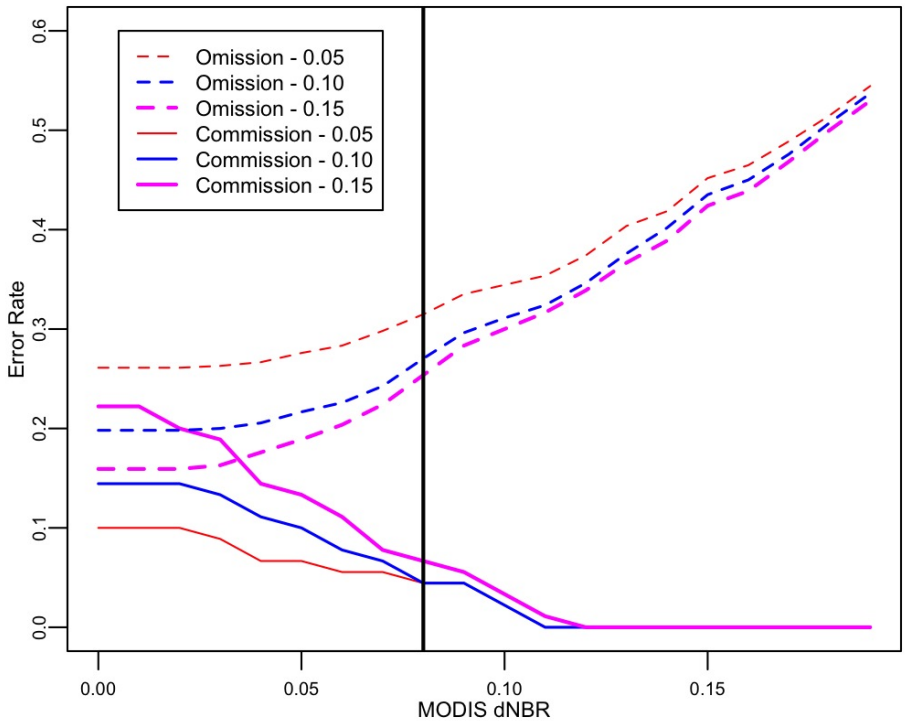

Figure 2.3: Selection of the pval parameter and development of a noise threshold in MODIS dNBR for a stratified random sample of 630 MODIS pixels. The chosen values of the noise threshold (0.08 dNBR; bold vertical line) and pval parameter (0.1) were based on the tradeoff between omission and commission errors in the MODTrendr results relative to the NWFP-DB. The commission error rates are shown as solid lines and the omission error rates are shown as dashed lines. The different line colors represent the three values of the pval parameter tested (0.05, 0.1, and 0.15).

2.3.2 Effects of Low-Resolution Bias

Figure 2.4 summarizes MODTrendr results for the sample of 630 pixels used in Figure 2.3 (described in Section 2.2.3) that includes both undisturbed and disturbed pixels, and where the latter group includes a range of disturbance timing, size, and

severity. For undisturbed pixels in this sample, the false positive rate in MODTrendr results (errors of commission) was less than 5%. As expected, the rate of successful detection was higher for pixels located over larger disturbances: 88% of disturbance events that affected more than 0.3 MODIS pixels were successfully detected within this sample. Conversely, the ability of MODTrendr to detect disturbance was much lower for smaller disturbance events: only 43% of events with areas less than 0.3 MODIS pixels were successfully detected. However, disturbance severity clearly influenced these results. High severity disturbance events tended to be detected more accurately, and disturbances with medium size but high severity had successful detection rates comparable with those for large area disturbances (Figure 2.4). The results for larger and higher severity disturbances also contained fewer timing errors relative to those for the smaller and less severe disturbance events. The most common timing error was associated with disturbance segments with onsets in 2001 and durations of 10 years, suggesting that these errors were caused by smoothing of abrupt changes to create a spurious long-term trend. Thus, the reliability of disturbance detection from MODTrendr depends on the area affected by the event, but even relatively small disturbances can be detected if the severity is high; for events with $A_c \leq 0.3$ MODIS pixels, the detection rate increased from 32% to 54% for low severity and high severity disturbances, respectively (Figure 2.4).

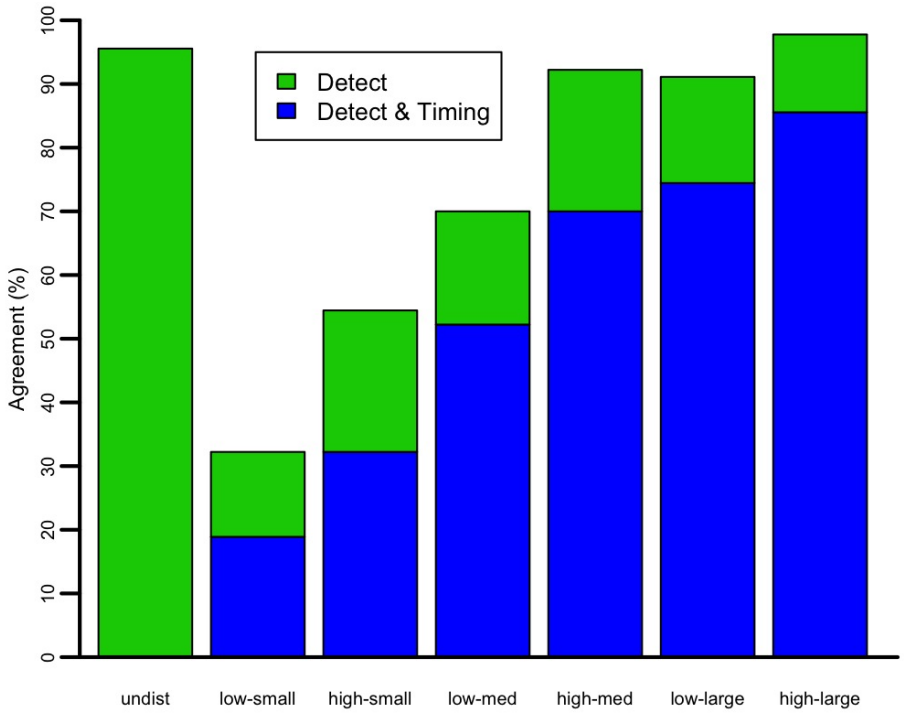

Figure 2.4: The agreement between disturbance information from the NWFP-DB and the MODTrendr results for the stratified random sample of 630 MODIS pixels also used in Figure 2.3. The strata shown here include undisturbed (undist) and combinations of severity (low and high) and size (small, medium or med, and large) classes. The "Detect" category indicates that MODTrendr correctly detected a disturbance event (or there was no detection in the case of undisturbed) but the algorithm missed the timing of the event. The "Detect & Timing" category indicates that MODTrendr also captured the timing of the disturbance event and is not applicable to the undisturbed case.

2.3.3 Effects of Gridding Artifacts

Using a sample of 2,000 MODIS pixels where MODTrendr successfully detected disturbance events between 2001 and 2008, we found positive relationships between

MODIS dNBR and two similar metrics derived from Landsat dNBR (Figure 2.5). The first metric (DM_p) uses the sum of Landsat dNBR values inside a single MODIS pixel, while the second metric (DM_{NB}) takes into account the disturbed area from neighboring pixels (see Section 2.2.4). Linear models for the relationship between MODIS dNBR and each of these metrics showed strong correlations, with a large cluster of points corresponding to lower severity events that are associated with either harvest or insect disturbances. MODIS dNBR under-predicted the first metric (DM_p; $R^2 = 0.66$) for many pixels affected by harvest, while the second metric (DM_{NB}; $R^2 = 0.75$) did not suffer from this effect and the relationship was closer to the 1:1 line. The shift in position of the cluster corresponding to harvested pixels is likely more related to the fact that small logging events tend to be widely distributed across the landscape than to a distinct spectral signature of logging. These results suggest that MODIS dNBR data capture information that is comparable to equivalent metrics at the Landsat scale, but that MODIS NBR values often include information from adjacent pixels that contribute to the disturbance signal at some pixels.

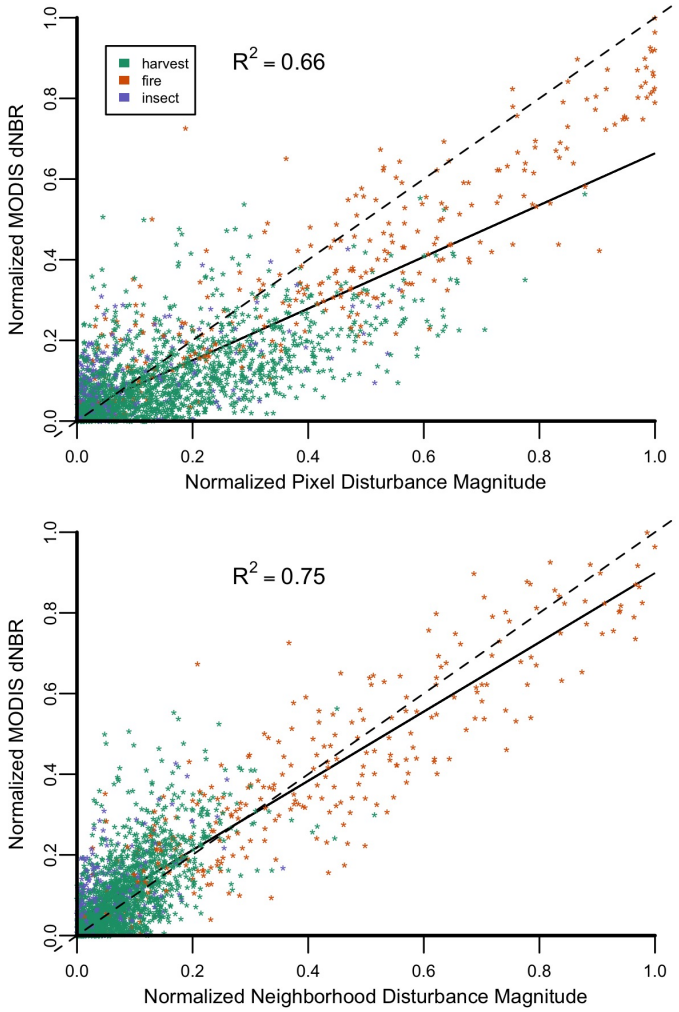

Figure 2.5: The relationship between MODIS dNBR and disturbance magnitude from the NWFP-DB for a random sample of 2,000 MODIS pixels that were disturbed once between 2001-2008. The points have been colored according to the disturbance type layer from the NWFP-DB. Two versions of disturbance magnitude are compared with MODIS dNBR: DM_p and DM_{NB}. Values of each metric have been normalized to range from 0 to 1 for comparison purposes. The solid line shows the best linear model fit with the R^2 value and the dashed line represents the 1:1 line.

2.3.4 Effects of Disturbance History

Of the 11.6 million hectares of forest (∼540,000 MODIS pixels) included in the study area, 28% were disturbed once and 62% were disturbed more than once between 1985 and 2008 according to the NWFP-DB. Of the forested pixels with at least one disturbance, 88% were disturbed between 1985 and 2000 and 50% were disturbed between 2001 and 2008. Hence, the spectral trajectory of many MODIS pixels includes information related not only to disturbance, but also to forest recovery and regeneration. Disturbance history prior to 2001 affects the trajectory of MODIS NBR values, and by extension, also affects results from MODTrendr. To explore this, we compared MODTrendr results for MODIS pixels in the study area that were undisturbed between 1985 and 2000 with results from pixels that were disturbed during the same period (Figure 2.6; Table 2.2). Before we review those results it is important to reiterate that the majority of errors in the MODTrendr results were associated with disturbance phenomena in the study area occurring at a scale that is well below the spatial resolution of MODIS pixels (Section 2.3.2; Jin and Sader 2005). The first panel in Figure 2.7 shows the size frequency distribution for disturbance events that occurred in the study area between 2001 and 2008, where the size of events is expressed as a proportion of 500-m MODIS pixels (A_p). Notably, about 75% of disturbance events in the NWFP-DB had areas smaller than 0.3 MODIS pixels. This size frequency distribution explains why fire events, which were generally much larger, were easier to detect with MODIS relative to harvest and insect disturbances, which tended to be much smaller. Further, as we demonstrated in Section 2.3.2, the signature of disturbance in MODIS time series is also related to the severity of the events. The second panel in Figure 2.7 shows the frequency distribution for DM_c (which combines the effects of size and severity; Section 2.2.4) across the study area

for all disturbance events that occurred in the study area between 2001 and 2008. Relative to the frequency distribution for A_p, the distribution of DM_c reached a maximum at lower values and had a longer tail; about 60% of disturbed pixels had DM_c values that were ≤ 0.1 dNBR. Since the noise threshold chosen for this work was 0.08 MODIS dNBR and the disturbance magnitude metrics are correlated with MODIS dNBR (Figure 2.5), this result demonstrates why MODTrendr does not capture a large proportion of disturbance events in the study area regardless of the effects of disturbance history discussed next.

Table 2.2: Sources of omission and commission errors in the MODTrendr results relative to the NWFP-DB across the study area. Each column shows proportions of MODIS pixels grouped as either of two agreement categories (undisturbed and disturbed) or two error categories relative to the disturbed class (commission and omission).

Category	Total number of MODIS pixels	Period 1985-2000			Period 2001-2008	
		Affected by Harvest	Affected by Insects	Disturbed Frequently[2]	Low MODIS NBR[3]	Neighborhood Disturbance[4]
Undisturbed forest	363,346	0.31	0.14	0.18	0.18	0.05
Disturbed forest	73,622	0.30	0.19	0.21	0.18	0.89
Errors of commission	32,585	0.28	0.27	0.18	0.51	0.18
Errors of omission	69,629	0.47	0.20	0.36	0.22	0.62

In previous sections we only considered pixels that were undisturbed prior to 2001; to expand on this we also explored the relationship between MODIS dNBR and

[2]"Disturbed frequently" describes pixels that were affected by at least three separate disturbance events during the period 1985-2000.

[3]"Low MODIS NBR" describes pixels with values of MODIS NBR < 0.6 in year 2000.

[4]"Neighborhood disturbance" describes pixels with $A_{NB} > 0.3$ MODIS pixels during the period 2001-2008.

DM_c for the 2001-2008 period for every forested pixel in the study area (Figure 2.6; Table 2.2). To maintain consistency with our previous results, here we used the same threshold to identify disturbed areas in the NWFP-DB (i.e., $A_p > 0.05$ MODIS pixels). Results from this analysis indicate that disturbance history substantially influenced results from MODIS. Two thirds (67%) of omission errors corresponded to locations that experienced either harvest or insect disturbances between 1985 and 2000 (only 2% of these errors were previously affected by fire disturbance), and many of these errors (36%) were also affected by at least three disturbance events (Table 2.2). This suggests that disturbance (primarily from logging) in these locations was frequent throughout the 1980s and 1990s, and that these locations therefore included mosaics of forest stands with different ages between 2000 and 2008 (Kennedy et al., 2012). Further, many of the disturbances affected relatively small areas, which affected the ability of MODTrendr to detect them; the median size of successfully detected disturbances was 0.3 MODIS pixels but the median size of undetected events was 0.13 MODIS pixels. Thus, individual disturbance events contributing to the DM_c in each pixel were frequently small, spread out in time, and included forest change at scales well below the resolution of MODIS. Further, post-disturbance afforestation between 2001 and 2008 may be masking spatially coincident disturbance events, leading to more errors of omission.

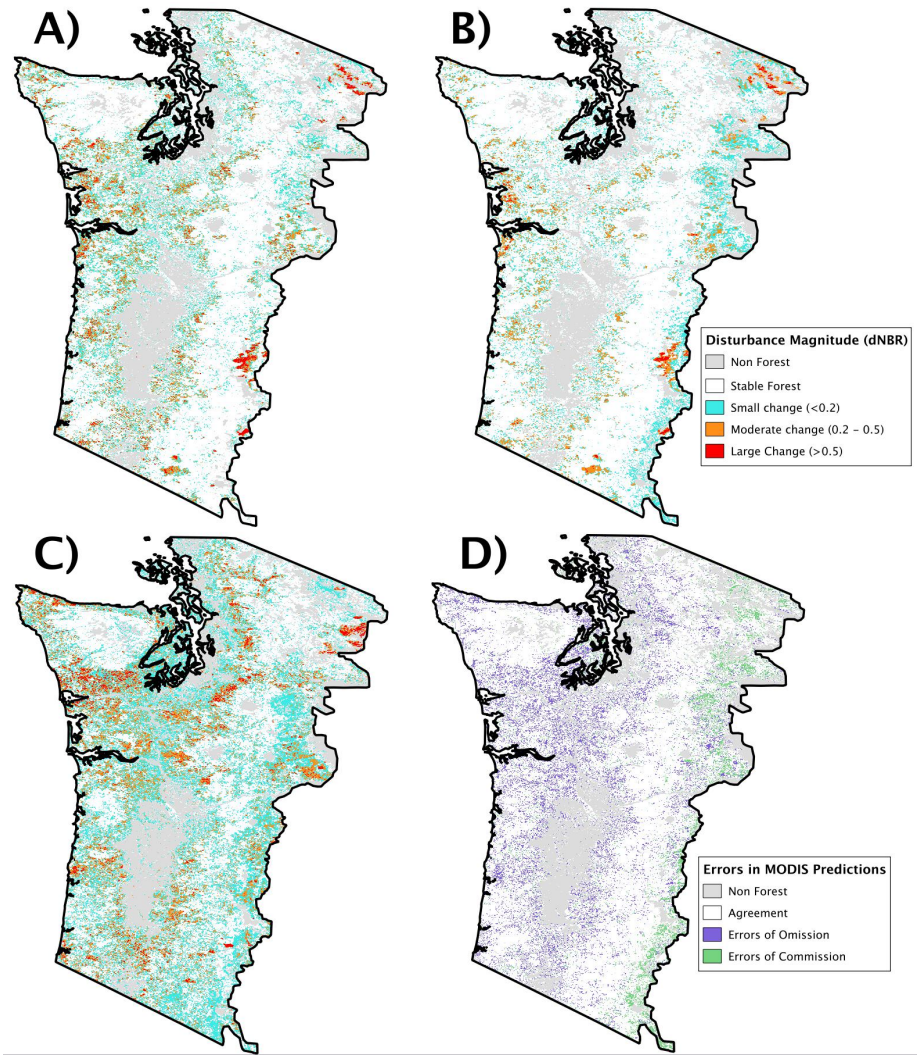

Figure 2.6: (A) Spatial distribution of the DM_c metric across the study area for the period 2001-2008. (B) Spatial distribution of MODIS dNBR for the period 2001-2008. (C) Spatial distribution of DM_c for the historical period 1985-2000. (D) Omission (purple) and commission (green) errors in MODTrendr results relative to the NWFP-DB for the period 2001-2008. Panels A-C are colored according to their dNBR values: a small change (cyan) is defined to be less than 0.2 dNBR, a moderate change (orange) as between 0.2 and 0.5 dNBR, and a large change (red) as greater than 0.5 dNBR. Panels A and C consider a pixel stable forest if $A_p \leq 0.05$ MODIS pixels and Panel B considers a pixel stable forest if MODIS dNBR ≤ 0.08.

The effect of disturbance history on commission errors, on the other hand, was less clear. More than one fourth (27%) of commission errors were located in pixels affected by long duration disturbances between 1985 and 2000, including areas that were affected by mountain pine beetle and western spruce budworm in the 1980s and 1990s (Meigs et al., 2011). Over half of these pixels had MODIS NBR values that were relatively low in 2000, indicating below average forest cover early in the time series (Table 2.2). The lower NBR values caused by these disturbances may have contributed to increased rates of commission errors by decreasing the signal-to-noise ratio within the time series, making MODTrendr more sensitive to noisy input data. Indeed, nearly 80% of the falsely-identified disturbance segments were estimated to occur in 2001 and had dNBR values less than 0.2 (Figure 2.6). Together, patterns in errors of omission and commission indicate that disturbance events prior to 2001 affect MODTrendr results from 2001-2008. At the same time, regional patterns in errors seem to reflect ecological differences between mixed-conifer forests dominated by Douglas-fir (*Pseudotsuga menziesii*) in the wetter western portions of the study area and the sparser forests dominated by Ponderosa pine (*Pinus ponderosa*) east of the Cascade Range (Lefsky et al., 2005; Kennedy et al., 2012), where commission errors tended to be concentrated.

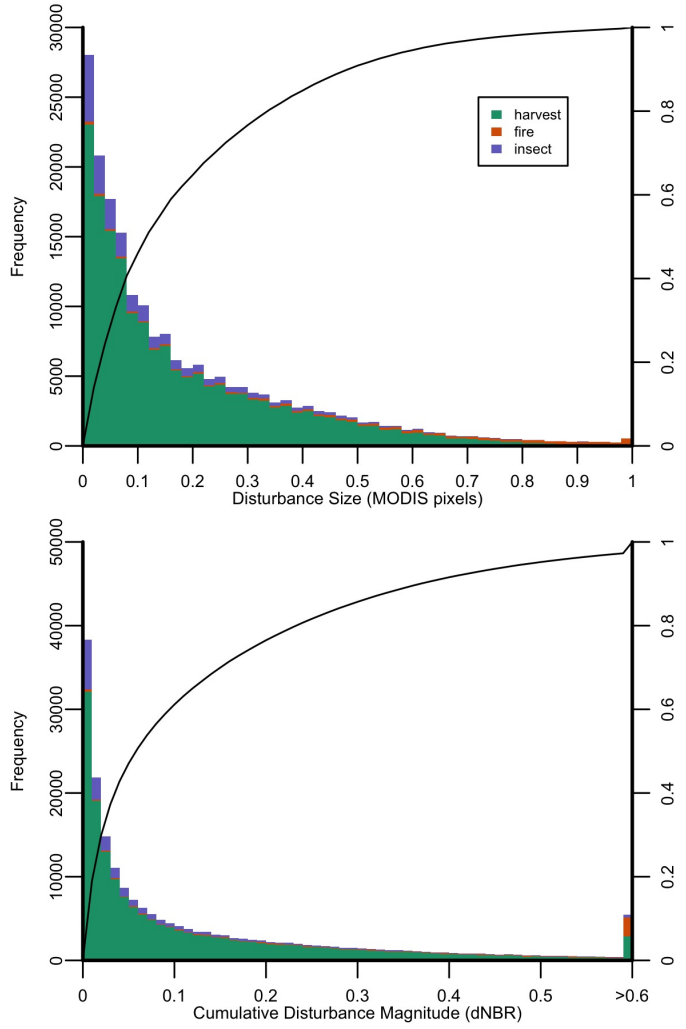

Figure 2.7: Distribution of disturbance event size and DM_c across the study area for the period 2001-2008. The disturbance size describes the proportion of a MODIS pixel affected by each event. The DM_c combines size and severity information from the NWFP-DB and is shown in units of dNBR. These two histograms are colored according to the relative proportion of three disturbance types from the NWFP-DB: harvest, fire, and insects/other. The solid lines show the cumulative frequency of the distribution along the right axis. For the DM_c distribution, all values of DM_c exceeding 0.6 dNBR were placed in the last bin.

2.4 Discussion

2.4.1 Effects of Disturbance Size, Disturbance Severity, and MODIS Gridding Artifacts

MODTrendr consistently detected disturbances larger than 0.3 MODIS pixels with high accuracy, correctly identifying 79% of these pixels across the study area (Figure 2.6). However, most disturbance events in the NWFP-DB affected less than one-third of a MODIS pixel (Figure 2.7). Previous results suggest that the so-called low-resolution bias inherent to analyses based on coarse spatial resolution instruments such as MODIS should preclude detection of these events by algorithms such as MODTrendr (e.g., Boschetti et al. 2004). Our results partially support this, but provide a more nuanced assessment. Specifically, our results indicate that across the study area 37% of forest disturbances affecting areas between 0.05 and 0.3 MODIS pixels were successfully detected by MODTrendr (Figure 2.6). For high severity events ($S_p > 0.6$ dNBR) within the same range in disturbance area, the percentage of successful detections increased to 52%. Thus, even though small disturbances were very common in the NWFP-DB (Figure 2.7), MODIS dNBR successfully captured the majority of disturbance information at the landscape scale. For example, sums of MODIS dNBR and Landsat-based DM_c (also in units of dNBR) across all forested MODIS pixels in the study area were remarkably similar (19,653 MODIS dNBR to 25,885 Landsat dNBR) for the period of 2001-2008, with MODIS capturing over 75% of the total disturbance magnitude from Landsat integrated over the entire study area and period. Disturbance size and severity also influenced the ability of MODTrendr to estimate the timing of events (Figure 2.4). MODTrendr assigned 56% of the spatially accumulated dNBR to disturbance segments with onsets in 2001, but the NWFP-DB only assigns 10% of the disturbance onsets to that year. If ac-

curate information related to disturbance timing is important, MODTrendr is likely to provide high quality information only for the larger and more severe events. That said, more research is required to better understand how interactions among sensor spatial resolution and disturbance size and severity influence errors of omission and commission from change detection algorithms.

Our results also suggest that gridding artifacts introduce modest amounts of information from neighboring pixels to dNBR values at each pixel (Figure 2.5). While MODIS data are geolocated with high accuracy, the MODIS daily surface reflectance data that are used to compute individual NBAR values at each pixel are obtained from a range of view zenith angles with fields of view that cover different projected areas on the ground. Daily surface reflectance measurements obtained at larger view zenith angles therefore include locations that are well outside the grid cell to which reflectance values are assigned (Huang et al., 2002); Tan et al. (2006) showed that 463-m MODIS pixels include information from an area that is 25% larger than the pixel grid cell. Indeed, even observations with small viewing angles have some geolocation uncertainty and may occasionally be assigned to the wrong grid cell. As a result, and as we demonstrate in Figure 2.5, the signature of disturbance events in adjacent pixels affects dNBR values in MODIS data. This conclusion is further supported by results shown in Table 2.2, which demonstrate that commission errors in MODTrendr results appear to be influenced by disturbance events in locations adjacent to the pixel of interest.

2.4.2 Effects of Disturbance History and Data Quality

Disturbance events that occurred prior to the launch of MODIS significantly affected MODTrendr results (Figure 2.6; Table 2.2). Specifically, errors of omission tended

to occur in locations with one or more disturbance events prior to 2001. MODIS NBR time series at these locations reflect complex interactions between disturbance and regrowth at sub-pixels scales. For pixels that were disturbed immediately prior to 2001, we expect changes in NBR from 2001-2008 to be slightly positive, reflecting forest regrowth. However, NBR time series at pixels that experienced multiple sub-pixel disturbance events between 1985 and 2008 may not show significant dynamics in NBR because regrowth at sub-pixel scales compensates for changes in NBR related to disturbance. Thus, errors of omission for sub-pixel disturbances occur not only because of low-resolution bias, but also because sub-pixel regrowth can mask the signature of disturbance in MODIS data (e.g., Healey et al. 2005). This is especially prevalent in the study area used for this work because logging activity creates a patchwork of forest clearing and regrowth below the spatial resolution of MODIS. As a result, errors of omission from MODTrendr tend to be clustered in those areas of the study area where logging is most common (Figure 2.2; Figure 2.6).

Commission errors from MODTrendr were influenced by noise in the MODIS NBR time series that were caused by factors other than disturbance history. Table 2.2 shows that many commission errors contained MODIS NBR values that were lower than average for forested pixels in the study area. This pattern may reflect changes in forest cover that occurred between the time depicted by the NWFP-DB forest mask and the MODIS era. However, a more likely explanation is that these lower than average NBR values reflect geographic differences in forest composition and stand structure (Lefsky et al., 2005). More generally, most commission errors from MODTrendr were associated with pixels that were estimated to have small severity disturbances (< 0.2 dNBR) in 2001. These two results are linked and reflect changes in the quality of NBR time series during the study period. Prior to 2003, MODIS

NBAR data were derived from MODIS-Terra only. After the launch of Aqua in 2003, the NBAR product algorithm was able to ingest surface reflectances from both MODIS-Aqua and MODIS-Terra, which significantly decreased the frequency of missing data and improved the quality of the product (Salomon et al., 2004). Because MODTrendr is sensitive to the first and last points of the time series (Kennedy et al., 2010), pixels that already have mixtures of forest and non-forest land cover (and lower NBR values) are more likely to show this type of commission error based on lower quality data from 2000-2002. Finally, a small proportion of MODTrendr commission errors may reflect timing errors for events that occurred between 2008 and 2010, or errors in the NWFP-DB caused by gaps in the Landsat archive, cloud-contaminated pixels, and the SLC-off problem of Landsat 7.

2.5 Conclusions

The research described in this paper includes two main elements. First, we adapted an existing algorithm for detecting forest disturbance using Landsat data for use with MODIS data; we call this version of the algorithm "MODTrendr." Second, we assessed the ability of MODTrendr to detect forest disturbance in the NWFP area and explored sources of error in MODTrendr results. Specifically, we examined how disturbance size, severity, and history affected errors of omission and commission in disturbance detection. In addition, we also examined if and how gridding artifacts inherent to MODIS data products affected the ability of MODTrendr to detect disturbance.

Our results provide several important insights regarding the strengths and weakness of MODTrendr (but also of MODIS data more generally) for detecting forest disturbance. Most importantly (and not surprisingly), successful detection of distur-

bance depended on the size and severity of the event, the level of noise in MODIS data, and the disturbance history at each MODIS pixel. Our results indicate that 79% of the disturbances affecting more than one-third of a MODIS pixel were detected by MODTrendr, but that smaller events were also detectable (albeit with less consistency), especially if the severity of the event was high. Disturbance history was shown to complicate the signature of disturbance in MODIS time series and introduced significant challenges for successful disturbance detection. Finally, the MODIS gridding algorithm can introduce signatures of disturbance from adjacent cells (and vice versa), which further complicate the signature of disturbance in MODIS NBR time series.

Future efforts with MODTrendr will focus on exploiting denser temporal information from MODIS time series, which is a particular strength of MODIS data. Further, extension of MODTrendr to use more spectral features (i.e., beyond NBR) also has the potential to improve results and might also help to discriminate different disturbance types (Schroeder et al., 2011). Another goal will be to test the use of MODIS 250-m data, which would help to resolve some of the challenges associated with sub-pixel disturbance detection that we have described in this paper. MODIS data have the advantage of being able to cover large areas in a timely fashion. However, MODIS lacks the spatial resolution provided by Landsat. In the long run, high-quality and timely detection of forest disturbances over large areas will require data from multiple sources that span a range of spatial, spectral, and temporal resolutions.

Chapter 3

Sources of Bias and Variability in Long-Term Landsat Time Series Over Canadian Boreal Forests

3.1 Introduction

The Earth's surface has warmed over the past 60 years at roughly 0.12°C per decade (Stocker et al., 2013). Climate warming has been most pronounced over Northern Hemisphere land areas during the winter and spring months (Hansen et al., 2006; Wang et al., 2006; Piao et al., 2008), and has been linked to longer growing seasons and changes to vegetation phenology and productivity (Piao et al., 2007; Kim et al., 2012; Xu et al., 2013; Jeganathan et al., 2014; Stow et al., 2004; Beck and Goetz, 2011), thermokarst dynamics (Smith et al., 2005), and forest dieback events (Allen et al., 2010; Michaelian et al., 2011). Boreal forest ecosystems are especially vulnerable to climate change because air temperatures exert strong control on boreal ecosystem function (Bonan, 2008), and continued warming has the potential to trigger a variety of climate feedbacks, including increased rates of ecosystem respiration (Angert et al., 2005), enhanced fire regimes (Flannigan et al., 2005; Wotton et al., 2010; de Groot et al., 2013), and melting permafrost (Anisimov, 1996; Schaefer et al.,

2011). Because boreal forests are geographically remote and extensive, monitoring and characterization of changes to the structure and composition of these forests is challenging. Remote sensing therefore provides a critical source of information related to how this important biome is responding to climate change.

Recent decades have witnessed an enormous increase in the volume of Earth-observation data from satellite-borne sensors that are available for climate change research. Several studies using the Normalized Difference Vegetation Index (NDVI), which is widely used as a proxy for primary productivity, have suggested that productivity has decreased across large regions of the North American boreal forest over the last 30 years (Tateishi and Ebata, 2004; Goetz et al., 2005; Beck and Goetz, 2011; Bi et al., 2013; Guay et al., 2014). Most of these studies are based on the Global Inventory Modeling and Mapping Studies (GIMMS) data set (newly released as version 3G), which provides 30 years of NDVI observations from the Advanced Very High Resolution Radiometer (AVHRR) at 8-km spatial resolution (Tucker et al., 2005; Pinzon et al., 2007; Pinzon and Tucker, 2014). The GIMMS data sets are based on maximum value NDVI composites for 15-day periods, and have been pre-processed to correct for clouds and atmospheric contamination, view angle effects, and changes to AVHRR sensor characteristics and calibration. Because observed changes in GIMMS NDVI time series over boreal forests are subtle, differences or refinements to methods that are used to generate AVHRR NDVI data sets can affect results from time series analyses. For example, the geographically extensive decreasing NDVI trends ("browning") observed across boreal North America in the GIMMS 3G data set were not detected in previously available AVHRR NDVI data sets (Slayback et al., 2003; Olthof and Latifovic, 2007; Pouliot et al., 2009; Alcaraz-Segura et al., 2010). More generally, challenges involved in cloud screening and atmospheric correction (Fontana

et al., 2012), the use of blended time series from different AVHRR sensors (Tucker et al., 2005; Pinzon and Tucker, 2014), natural and human disturbances (Goetz et al., 2005), and geolocation errors (Alcaraz-Segura et al., 2010) all introduce uncertainty to AVHRR time series.

In contrast to data from the AVHRR, the Landsat archive provides well-calibrated and precisely geolocated time series of remote sensing observations that span essentially the same time period as the GIMMS 3G data set (Wulder et al., 2012). The Landsat 4 and 5 missions (from 1982 to 2011) carried the Thematic Mapper sensor, which included six spectral bands designed for land cover and vegetation characterization at much finer spatial (30-m) resolution and with much better radiometric resolution and calibration relative to the AVHRR sensors (Markham et al., 2004). The Landsat 7 mission (launched in 1999) included the Enhanced Thematic Mapper Plus (ETM) sensor, which was developed as a more stable upgrade to the Thematic Mapper (Masek et al., 2001), and most recently, Landsat 8 was launched in 2013 and includes the Operational Land Imager (OLI), which extends and improves upon the Landsat legacy of Earth-observation science (Irons et al., 2012).

While a number of recent studies have used Landsat data to study long term changes in high latitude regions, these studies have generally used fewer than ten images for a single Landsat path/row, and have largely focused on greening trends in tundra ecosystems (Neigh et al., 2008; Pouliot et al., 2009; McManus et al., 2012). In this paper, we investigate a more general set of issues related to compiling and analyzing much denser Landsat time series (i.e., 150 to 300 images per scene) in support of long-term change studies in Canadian boreal forests. To do this, we selected eleven locations distributed across the Canadian boreal forest where Landsat acquisitions overlap according to the Worldwide Reference System (WRS2), and downloaded all

available TM5 and ETM data corresponding to peak-summer conditions (approximately July 1st to September 1st) for each of these locations. We then used these data to address the following questions:

1. Are red and near-infared (NIR) surface reflectances and derived spectral vegetation indices sufficiently stable over the 30-year Landsat record to support long-term trend analyses?

2. Do within-scene variations in sensor view geometry affect red and NIR surface reflectances and vegetation indices derived from Landsat data?

3. Can reflectances from the TM5 and ETM sensors be combined into a single time series, or do sensor-specific differences introduce artifacts in the data?

Results from our analyses show that while the radiometric and calibration quality of the TM5 and ETM sensors are exceptionally high, time series of Landsat surface reflectances and spectral vegetation indices include sources of variability that are unrelated to changes in surface properties, and which therefore need to be accounted for in time series analyses that exploit the deep and rich record of terrestrial observations provided by the Landsat archive.

3.2 Data and Methods

3.2.1 Study area

The boreal zone of North America extends from Alaska to Newfoundland, encompasses 627 million hectares, and is defined by climate regimes that support cold-tolerant tree species (Brandt, 2009). In this work we focus on the boreal forests east of the Canadian Rocky Mountains, using eleven sites that encompass a range in forest

types, disturbance regimes, and climates (Figure 3.1). Specifically, we selected areas located where two or more adjacent Landsat WRS2 paths overlap each other. This strategy doubled (or in some cases tripled) the number of Landsat images and compensated for the relatively low frequency of Landsat acquisitions at higher latitudes (Ju and Roy, 2008).

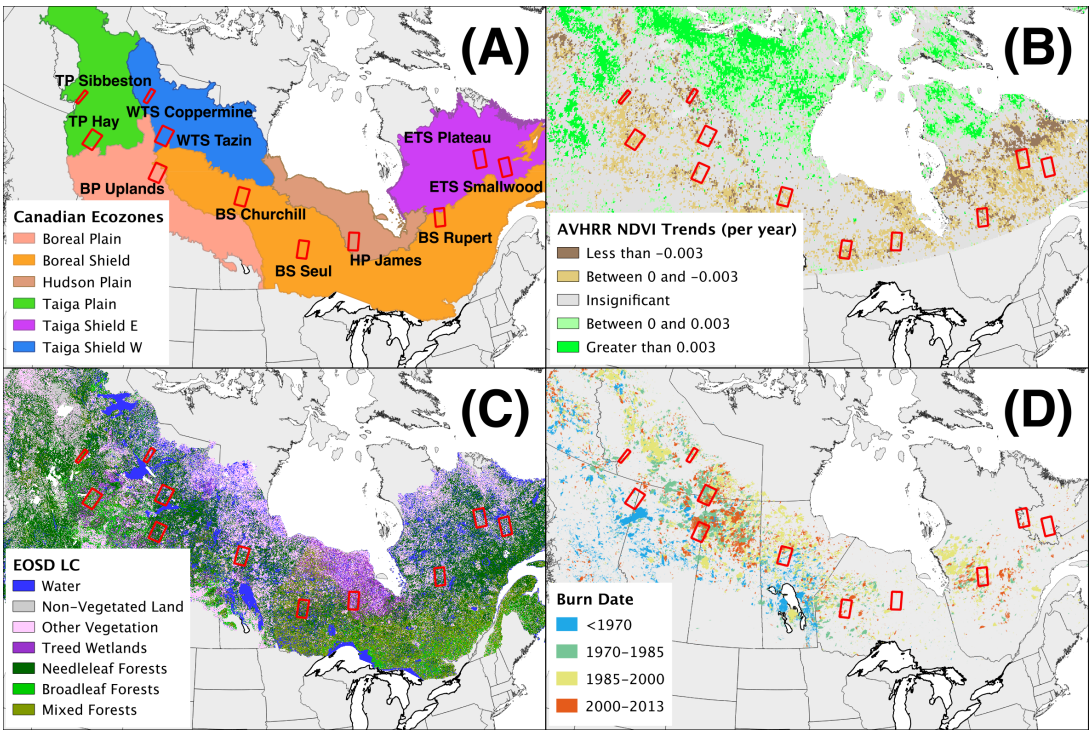

Figure 3.1: The Canadian boreal forest study area and the eleven scenes (identified by red boxes) selected according to (A) ecozones, (B) AVHRR NDVI trend slopes, (C) land cover, and (D) fire disturbance.

The final set of sites included eleven overlap regions that were selected according to two main criteria. First, nine of the sites included a substantial proportion of 8-km AVHRR pixels with statistically significant browning trends in peak-summer NDVI in the GIMMS 3G data set. To identify AVHRR pixels with browning trends, we

followed the same basic procedure as Beck and Goetz (2011) and Guay et al. (2014), where we first selected the maximum NDVI value for each AVHRR pixel from all July and August observations for each year between 1982 and 2012. We then used results from the Theil-Sen trend estimator (implemented in the *zyp* pacakage in R (Bronaugh and Werner, 2013)) at each pixel to select regions with widespread and statistically significant browning ($\alpha = 0.05$). Two scenes that contained relatively low proportions of pixels with statistically significant NDVI trends were also selected (i.e., WTS Tazin and ETS Smallwood; Figure 3.1). Second, the sites were selected to encompass the diverse range of climate zones, forest types, and disturbance histories that are found in the Canadian boreal forest zone (Figure 3.1). To do this, we used climate regimes (available at `http://sis.agr.gc.ca/cansis/nsdb/ecostrat/gis_data.html`), land cover derived from Landsat data circa 2000 (Wulder et al., 2008a), and fire disturbance history from the Canadian Large Fire Database (LFDB) (Stocks et al., 2002).

3.2.2 Landsat time series data

Several pre-processing steps were required to convert raw L1T Landsat stacks to annual composites representing the peak-summer "greenness" for each year. These included atmospheric correction and cloud screening, followed by manual inspection of images to further screen undetected atmospheric contamination. Finally, all of the images for each peak-summer period were condensed into a single cloud-free composite for each site. We define "peak-summer" as the eight-week window between day of year 180 and 240, which corresponds to the period from July 1 to September 1.

For each of the eleven sites (Figure 3.1), all available peak-summer images from

Landsat 5 (TM5) and Landsat 7 (ETM) between 1984 and 2012 were downloaded from the Google Earth Engine archive (available at `gs://earthengine-public/landsat`). Landsat L1T data were used because they have already been georeferenced and orthorectified by the USGS (Wulder et al., 2012). The Landsat Ecosystem Disturbance Adaptive Processing System (LEDAPS) (Masek et al., 2006) was used to convert the L1T data to at-sensor radiances, perform atmospheric correction, and compute surface reflectances. The Function of Mask (Fmask) algorithm (Zhu and Woodcock, 2012) was then used to identify pixels that contained clouds, cloud shadows, snow, or water. To screen errors in the Fmask results, we manually screened the resulting image time series, and any images with substantial amounts of undetected clouds, haze, and smoke were removed. To eliminate any remaining data contaminated by clouds or smoke (especially for sites with only a few images in a single summer season), we removed observations with red reflectance higher than 0.12 and NIR reflectance higher than 0.2. These thresholds were prescribed to be conservative, and eliminate extreme values only.

The final peak-summer composite for each year was created using a maximum value NDVI compositing procedure. This procedure eliminates most unscreened atmospheric effects over vegetated surfaces because cloud-contaminated pixels have lower NDVI values than clear-sky pixels (Roy et al., 2010). To perform the compositing, at each pixel surface reflectances for each Landsat band were retained from the image associated with the highest NDVI observation during the peak-summer period. To support further analysis, data from different Landsat WRS2 paths were composited separately for each sensor, thereby allowing us to create data sets that only included imagery from eastern or western images in overlap pairs, or that included data from only the TM5 or ETM sensor.

3.2.3 Ancillary information related to land cover and disturbance

Two sources of ancillary information were used to select undisturbed pixels with different land cover types in each of the eleven sites. First, to identify landscape patches with uniform land cover, we used a simplified version of the Earth Observation for Sustainable Development of Forests (EOSD) map, which provides a land cover classification at 30-m spatial resolution for all of Canada based on circa 2000 Landsat 7 ETM data (Wulder et al., 2008a). To reduce the impact of uncertainty in this product, we collapsed the 22-class EOSD legend into two simpler legends with four classes and seven classes (Table 3.1), where the four-class scheme collapsed all forest types into one class and the seven-class scheme retained differences related to leaf types. To identify homogeneous land cover patches in these simplified maps, we used morphology tools available in the Python Scipy library (Jones et al., 2001) to identify spatially contiguous land cover patches and to erode each patch inwards by one pixel, thereby reducing errors associated with patch edges. Second, to isolate pixels that were not disturbed by fire (which is the dominant source of disturbance in Canadian boreal forests (Amiro et al., 2001), we used the Canadian Large Fire Database (LFDB) to identify and remove pixels that had been burned at any time in the record.

Table 3.1: Aggregation of EOSD LC classes according to four (AGG4) and seven (AGG7) class schemes similar to Remmel et al. (2005).

AGG4	**AGG7**	**EOSD**
		Shadow
		Cloud
Water		Water
Non-Vegetated Land		Snow/Ice
		Rock/Rubble
		Exposed Land
Non-Forest Vegetation		Shrub-Tall
		Shrub-Low
		Herb
		Bryoids
		Wetland-Shrub
		Wetland-Herb
Forest	Treed Wetlands	Wetland-Treed
	Conifer Forests	Conifer-Dense
		Conifer-Open
		Conifer-Sparse
	Broadleaf Forests	Broadleaf-Dense
		Broadleaf-Open
		Broadleaf-Sparse
	Mixed Forests	Mixed-Dense
		Mixed-Open
		Mixed-Sparse

3.2.4 Analysis of Landsat data

We analyzed nearly three decades of Landsat imagery at each of the eleven study sites to explore sources of variability that influence detection of long-term trends in time series of annual maximum NDVI and corresponding values for EVI, red reflectance, and NIR reflectance. To perform these analyses, we used the four-class version of EOSD map (Table 3.1) in association with the LFDB to select random samples of unburned pixels from each land cover type (excluding water) in each site. Water pixels were excluded because the maximum-NDVI compositing approach is not appropriate for water bodies, which can have lower clear-sky NDVI values than cloud-contaminated pixels. The resulting data set provided time series of Landsat surface reflectances for each cover type that were then used to explore if and how vegetation indices and surface reflectances varied as a function of time, view angle (eastern versus western portion of images), and instrument (TM5 versus ETM).

The first set of analyses we performed was designed to assess the nature and magnitude of systematic biases introduced by intra-sensor geometry and both intra- and inter-sensor calibration. To do this, we selected 100 samples, each of 2,000 undisturbed pixels, for each land cover type within each site. Land cover types that made up less than 5 percent of the site's area were excluded. Each sample of pixels was used to calculate five-year medians in red and NIR surface reflectances (values for the medians of the other visible and IR bands are provided in the Appendix), the NDVI, and the Enhanced Vegetation Index (EVI). The EVI was used because it is less affected by residual atmospheric effects not captured by LEDAPS and is less prone to saturation at high values relative to the NDVI (Huete et al., 2002). Medians based on 100 bootstrapped sample means (Efron and Tibshirani, 1986) were compiled for each five-year interval and used to perform three assessments. First, to characterize the

long-term stability of the TM5 calibration, we assessed if and how TM5 data changed through time by comparing data from 1985-1989 to values for the same undisturbed pixels in 2005-2009. Second, to quantify the magnitude of variance introduced by view geometry, we took advantage of the fact that all of our sites are located in the overlap zone between adjacent Landsat scenes, and compared TM5 and ETM data from the eastern-most portion of Landsat images with co-located data from the western-most portion of adjacent Landsat images at each site for 2005-2009. Third, we quantified differences between TM5 and ETM using data from each instrument acquired with consistent geometry (i.e., within the same WRS2 scene) for 2005-2009.

In the second set of analyses, we assessed if and how subtle differences in calibration between the TM5 and ETM sensors affect the nature and magnitude of NDVI trends over undisturbed forest pixels. To do this, we used two 28-year Landsat time series (1984-2011): the first data set included only TM5 data, and the second data set pooled all available TM5 and ETM data into a single time series. Using these data we randomly selected 400 undisturbed forested pixels from each site (total n=4,400 pixels). We then used the Theil-Sen trend estimator to characterize the magnitude and statistical significance of temporal trends in NDVI in each data set (i.e., TM5-only versus TM5 and ETM combined). As part of this analysis, we also analyzed differences between the annual maximum NDVI computed from TM5 versus ETM for each sampled forest pixel for the period when both Landsat 5 and Landsat 7 were collecting data (from 1999 to 2011).

3.3 Results

3.3.1 Landsat compositing and cloud screening

Figure 3.2A shows the number of TM5 and ETM images acquired for each year across all eleven study sites that were used in our analyses (2,439 images total). These images were all acquired between day of year 180 and 240 between 1984 and 2012. The number of TM5 images acquired each year was relatively constant (roughly 60) until 1999 when Landsat 7 was launched; thereafter, the combined rate of image acquisitions nearly doubled to 115 images per year. In 2000, and to a lesser extent in 2001, the number of TM5 images decreased substantially over boreal Canada because the acquisition strategy focused on ETM data during this period (White and Wulder, 2014). After 2001, acquisitions of TM5 and ETM data were roughly equivalent until Landsat 5 was decommissioned in late 2011.

Figure 3.2: (A) Distribution of all peak-summer Landsat acquisitions by year. (B) Summary of good quality data frequency at ten percent intervals. Discarded scenes are represented as N/A.

Figure 3.2B summarizes the proportion of good quality data in peak-summer TM5 and ETM images after the pre-processing steps described in Section 3.3.1 were applied. We define a "good quality" observation as having a valid value in both red and NIR reflectances. Of the 2,439 total scenes, 11 percent were excluded because of

errors during pre-processing, including problems with the Fmask-based cloud screening. Roughly 21 percent of the remaining images had more than 90 percent missing data, and 37 percent of the images had less than 50 percent missing data. Relative to TM5 data, ETM data had higher frequencies of missing observations because of the scan-line corrector failure of Landsat 7 in 2003 (Arvidson et al., 2006).

Figure 3.3 shows the impact of manual cloud screening (performed after applying Fmask and LEDAPS) on red band reflectance values at each site. In general, sites with more cloud cover in summer months tended to be located in the eastern part of the study area (i.e., ETS Smallwood, ETS Plateau, and BS Rupert; Figure 3.1) and exhibited more variance in red reflectance. After we manually screened for clouds, there were fewer outliers in most sites and both the median and the overall spread in red reflectance decreased. The decrease in the magnitude of red band reflectances for ETS Plateau, BS Churchill, BP Uplands, and WTS Coppermine suggests that this procedure successfully removed previously undetected clouds.

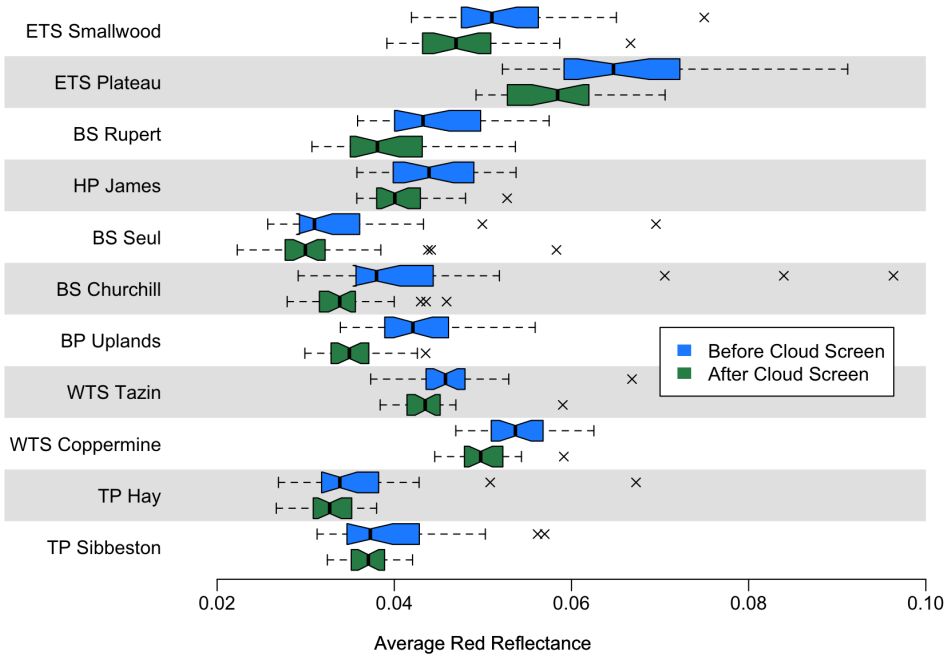

Figure 3.3: The average red reflectance of TM5 data for each study site is compared before and after manual cloud screening. Each box represents the range of 28 years of site-wide averages.

3.3.2 Sources of variation in Landsat time series

To investigate sources of variability in TM5 and ETM data related to intra- and inter-sensor calibration differences, we compared surface reflectances and vegetation indices for co-located undisturbed pixels across different time periods, sensor view angles, and instruments. Specifically, we performed three distinct assessments using time series of red reflectance, NIR reflectance, and corresponding NDVI and EVI values. The same assessments were performed for the blue, green, and two shortwave infrared channels (Landsat bands 1, 2, 5, and 7) and are provided in the Appendix.

First, we compared values from 1985-1989 for each of these quantities against

values from 2005-2009 for TM5 data only. Figure 3.4 presents scatter plots showing mean values for each of these quantities, stratified by site and land cover class (Figure 3.9 shows these relationships for the other visible and infrared bands). The solid red line presents the result from a linear major axis regression (Sokal and Rohlf, 1995), along with 95 percent confidence intervals on the slope of the estimated model plotted as dashed red lines. In all four cases, values are close to the 1:1 line, which strongly suggests that the calibration for TM5 is stable across the twenty year time period considered here. The only exceptions to this general conclusion are that forested pixels in some sites had higher NIR reflectance in 1985-1989 relative to 2005-2009 and, conversely, non-forested pixels in some sites had lower NIR reflectance in 1985-1989 relative to 2005-2009. However, these differences were not sufficiently large to affect corresponding NDVI or EVI values.

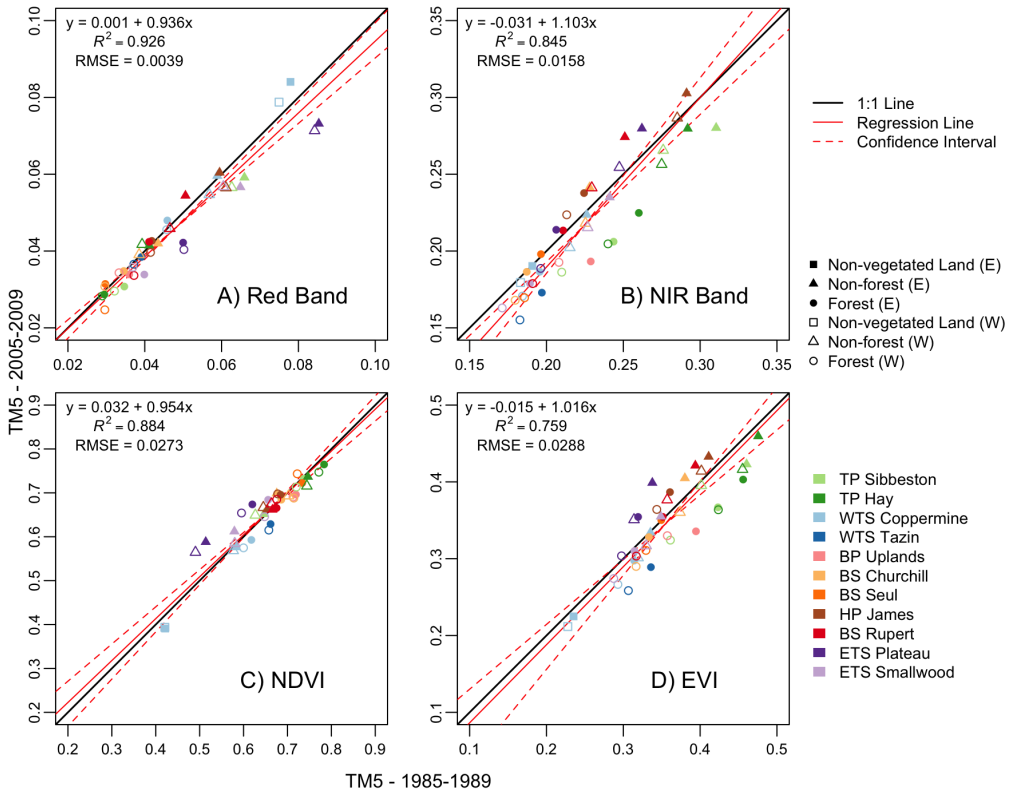

Figure 3.4: Comparisons of median red reflectance, NIR reflectance, NDVI, and EVI values between TM5 data sets for undisturbed landscape patches separated by 20 years. The values plotted are medians for five year periods, stratified by land cover type and study site.

Second, we assessed if and how modest variation in TM5 and ETM view geometry between the eastern and western portions of Landsat scenes introduces systematic variation in surface reflectances and vegetation indices derived from these instruments. To do this, we exploited the fact that each of our sites is located in the overlap region between adjacent Landsat scenes, and compared values for surface reflectances and vegetation indices that were acquired by the same sensor during the same time period from different view geometries (i.e., pixels located on the western

portion of one scene versus the eastern portion of the adjacent overlapping scene). Figure 3.5 clearly shows that red and NIR reflectances from pixels taken from the western side of Landsat scenes (i.e., from the eastern-most WRS2 path) were higher on average than those from the eastern side (Figure 3.10 shows that these relationships are similar for the other visible and infrared bands), and that this bias was stronger in the NIR band than in the red band. While NDVI values did not show this pattern, EVI values for the western side of Landsat images were also higher than those on the eastern side.

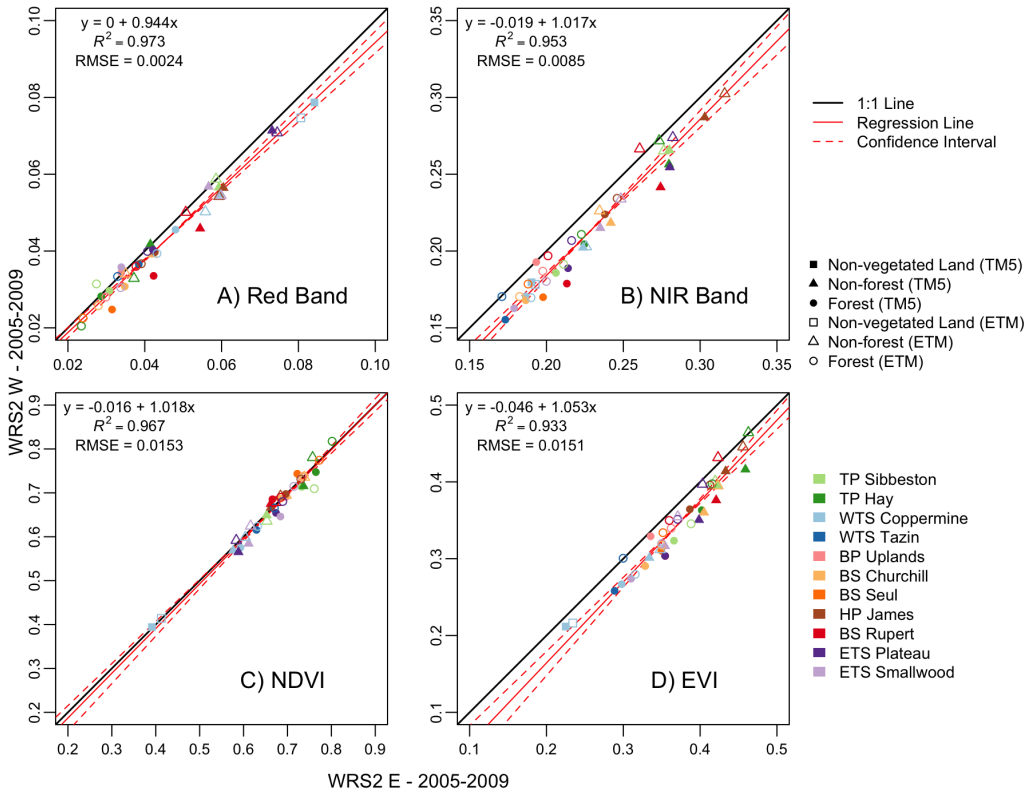

Figure 3.5: Comparisons of median red reflectance, NIR reflectance, NDVI, and EVI values from Landsat data between eastern and western edges of adjacent scenes over undisturbed landscape patches. Values plotted are medians for 2005-2009, stratified by land cover type and study site.

Third, we used the period 2005-2009, when both Landsat 5 and Landsat 7 were acquiring data, to assess differences between TM5 and ETM surface reflectances and vegetation indices. Figure 3.6 presents a comparison of red reflectance, NIR reflectance, and values of the EVI and NDVI from TM5 versus ETM for co-located pixels extracted from peak-summer image acquisitions (Figure 3.11 shows these relationships for the other visible and infrared bands), and reveals that red reflectance values from the TM5 sensor were systematically higher than those from the ETM

sensor, but that NIR reflectance values were very similar across the TM5 and ETM sensors. As a result, average NDVI and EVI values derived from ETM data were higher than those from TM5 data. Relative to changes over time or biases imposed by changing view geometries, relationships between TM5 and ETM reflectances and vegetation indices showed the strongest agreement with very little scatter around the fitted regression. In the next section, we show that even though differences in red reflectance between the TM5 and ETM data were small, these differences can introduce spurious trends in time series if they are combined to create a single time series.

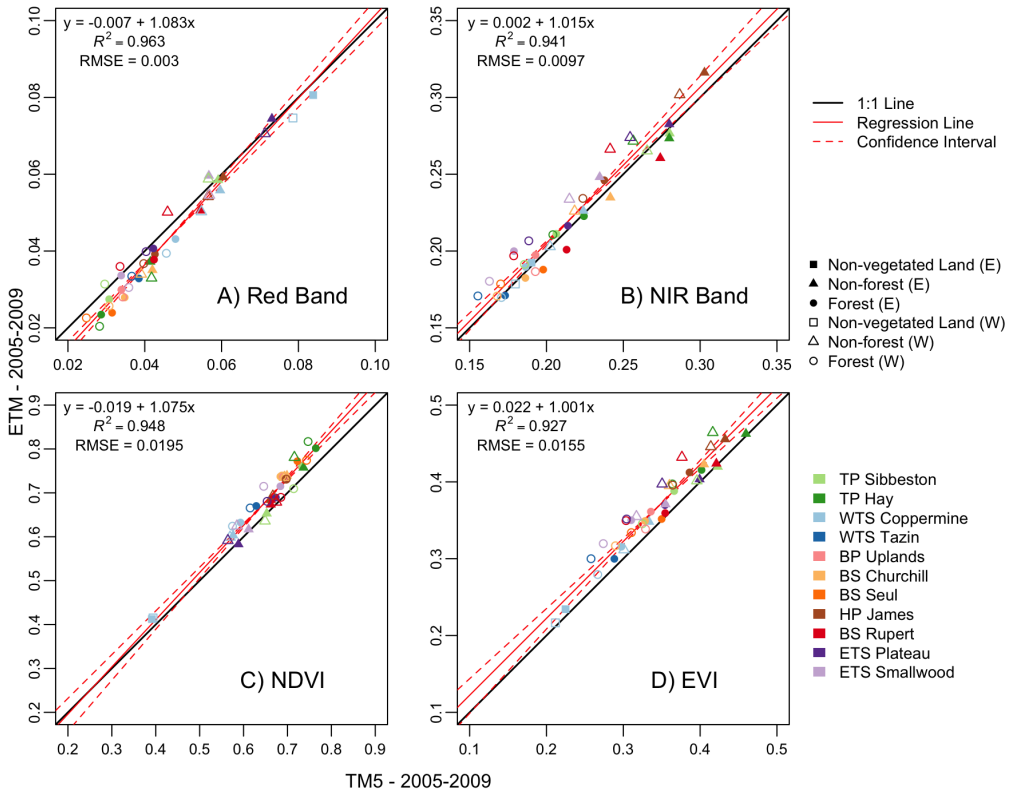

Figure 3.6: Comparisons of median red reflectance, NIR reflectance, NDVI, and EVI values between TM5 and ETM data over undisturbed landscape patches. Values plotted are medians for 2005-2009, stratified by land cover type and study site.

3.3.3 Impact of cross-sensor bias on NDVI trends

In the final set of analyses performed for this work, we assessed if and how the systematic differences in red band reflectance from TM5 versus ETM discussed in Section 3.3.2 affect long-term NDVI trends over undisturbed forest pixels in our study sites. To do this, we used the same non-parametric Theil-Sen estimator that was used in Section 3.2.1 to compute the magnitude and statistical significance of trends in Landsat NDVI over time using two different data sets. The first data set

was created using surface reflectances from TM5 data only, while the second data set combined NDVI data from both TM5 and ETM. Figure 3.7 plots the distribution of estimated trends across 4,400 undisturbed forest pixels sampled from each data set, and clearly shows substantial differences between trends estimated from only TM5 data versus those estimated using the pooled data set that combines data from the TM5 and ETM. In the data set that combines TM5 data with ETM data, 36 percent of pixels exhibit statistically significant trends (α =0.05), while in the TM5-only data set only 18 percent of pixels do. Further, nearly all of the pixels showing statistically significant trends in the combined data set have positive slopes (i.e., NDVI increasing with time), while pixels showing statistically significant trends in the TM5-only data set are more evenly split between positive and negative slopes (47 percent versus 53 percent, respectively).

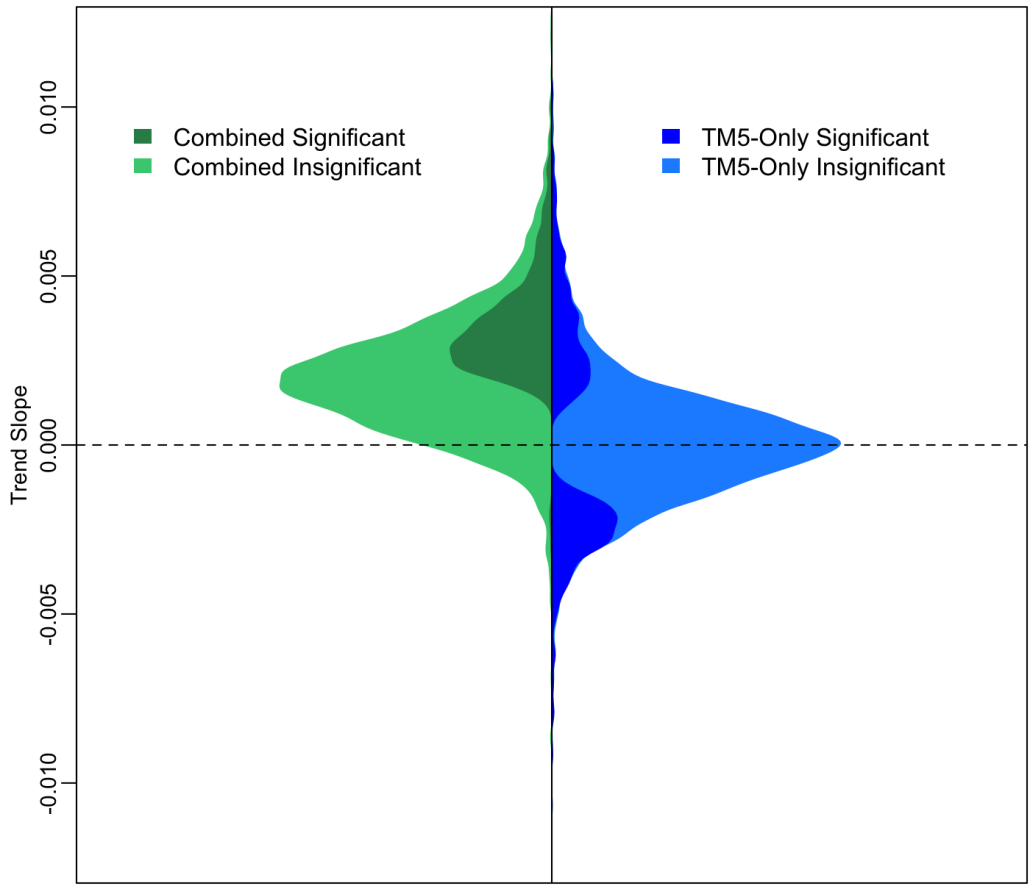

Figure 3.7: Distribution of NDVI trend slopes for the combined TM5/ETM data set and the TM5-only data set for a sample of 4,400 undisturbed forest pixels.

Over the period from 1999 to 2011, the combined data set has a median bias of 0.03 NDVI units greater than the TM5-only data set for the same period (Figure 3.8). It is interesting to note, however, that the magnitude of this bias seems to modestly vary over time; from 1999 to 2002 the median bias was 0.042 NDVI units but from 2003 to 2011 the median bias was 0.027 NDVI units. These results demonstrate that systematic differences in NDVI values derived from ETM data relative to those derived from TM5 data influence long-term trends estimated from NDVI time series that combine TM5 data with ETM data. Specifically, because ETM NDVI values are

systematically higher than those from TM5, inclusion of ETM data from 1999-2011 can cause spurious positive trends in NDVI time series.

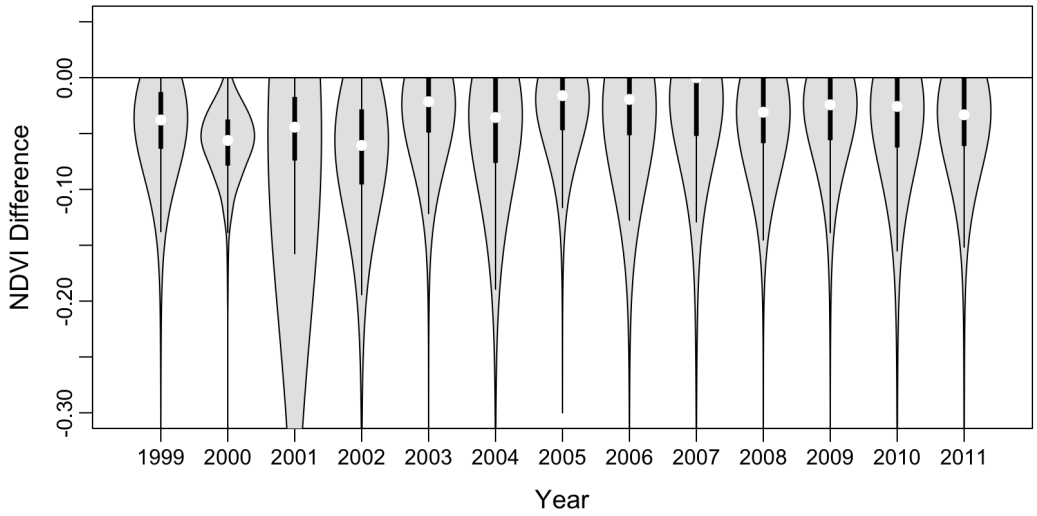

Figure 3.8: The distribution of absolute differences in peak-summer NDVI values between the TM5-only data set and the combined TM5/ETM data set for all years between 1999 and 2011 for a sample of 4,400 undisturbed forest pixels.

3.4 Discussion and Conclusions

In this paper we explored sources of variability in time series of Landsat data that are unrelated to surface properties, which can therefore influence interpretation and statistical inferences related to long-term trends in surface properties. Specifically, we addressed the three research questions posed at the end of Section 3.1. Results from our investigation point to three main conclusions.

First, the results presented in Figure 3.4 demonstrate that the radiometric calibration of the TM5 instrument, at least in the red and NIR bands, is sufficiently stable over the nearly three decade lifespan of Landsat 5 to support long-term trend

analyses. However, several outliers are clearly evident in the NIR reflectance shown in Figure 3.4B. In all likelihood, these outliers reflect changes in vegetation cover that occurred during the 20 year period represented in this Figure. For example, increases in the NDVI of non-forest vegetation in the ETS Plateau and ETS Smallwood sites may reflect increases in the vigor of shrub vegetation in response to climate warming (Fraser et al., 2011; McManus et al., 2012). Similarly, decreases in NIR (and by extension, NDVI) in forested pixels could be related to responses to drought stress or to succession from hardwood to conifer species in pixel containing undetected fires in the LFDB. Indeed, it is important to note that even though the LFDB provides a record of fire that extends back to the early 1900's, it is less accurate for earlier periods (i.e., before Landsat) (Stocks et al., 2002). Further, fires that were smaller than 200-ha are not recorded in the LFDB, nor are other disturbances such as logging and mining development. In cases where a disturbance was missed and the affected pixels were labeled as undisturbed, ecological succession from shrubs and broadleaf deciduous trees to evergreen needleleaf forests would first exhibit an increase in NIR reflectance, followed by a gradual decline over many years (Song et al., 2002). Overall, however, the results we found strongly support the conclusion that the calibration coefficients of the red and NIR bands for TM5 are of high quality.

Second, modest differences in view geometry between the eastern and western portions of Landsat scenes introduce small but statistically significant differences in surface reflectances. Specifically, surface reflectances for pixels on the western edge of Landsat images are higher than corresponding reflectances from the eastern edge of the adjacent image because the western portion of images include a higher proportion of illuminated tree crowns, while the eastern portion of images include a higher proportion of shadows (Li and Strahler, 1986). Because of this effect, care

must be taken when Landsat time series are created by combining data from overlapping WRS2 paths. The impact of the directional effect on NDVI values is small because the the red and NIR values are weighted equally in the computation of the NDVI and the bias introduced by view geometry has the same sign and roughly the same magnitude in each band (Figure 3.5). Conversely, the EVI values from the western edges of images show systematic positive biases because the NIR band is weighted more heavily in the EVI relative to the NDVI. Hence, compositing procedures that use data combined from adjacent paths based on maximum EVI values will preferentially select data from the eastern path.

Third, we found modest, but potentially significant, differences in red reflectance between the TM5 and ETM sensors, which probably arise from bandwidth differences of the TM5 and ETM sensors that are not corrected for by cross-calibration (Teillet et al., 2001; Vogelmann et al., 2001; Chander et al., 2009). Because most of the ground targets used for this procedure in the past have had high reflectances in the red and NIR wavelengths (Teillet et al., 2004), the collection of more low-radiance targets for this purpose may correct the problem. While the differences we found are small, they are sufficiently large to introduce spurious trends in time series of the NDVI in a substantial proportion of undisturbed pixels across the eleven sites we examined. Hence, depending on the application, NDVI time series that have been generated using data combined from both of these sensors should be used with care (Figure 3.6).

Of the three main results that we identify above, differences in red reflectance between the TM5 and ETM sensors have the largest impact on detection of long-term NDVI trends over boreal forests (Figure 3.7). Specifically, peak-summer NDVI values derived from data that combine TM5 and ETM reflectances were on average

0.03 NDVI units higher than NDVI based on TM5 data only (Figure 3.8). Results from non-parametric trend tests show that this bias introduced spurious trends in NDVI for a substantial number of pixels in the combined data set (Figure 3.7). A related finding was that the magnitude in the NDVI bias was not constant through time. Figure 3.8 shows that the magnitude seems to change in 2003. This shift could either be related to the scan-line corrector (SLC) failure of Landsat 7 in 2003 (Arvidson et al., 2006) or the unequal acquisition of TM5 and ETM data during the period 1999-2002 (White and Wulder, 2014) (Figure 3.2).

The Landsat archive is one of the best sources of remote sensing information for investigating trends related to forest health and productivity at regional to global scales. The archive is freely accessible and deep enough to address many important questions regarding the nature and consequences of changes in the biosphere over the last 30 years. In remote regions such as the Canadian boreal forest and arctic where the depth of the Landsat archive can be an important limiting factor, focusing studies in areas where Landsat acquisitions overlap can substantially increase the amount of data available. However, because these environments are naturally dynamic and many of the changes that are occurring are subtle and gradual, effective analysis of Landsat times series requires high quality data that have been carefully screened for artifacts and sources of variance that are unrelated to processes on the ground.

While this work focused on red and NIR reflectances (see the Appendix for analyses of other Landsat bands) and commonly used spectral vegetation indices such as the NDVI, future work will benefit from the use of other spectral indices such as the Normalized Burn Ratio (Kennedy et al., 2010), or the wetness component of the Tasseled Cap transform (Czerwinski et al., 2014). These indices may be less affected by unscreened atmospheric effects and have been shown to provide useful informa-

tion related to spatial and temporal variation in forest productivity and biomass (Cohen and Spies, 1992; Roberts et al., 2006; Baccini et al., 2012; Ji et al., 2012). As new data from TM5-like sensors become available, such as the recently launched OLI sensor onboard Landsat 8 or the Sentinel-2 missions, it will also become increasingly feasible to monitor and explore patterns of change over large swaths of the Earth's terrestrial ecosystems. As this paper shows, however, careful attention to data quality will be essential to the success of these studies.

3.5 Appendix

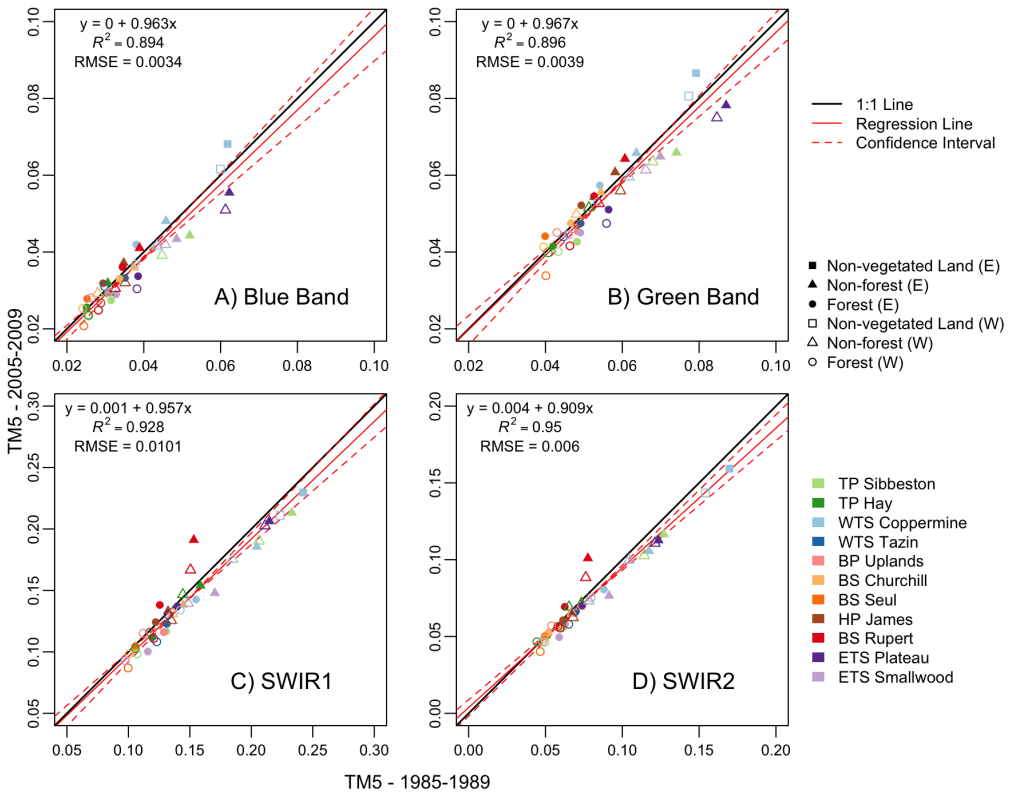

Figure 3.9: Comparisons of median blue reflectance, green reflectance, SWIR1 reflectance, and SWIR2 reflectance values between TM5 data sets for undisturbed landscape patches separated by 20 years. The values plotted are medians for five year periods, stratified by land cover type and study site.

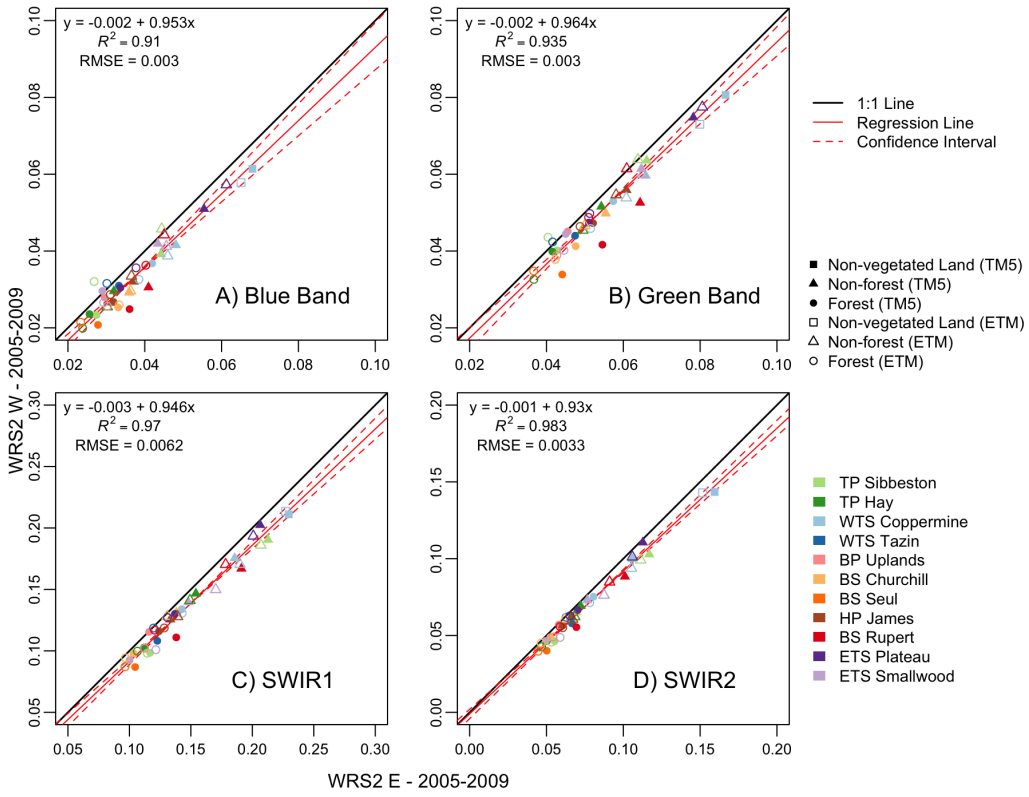

Figure 3.10: Comparisons of median blue reflectance, green reflectance, SWIR1 reflectance, and SWIR2 reflectance values from Landsat data between eastern and western edges of adjacent scenes over undisturbed landscape patches. Values plotted are medians for 2005-2009, stratified by land cover type and study site.

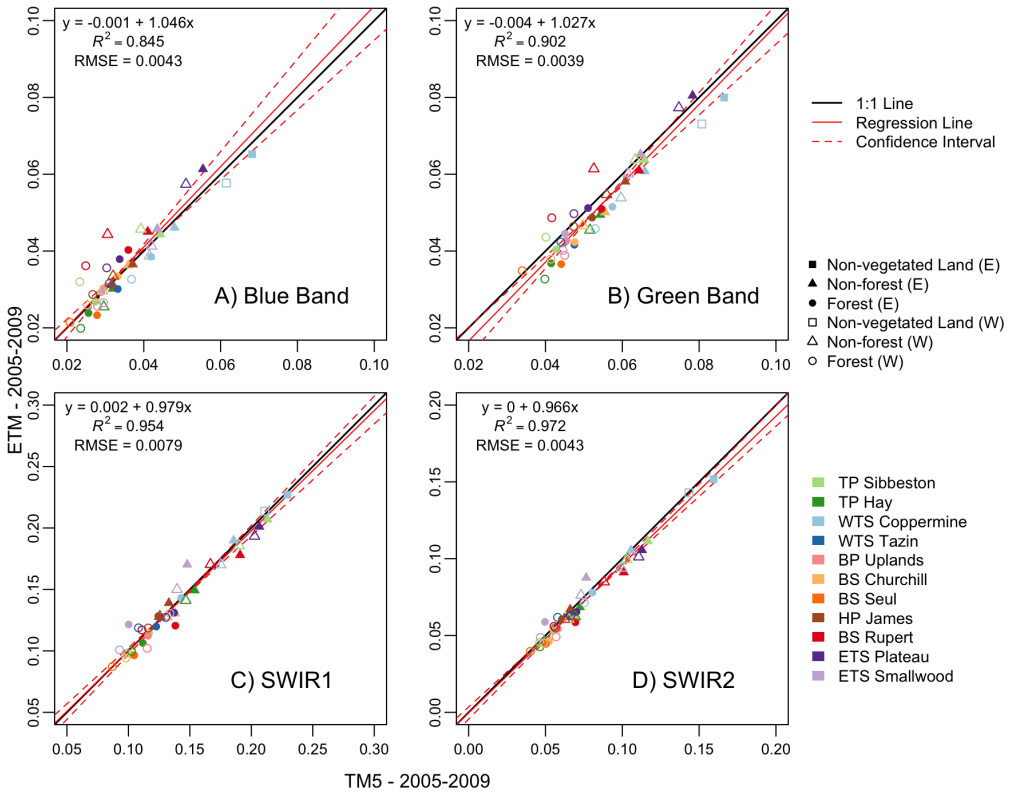

Figure 3.11: Comparisons of median blue reflectance, green reflectance, SWIR1 reflectance, and SWIR2 reflectance values between TM5 and ETM data over undisturbed landscape patches. Values plotted are medians for 2005-2009, stratified by land cover type and study site.

Chapter 4

Divergent Responses of Canadian Boreal Forests to Climate Warming

4.1 Introduction

Over the past 40 years the Earth's climate has warmed at a rate of 0.15-0.2°C per decade with much of this warming concentrated in the Northern Hemisphere (Hansen et al., 2010a; Stocker et al., 2013). The changing climate has major implications for the function and productivity of natural ecosystems in arctic and boreal regions, including longer growing seasons (Keyser et al., 2002; Piao et al., 2008; Xu et al., 2013), drier summers (Angert et al., 2005; Parida and Buermann, 2014), and enhanced fire regimes (Kasischke and Turetsky, 2006; Turetsky et al., 2010). Ground-based studies in these regions have described permafrost loss (Osterkamp et al., 2000), increased shrub growth in arctic ecosystems (Sturm et al., 2001; Tape et al., 2006), and both increasing and decreasing rates of boreal tree growth (Wilmking et al., 2004; Ma et al., 2012). Many of these changes have important implications for global climate models, which project an enhanced role for boreal and arctic ecosystems in the global carbon and radiation budgets (Eugster et al., 2000; Balshi et al., 2007; Euskirchen et al., 2009; Schaefer et al., 2011). Further, in large regions of boreal North America, observations of declining tree growth (Lloyd and Bunn, 2007), including wide-spread

tree mortality events (Allen et al., 2010; Peng et al., 2011), provide evidence for potentially large errors and uncertainties in current models.

Forest health in boreal regions is intimately linked to the seasonal co-occurrence of temperature and precipitation (Bonan and Shugart, 1989), and warming temperatures are affecting the depth of the snow-pack (Kim et al., 2012), the length of summer-time droughts (Michels et al., 2007; Dai, 2012), and the prevalence of fires (Flannigan et al., 2005). In the drier central regions of Canada, increased summertime drought stress has caused widespread aspen diebacks in Saskatchwan and Alberta, especially following the extreme 2001 drought (Hogg et al., 2008; Michaelian et al., 2011). However, in more humid eastern regions of Canada, growth rates of conifer and shrub species in open woodlands and treeless tundra continue to increase, possibly in response to the longer and warmer growing seasons (Ma et al., 2012; Fraser et al., 2011; McManus et al., 2012).

While it is clear that the function and productivity of the boreal forests of Canada are responding to climate warming, studying these processes across the entire boreal region of Canada requires remote sensing data. Recent studies have attempted to do this using 30-year time series of the Normalized Difference Vegetation Index (NDVI) acquired from the Advanced Very High Resolution Radiometer (AVHRR), and have linked negative trends in NDVI to declines in photosynthetic capacity and productivity (Beck and Goetz, 2011; Bi et al., 2013; Guay et al., 2014). However, time series from AVHRR have large uncertainties (Pouliot et al., 2009; Alcaraz-Segura et al., 2010) and questions remain about the ecological meaning of observed NDVI changes.

In this work we investigate long-term records of boreal forest productivity from remote sensing data with improved spatial and radiometric properties compared to the AVHRR sensor. Specifically, we use 28-year time series (1984-2011) of Landsat 5

imagery from the Thematic Mapper (TM) instrument to identify subtle changes to forest ecosystems with unprecedented precision. The main objective of this research is to improve understanding of the major sources of variability and trends in Landsat vegetation index (VI) data within Canadian boreal forests over the past three decades. To achieve this goal, we ask the following two research questions:

1. How do spatial patterns in disturbance and land cover influence VI trends from 28-year Landsat time series in Canadian boreal forests?

2. How do spatial patterns and changes in climate influence VI trends from Landsat time series for undisturbed forests in the boreal region of Canada?

To address these questions we upscaled Landsat-scale time series to the spatial scale of the Moderate Resolution Imaging Spectroradiometer (MODIS) and intersected these data with ancillary information on disturbance, land cover, and climate. By characterizing the major sources of spatial variability in long-term VI trends, we can identify the regions that are vulnerable to transitioning to a less productive state as a result of climate change (Lenton et al., 2008; Scheffer et al., 2012).

4.2 Data and Methods

4.2.1 Study Area

The study area for this work included five major Canadian ecozones: Boreal Plain, Boreal Shield, Taiga Plain, Taiga Shield, and Hudson Plain (downloaded from `http://canadianbiodiversity.mcgill.ca/english/ecozones/index.htm`; Figure 4.1A). These ecozones include a large proportion of the AVHRR pixels that have previously shown negative NDVI trends in the Global Inventory Modeling and Mapping Studies (GIMMS 3G) data set (Pinzon et al., 2007; Beck and Goetz, 2011). In addition,

these ecozones include a range in climate and fire regimes. Within the study area, 46 sites were chosen that were located in the overlap area between two or more adjacent Landsat World Reference System (WRS2) acquisition paths (Figure 4.1). These sites were randomly selected based on the criterion that each contained at least 10% tree cover according to the MODIS Vegetation Continuous Fields (VCF) product (Hansen et al., 2003).

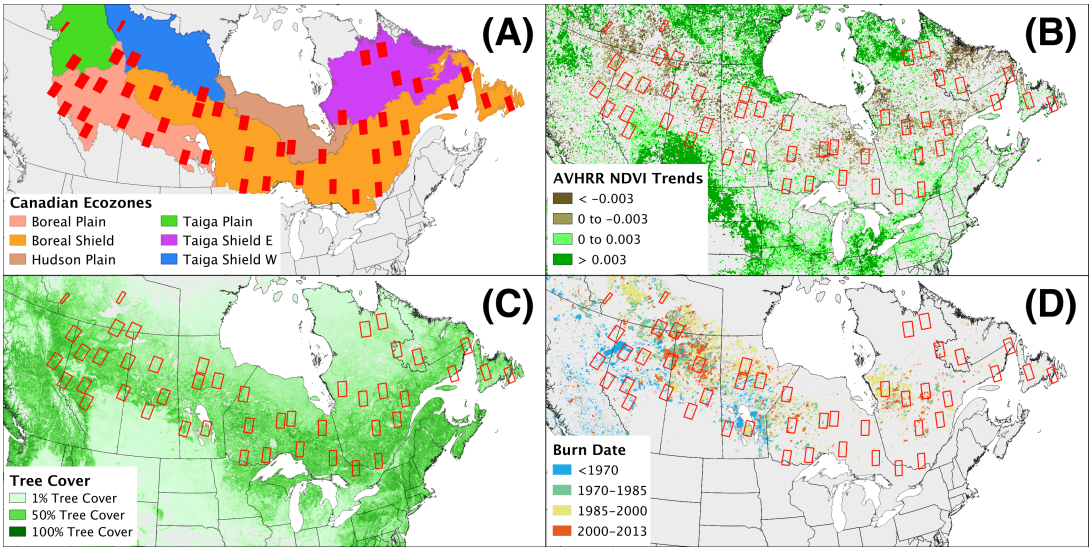

Figure 4.1: The Canadian boreal forest study area and the 46 Landsat overlap scenes (identified by red boxes) shown according to (A) Canadian ecozones, (B) AVHRR NDVI trends from the GIMMS 3G data set, (C) tree cover from the MODIS VCF product, and (D) fire disturbance from the Canadian LFDB.

4.2.2 Pre-processing Landsat Data

For each site, all available Landsat 5 Thematic Mapper (TM) L1T data between 1984 and 2011 were downloaded from the USGS archive (`http://earthexplorer.usgs.gov/`). These data have been orthorectified, atmospherically corrected, and

converted to surface reflectances by the USGS (Masek et al., 2006). Before further analyses, the data were pre-processed to remove ephemeral contamination from clouds and other atmospheric effects. The cloud screening was done in two parts. In the first step, we used a recently developed algorithm called Function of Mask (FMask) that uses thresholds in reflectance and brightness temperatures to identify clouds and then matches clouds with cloud shadows using sun-sensor geometry (Zhu and Woodcock, 2012). Fmask has an overall cloud-detection accuracy higher than 95%. However, it does miss haze and smoke contamination (Zhu and Woodcock, 2012), which commonly occur in the study region. Therefore, we used a second procedure to remove scenes that were still contaminated by unscreened clouds, haze, and smoke after applying FMask. To do this, we calculated scene-wide averages of red band reflectance for each image in the peak-summer period (defined as all dates between day of year 180 and 240). Since these atmospheric effects significantly increase red band reflectances above normal conditions (Sulla-Menashe et al., in review; see Figure 3.3), we removed images with average scene-wide red band reflectances that were more than one standard deviation greater than the mean value across all dates.

Following these pre-processing steps, peak-summer composites for each Landsat band were produced for each growing season using a maximum NDVI compositing approach (Cihlar et al., 1994). To do this, the cloud-free NDVI values in the peak-summer period were sorted and the reflectances corresponding to the image with the highest NDVI value were selected at each pixel and for each year. Two spectral vegetation indices were calculated from these composites, the NDVI and the Normalized Burn Ratio (NBR; García and Caselles, 1991), which is a widely used index for detecting changes in forest cover (Key and Benson, 1999; van Wagtendonk et al., 2004; Cohen et al., 2010), canopy water content (Roberts et al., 2006), and above-ground

biomass (Baccini et al., 2012; Ji et al., 2012).

4.2.3 Ancillary Information on Land Cover, Climate, and Disturbance

Four sources of ancillary information were used to help characterize the influence of land cover, climate, and disturbance on trends in Landsat vegetation indices. First, for land cover, we used an existing Landsat-scale land cover map from the Earth Observation for Sustainable Development of Forests (EOSD) project that covers 80% of Canada's land area and was created using Landsat Enhanced Thematic Plus (ETM+) data circa 2000 (Wulder et al., 2008a). The original twenty classes provided by this map were aggregated to four classes (water, non-vegetated land, non-forest vegetation, and forest) because, at this level of aggregation, the map has an overall accuracy of nearly 80% (Remmel et al., 2005).

Second, for climate, we obtained monthly climate data including temperature, precipitation, and potential evapotranspiration data at 0.5° spatial resolution from the Climatic Research Unit (CRU) data set for the period of 1984-2011 (New et al., 2002). CRU data were obtained for each site by identifying the nearest 0.5° grid cell to the site centroid. To characterize the sites according to moisture regime, we calculated the Climate Moisture Index (CMI) for the growing season from these data, defined here as the six-month period from April through September. CMI was calculated as the accumulated difference (in millimeters) between monthly precipitation and potential evapotranspiration across the growing season.

The final ancillary data sources used in the analyses were two maps of disturbance. The first of these was developed from the Canadian Large Fire Database (LFDB), which combines all Canadian fire agency records of fires larger than 200 hectares from 1959 to present based on analysis of aerial surveys and satellite imagery (Stocks et al.,

2002). The polygons of burned areas obtained from this database were reprojected, clipped, and rasterized to match the resolution and extent of each Landsat site. At each Landsat pixel, the date of the most recent burn was recorded.

The second disturbance map used in the analyses was created directly from the pre-processed Landsat stacks (Section 4.2.2) using an algorithm called Continuous Change Detection and Classification (CCDC; Zhu and Woodcock, 2014). This algorithm fits models to the time series of reflectances at each Landsat pixel and identifies breakpoints in these time series based on persistent deviations of the observations from their modeled values. At each Landsat pixel, we applied a simplified version of the CCDC algorithm written in Python (Holden, 2015) to the entire Landsat TM time series (1984-2011) to detect breakpoints corresponding to land cover changes. From these results we produced a single map for each site with values corresponding to the year of the first disturbance in the record. Since the Canadian LFDB only records fires larger than 200 hectares, this second disturbance map was used to identify small fires and other disturbances, including logging, insect defoliation, storm damage, and flooding.

4.2.4 Analyses of Landsat Trends

To analyze trends in Landsat vegetation indices, peak-summer Landsat 5 TM composites for each year were intersected with the MODIS Sinusoidal grid and each Landsat pixel was assigned to a MODIS pixel ID. The ∼225 Landsat pixels within each MODIS pixel were treated as a panel, and panel linear models (PLMs) were applied to each panel using the *plm* package in R (Baltagi, 2008; Croissant and Millo, 2008). Specifically, the linear models were used to investigate the slope of the relationship between two spectral indices (NDVI and NBR) and time. By combining

spatially contiguous groups of pixels into panels, we minimized problems associated with missing or noisy data influencing the results. In assessing the PLM results, we excluded pixels with p-values greater than 0.05. However, one of the strengths of the PLM approach is that it pools data across pixels in the same region, thereby substantially increasing the degrees of freedom in the estimated model. As a result, panel models effectively identify subtle trends. Because it is difficult to interpret the meaning of very small changes in VIs over a 28-year period, we excluded panels that had trends with absolute values less than 0.001 VI units/year.

To summarize the land cover map for each panel, we counted the number of Landsat pixels in each of the four classes. Panels with more than 40% water were removed from further analyses. The remaining panels were categorized into four classes, including non-vegetated land, non-forest vegetation, open forest, and dense forest. Non-vegetated land was defined as having less than 30% vegetation. Non-forest vegetation was defined as having more than 30% vegetation and less than 40% forest vegetation. Open forest and dense forest were defined as having between 40 and 80% and greater than 80% forest vegetation, respectively.

To summarize the disturbance information for each panel, we counted the number of Landsat pixels that were disturbed in each year from each disturbance map (LFDB and CCDC). For each year and panel, the sums of disturbed Landsat pixels for each disturbance map were compared and the largest sum was used as the proportion of disturbance in that year. To determine the total proportion of disturbance occurring in each panel, the annual sums were tallied across the entire time series. Panels that contained at least 70% disturbed Landsat pixels were categorized as disturbed and panels that contained less than 10% disturbed Landsat pixels were categorized as undisturbed, thereby avoiding sub-panel mixtures of disturbed and undisturbed

pixels. Figure 4.2 shows how the spatially aggregated land cover and disturbance information corresponds with the VI trends from the PLM results for a site centered on the Northern Old Black Spruce BOREAS site in Manitoba.

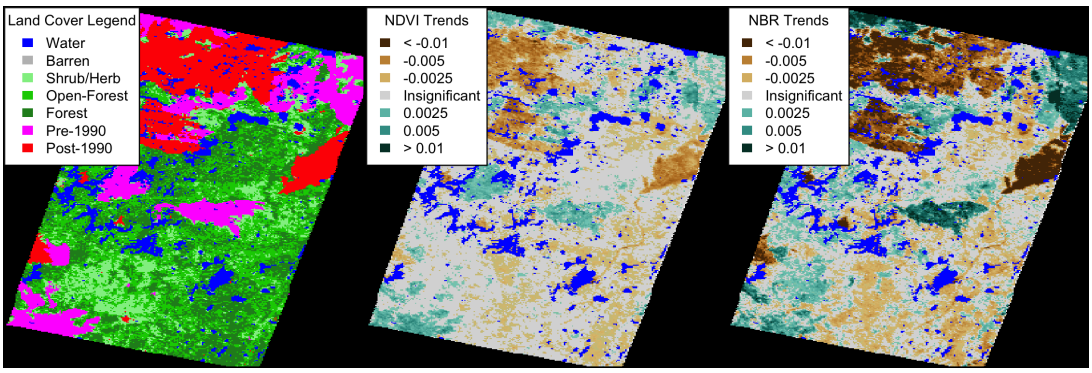

Figure 4.2: An example of the spatial distribution of land cover, disturbance, and Landsat VI trends for a site centered on the Northern Old Black Spruce BOREAS flux tower site in Manitoba. In the first panel, land cover and disturbance information have been aggregated from Landsat-scale maps to the MODIS pixel-sized panels used in analyses. Estimated trends and significances in the second (NDVI) and third (NBR) panels are based on panel linear models and significant trends were required to have p-values less than 0.05 and slopes with absolute values greater than 0.001 VI units/year.

We performed three analyses on the Landsat time series using the ancillary information on land cover, climate, and disturbance described in Section 4.2.3. In the first analysis, we examined how disturbance timing affects the nature and magnitude of trends from each vegetation index. To do this, we grouped the disturbed panels into two categories: disturbed early and disturbed late, where disturbed early refers to panels that were disturbed between 1970 and 1989 and disturbed late refers to panels that were disturbed between 1990 and 2011. To determine the presence and

timing of disturbance events in each panel, we assigned the disturbed panels to the early or late category based on the annual counts of disturbance occurrence from the combined disturbance map. Using a random sample of 5,000 panels from each category, we estimated probability density functions (PDFs) for the estimated NDVI and NBR trends. As part of this analysis, we randomly sampled panels that had been disturbed by fire according to the LFDB map and characterized the time series of each index (NDVI and NBR) as a function of time since fire relative to samples of undisturbed panels, including non-forest, open forest, and dense forest.

In the second analysis, we examined trends in Landsat NDVI and NBR for undisturbed panels. To do this, we randomly selected 5,000 panels from each of three categories of undisturbed cover types: non-forest vegetation, open forest, and dense forest. For each sample, we again estimated PDFs of the NDVI and NBR trends.

In the third analysis, we explored how the trends within the undisturbed dense forest category varied according to climatically available moisture (Figure 4.6). The sites were separated into dry, moderate, or wet categories according to 33% quantiles in mean CMI values across the study area, where higher CMI values indicate more moisture availability. For each category, we again estimated PDFs of the NDVI and NBR trends for a random sample of 5,000 panels.

4.3 Results

4.3.1 Effects of Disturbance on Landsat VI Trends

For the first analysis, we sampled from a set of panels, distributed across all the study sites, that contained more than than 70% disturbed Landsat pixels. Disturbed panels represented about 25% of all land panels, with 9% in the disturbed early category, 13% in the disturbed late category, and 3% belonging to neither category (either

disturbed before 1970 or disturbed in both early and late periods). Of the disturbed panels, 86% were affected by fire (disturbed according to the LFDB) and 14% were affected by other disturbances (disturbed according to the CCDC results but not according to the LFDB). Figure 4.3 shows how the trends in NDVI and NBR varied according to disturbance timing, which was a strong predictor of the sign of the VI trend (e.g., Figure 4.2). Specifically, disturbances that occurred near the beginning of the time series were associated with statistically significant positive VI trends (71% for NDVI and 79% for NBR) and disturbances that occurred in the middle or the end of the time series were associated with significant negative VI trends (53% for NDVI and 76% for NBR). In general, NBR trends associated with disturbance had larger ranges and higher median absolute values than those of NDVI trends (Figure 4.2; Figure 4.3).

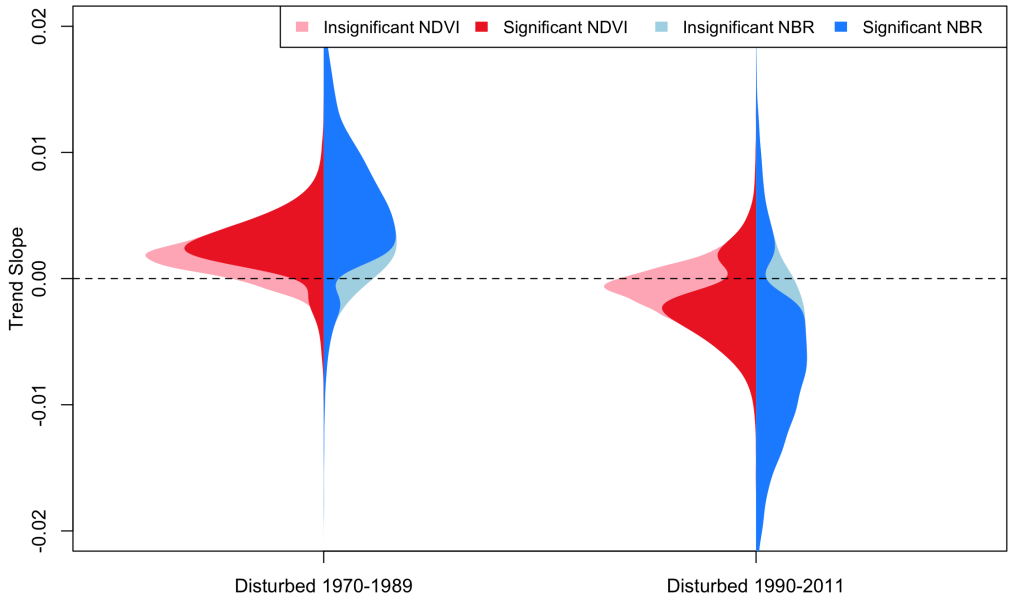

Figure 4.3: Distributions of NDVI and NBR trends for two samples of 5,000 panels for Landsat time series that were disturbed between 1970-1989 (first column) or between 1990-2011 (second column). Estimated trends and significances are based on panel linear models and significant trends were required to have p-values less than 0.05 and slopes with absolute values greater than 0.001 VI units/year.

Figure 4.4 shows how Landsat NDVI and NBR values change after a fire disturbance for a random sample of disturbed panels. In general, NDVI and NBR values in disturbed panels increased for the first five years following a fire event, after which the median values plateaued. NBR values had a larger range than NDVI during the initial five years after fire. After twenty years, values for each index were closer to those of open forest than dense forest.

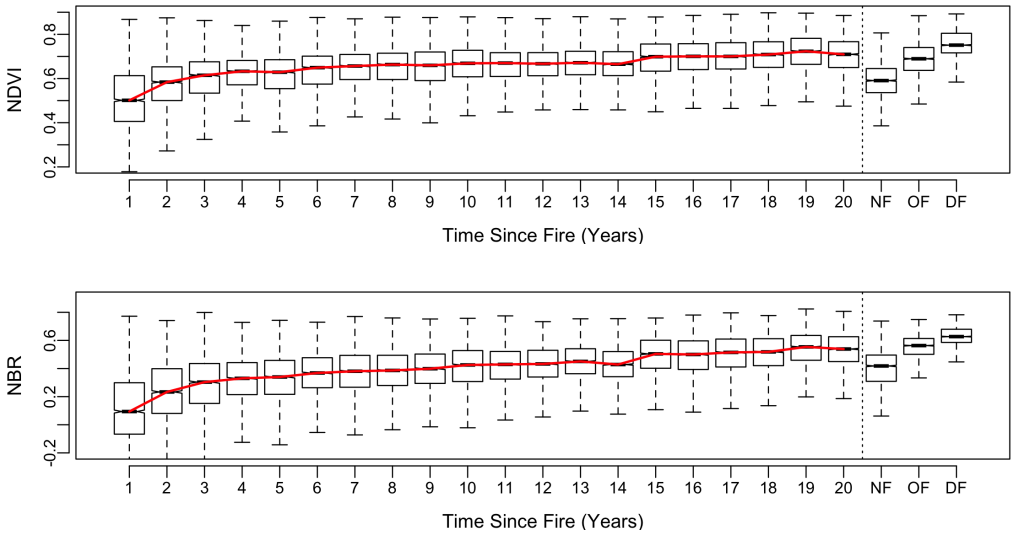

Figure 4.4: Boxplots of NDVI (top panel) and NBR (bottom panel) values for the first twenty years after a fire event. Each box represents a random sample of 3,000 panels that had been burned once according to the Canadian LFDB. The red line plots the time series for the median value of each box. The three boxplots on the far right of each panel are from undisturbed panels from non-forest (NF) vegetation, open forest (OF), and dense forest (DF) land cover types, respectively.

4.3.2 Variance in Landsat VI Trends According to Land Cover

In the second analysis, we sampled from a set of undisturbed panels across all the study sites, defined as panels containing less than 10% disturbed Landsat pixels. Figure 4.5 shows how the trends in NDVI and NBR varied according to land cover. The three undisturbed land cover types used in this analysis made up 55% of all land panels, with 9% non-forest, 15% open forest, and 31% dense forest. Non-forest vegetation such as steppe grasslands, agriculture, herbaceous bogs, and treeless tundra generally showed statistically significant positive VI trends (71% for NDVI and

72% for NBR). The open forest category included a higher proportion of significant positive VI trends relative to significant negative trends (42% for NDVI and 41% for NBR were significant and positive; 10% for NDVI and 16% for NBR were significant and negative). The dense forest category had a median slope close to zero for both indices, with 21% of panels for NDVI and 24% for NBR showing significant and positive trends, and 12% for NDVI and 27% for NBR showing significant and negative trends.

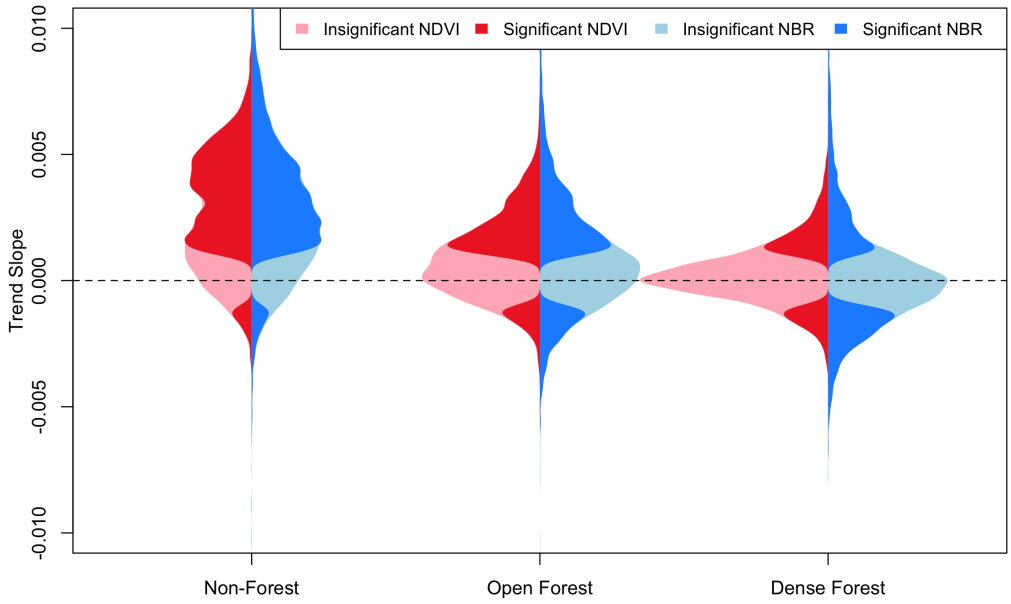

Figure 4.5: Distributions of NDVI and NBR trends for three samples of 5,000 undisturbed panels belonging to non-forest, open forest, and dense forest categories. Trends and significances are based on panel linear models and significant trends were required to have p-values less than 0.05 and slopes with absolute values greater than 0.001 VI units/year.

4.3.3 Landsat VI Trends in Undisturbed Forests Across a Climate Gradient

Figures 4.7 and 4.6 show how the trends in NDVI and NBR for undisturbed dense forest panels varied according to climatically available water during the growing season. The three climate categories were chosen according to quantiles in mean CMI across the study area, where these quantiles correspond to CMI values less than -127 mm for dry, between -127 and 47 mm for moderate, and greater than 47 mm for wet. Figure 4.6 shows how these CMI categories vary spatially across Canada relative to the scene-wide medians of NDVI and NBR trends for undisturbed dense forest panels. The average proportion of undisturbed dense forest panels within a site was 29% with a range of 3% to 74%. The 20 sites in the moderate region had the highest average proportion of undisturbed dense forest panels (37%) relative to the 15 western sites (23%) and 11 eastern sites (24%). The dry CMI regions mostly correspond to regions in central Canada east of the Canadian Rockies but west of the Hudson Bay, including most of the Northwest Territories, Alberta, Saskatchewan, and southern Manitoba. The moderate regions correspond to regions on the eastern edge of the Canadian Rockies and along the western and southern shore of the Hudson Bay, including northern Manitoba and most of Ontario. The wet regions include small portions of the Canadian Rockies and Ontario, and then a large portion of eastern Canada, including Quebec, Labrador, and Newfoundland.

The statistically significant VI trends in the dry regions were generally negative (22% for NDVI and 42% for NBR; Figure 4.7). The moderate CMI regions had a median slope close to zero for both indices but a higher proportion of significant positive trends relative to significant negative trends (21% for NDVI and 27% for NBR were significant and positive; 6% for NDVI and 19% for NBR were significant

and negative), and the significant VI trends in the wet region were mostly positive (46% for NDVI and 44% for NBR). In general, there are a higher proportion of significant trends for NBR than for NDVI across all categories and for all three trend analyses described in this section (e.g., Figure 4.2).

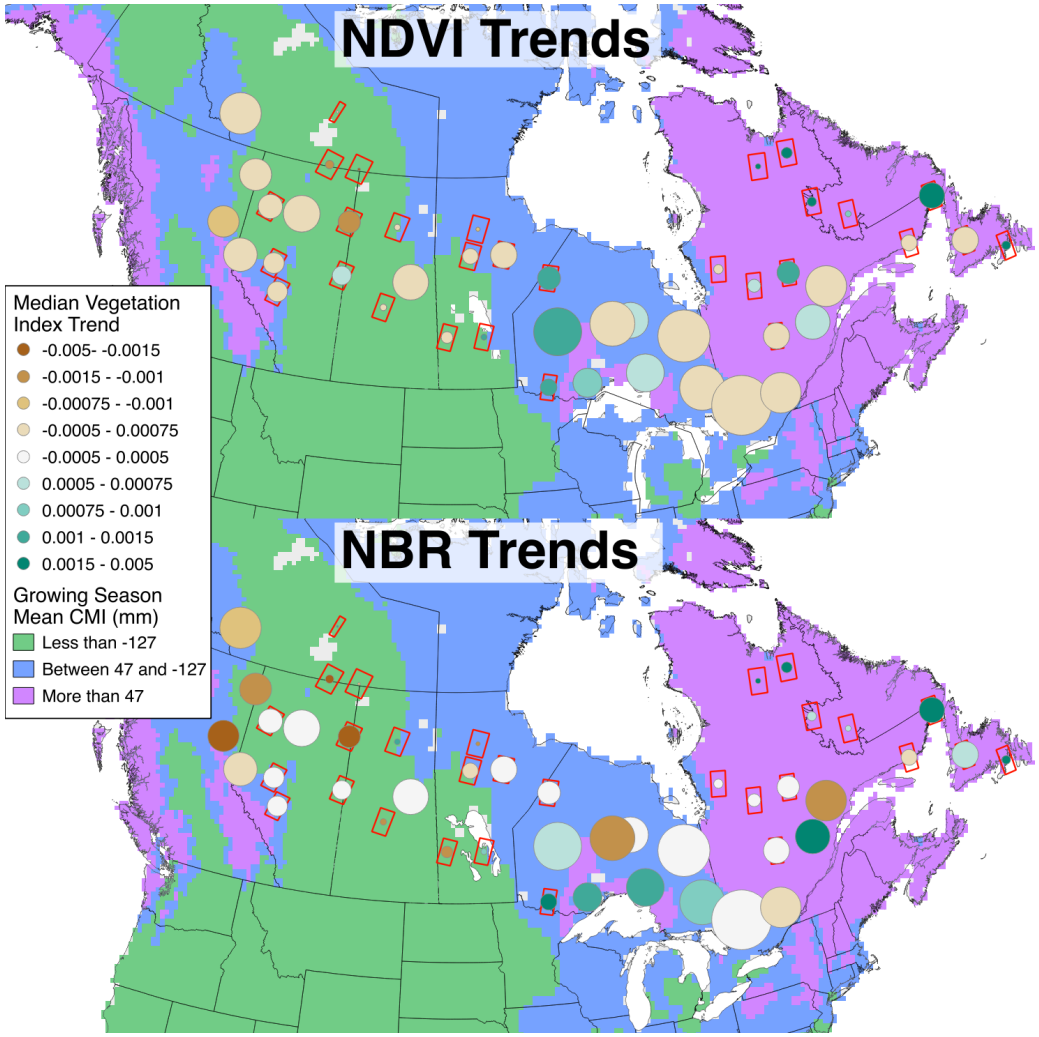

Figure 4.6: A map showing the scene-wide median trends in NDVI (top panel) and NBR (bottom panel) for undisturbed dense forest panels. The size of each circle is shown relative to the proportion of undisturbed dense forest panels in that site and the color of each circle describes the magnitude and sign of that median slope value. The background colors represent the three climate categories used in the analyses corresponding to dry (green), moderate (blue), and wet (purple) climate regimes.

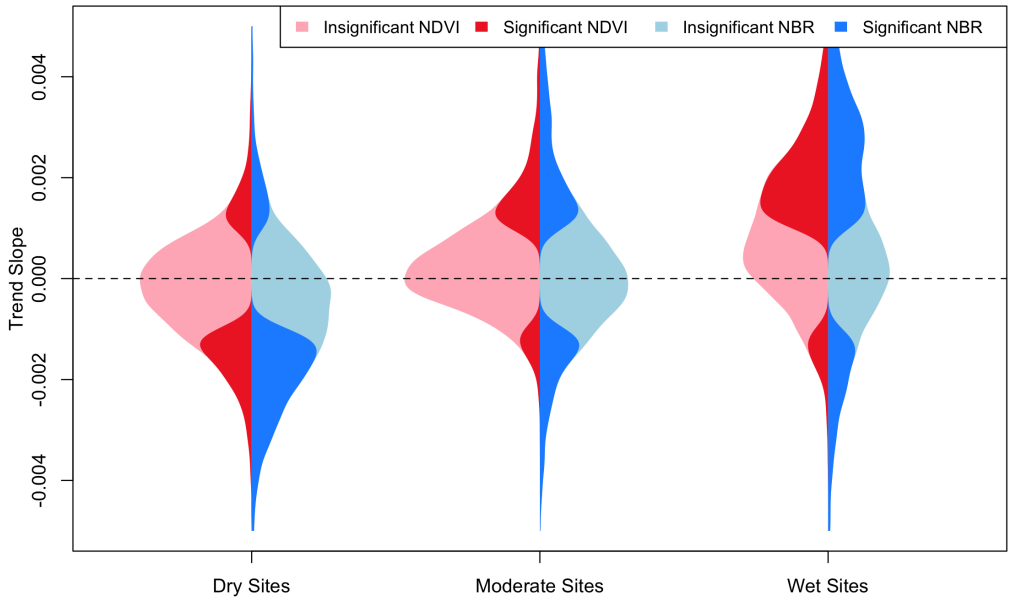

Figure 4.7: Distributions of NDVI and NBR trends for three samples of 5,000 undisturbed dense forest panels belonging to dry, moderate, and wet climate regimes. Trends and significances are based on panel linear models and significant trends were required to have a p-values less than 0.05 and slopes with absolute values greater than 0.001 VI units/year.

4.4 Discussion

Relative to the NDVI trends detected from the AVHRR time series (e.g., Beck and Goetz, 2011), our analysis using Landsat data suggest the total area of decreasing or browning trends in the boreal forests of Canada is much smaller than previously reported (Figure 4.6). There are several possibilities for this discrepancy. The first is that disturbances other than fire could be causing many of the negative trends. The second is that data quality issues unique to the GIMMS 3G data set introduces

negative trends because of uneven cloud screening, uncertain geolocation, and the combination of data from multiple AVHRR sensors. Relative to these coarse AVHRR records, Landsat data have higher spatial and radiometric resolution and we used more advanced cloud screening and disturbance detection algorithms. Since most of these discrepancies occur in the wetter eastern portion of the study area where forest disturbances are less common, it seems likely that at least some of the previously reported negative AVHRR trends were over-estimated because of issues with AVHRR data quality. In the next few sections we summarize the major findings of this work and describe sources of uncertainty in the Landsat-based trend analyses.

4.4.1 Disturbance Timing Affects Trends from Landsat Data

Disturbance, especially fire, is a major factor affecting carbon dynamics in the boreal forest zone of North America, impacting millions of hectares in Canada alone each year (Stocks et al., 2002). Our analysis showed that the timing of disturbance events relative to the first year in the remote sensing time series had a large impact on the direction and magnitude of the observed trends in vegetation indices. Specifically, disturbances that occurred near the beginning of the time series were associated with positive trends but disturbances that occurred in the middle or end of the time series led to much higher proportions of negative trends (Figure 4.3). The source of these patterns is that disturbance events reduce VI values in the short term, followed by regrowth of shrubs to trees that takes over 20 years to complete (Bond-Lamberty et al., 2002; Serbin et al., 2009; Figure 4.4).

Since forest disturbances have a large impact on VI trends (Figure 4.3), accurate detection of disturbances was important to ensuring the integrity of time series extracted over undisturbed land cover types. The Canadian LFDB identifies most

fire disturbances and the new time series method (CCDC; Zhu and Woodcock, 2014) used in this work was able to detect additional disturbances that were not captured in the LFDB. More importantly, fire disturbances that occurred before the Landsat era are often missed by the LFDB and are altogether missed by CCDC. Hence, regrowth from these disturbances can be misinterpreted as gradual changes in VIs (Figure 4.4) and probably added substantial noise to the analyses of "undisturbed" land cover types.

4.4.2 Land Cover and Climate Explain Spatial Variability in Landsat Trends

Analysis of vegetation index trends across land cover types (Figure 4.5) indicates that tree, shrub, and herbaceous vegetation are responding differently to recent climate warming. Positive trends in non-forest vegetation indicate that they are responding positively to the increasing temperatures and longer growing seasons. This is consistent with observations of increased shrub productivity in tundra ecosystems (Hinzman et al., 2005; McManus et al., 2012; Myers-Smith et al., 2011) and agricultural expansion along the heavily managed southern edge of the boreal forests (Neigh et al., 2008). Open forests also showed mostly positive trends, which may be caused by increases in growth and productivity in the understory of these heterogeneous landscapes. In contrast, dense forests were less likely to show significant trends than non-forest or open forest classes, with more positive trends observed in the wetter region of eastern Canada and more negative trends observed in the drier central and western regions (Figures 4.6 and 4.7).

While generally consistent with observations of changes in the rates of tree growth in forest inventory plots (Ma et al., 2012), this study examines changes over a much

larger area (∼50 million hectares) of the boreal forest zone in Canada. One major caveat to these findings is that because the EOSD land cover map used in this study is from Landsat imagery acquired *circa* 2000 (Wulder et al., 2008a), classification errors, along with regrowth processes from undetected disturbances prior to the Landsat era, add uncertainty to results from trend analyses that is difficult to quantify. Further, the impact of climate changes on the observed VI trends in this work is still incompletely assessed. Although drier sites contain more forests with decreasing VI trends than those that are less moisture limited (Figure 4.6), the impacts of inter-annual variability in precipitation, drought stress from higher growing season temperatures, and decreases in winter snow-pack depth is not addressed in this paper (Kim et al., 2012; Barichivich et al., 2014; Parida and Buermann, 2014). However, the connection between water availability and both VI trends and increased forest mortality in these regions has been documented by other work (Hogg et al., 2008; Peng et al., 2011; Buermann et al., 2013), and the results presented here provide new evidence to support those findings.

4.5 Conclusions

Our results show that the response of Canadian boreal forests to climate warming is more nuanced than had been suggested by previous studies using long-term AVHRR records. In dry central regions of Canada, declines in vegetation indices such as the NDVI indicate drought stress and reduced tree growth. Evaporative demand in these regions outpaces precipitation inputs during the growing season (Section 4.3.3) and the fire regime has been intensified by the longer, drier summers (Turetsky et al., 2010). In eastern regions of Canada, positive trends in vegetation indices were detected for forests and treeless tundra. These trends are consistent with increased

tree and shrub growth in response to longer growing seasons without the water limitations present in the western boreal forests of Canada.

With increasing drought stress predicted into the future (Dai, 2012), results from this work suggest that the drier central region of Canada may experience a transition from boreal forests to treeless steppe (Scheffer et al., 2012) and that the wetter eastern region may experience overall declines in forest health, including higher fire frequency (Flannigan et al., 2005; Kasischke and Turetsky, 2006). These changes have the potential to reduce the boreal forest carbon sink and could cause the region to become a net carbon source to the atmosphere sooner than has been predicted by climate models (Kasischke et al., 1995; Sitch et al., 2007).

More generally, results from this work demonstrate that Landsat time series represent an important record for assessing climate change impacts in boreal forest ecosystems. Time series from other sensors have been used for this purpose, most notably AVHRR and MODIS, but these data are limited by either poor radiometric and spatial resolutions or by short time series, respectively. In contrast, Landsat data are able to resolve subtle changes in boreal forests that may indicate gradual shifts in photosynthetic activity over time. Although the NDVI has been commonly used to assess forest productivity trends (e.g., Guay et al., 2014), here we argue that the NBR index is more sensitive to disturbance (Figure 4.4) and may provide a better proxy for productivity changes in undisturbed forests (Figure 4.7).

The major disadvantages to using Landsat data to study forest change processes are (1) the large computing resources needed to process and store the data relative to AVHRR or MODIS and (2) the uneven temporal sampling of Landsat data at higher latitudes. Recent improvements in computing have made the former concern less limiting and by using a strategy that combines data across adjacent WRS2 paths

it is nearly possible to achieve wall-to-wall mapping of the North American boreal zone with between 500 and 1400 total images available per overlap area. Future directions for this research include an expansion of this approach to a larger region of the Northern Hemisphere and a deeper exploration of the link between climate change and the observed VI trends from Landsat data.

Chapter 5

Concluding Remarks

Northern high latitudes have experienced substantial warming over the past several decades (Stocker et al., 2013). Since these regions contain large stocks of carbon in their soils and biomass (Bonan, 2008), there is concern that recent warming will lead to large positive feedbacks between the biosphere and the atmosphere, leading to even more changes in climate (Eugster et al., 2000; Soja et al., 2007; Euskirchen et al., 2009; Schaefer et al., 2011). Because forested ecosystems are major regulators of the climate system, changes to forest cover and productivity have important implications to future human well-being and food security.

Results from the research presented in this dissertation provide improved understanding regarding spatial and temporal patterns of forest cover and productivity changes in Northern Hemisphere temperate and boreal regions using remote sensing data from the Landsat and MODIS sensors. By developing new methods for detecting disturbance and trends using dense sets of remote sensing observations, I demonstrate that remote sensing provides valuable information for understanding climate change impacts on forested ecosystems, but also that there are many challenges to making such inferences from remote sensing data. These challenges include trade-offs between spatial and temporal resolutions, inconsistent atmospheric correction and cloud screening, a relatively short available time series for performing statistical

analyses, and difficulties in distinguishing subtle changes in inter- and intra-sensor calibration and sun-sensor geometry from real trends in vegetation productivity. Despite these challenges, advances in computing and opening of the Landsat archive to the public (Wulder et al., 2008b) have enabled the development of new techniques for time series analyses of multi-resolution remote sensing data sets that have substantial potential to provide high quality information about forest change. Here I summarize the major findings and future directions of my research, which I hope will influence the way dense time series of remote sensing data are used to study important questions about the effects of climate change on the biosphere.

In the first chapter, I showed that MODIS can be used to monitor forest change over large areas, but that detection of disturbance processes using coarse spatial resolution MODIS time series has several limitations relative to using Landsat data for this purpose. These limitations include complications introduced by spatially co-occurring disturbance and regrowth processes and gridding artifacts inherent in MODIS data. One of the strengths of this study is the focus on a region (the Pacific Northwest of the conterminous United States) that contains a complex mosaic of forest management strategies, disturbance regimes, and tree species compositions. Since the MODTrendr algorithm worked well in such a difficult landscape, detecting nearly 80% of disturbance events occupying more than one-third of a MODIS pixel, there is potential for using this algorithm to detect disturbance in much larger regions or even at the global scale. The major benefits to using the MODTrendr algorithm relative to the Landsat-based version (LandTrendr; Kennedy et al., 2010) are that there are very few pre-processing steps, it can be adapted to many different vegetation indices, and it is computationally easy to process very large regions.

In the second chapter, I showed that several factors unrelated to surface processes

can affect detection of long-term trends in vegetation indices derived from Landsat time series of surface reflectance. Specifically, spatial and temporal variation in vegetation indices from Landsat data can be influenced by inter- and intra-sensor calibration and within-scene variation of sensor view geometry. In addition, Landsat data require careful pre-processing to remove the effects of clouds and other atmospheric effects as well as accurate detection of disturbance. An important finding from this study was that the strategy used to combine Landsat data across adjacent WRS2 paths is an effective way to increase the density of observations in many high latitude regions where acquisitions are limited. A second important finding is that subtle differences in red band reflectances between Landsat 5 TM and Landsat 7 ETM+ data introduce bias in VI time series when data from the two sensors are combined into a single time series.

In the third chapter, I showed how spatial patterns in land cover and disturbance explain most of the variability in observed VI trends in the boreal forests of Canada. Residual variability in the magnitude and direction of VI trends for densely forested regions can be attributed to spatial patterns in climatically available water during the growing season, with the drier western and central regions of interior Canada showing declining VI trends and the wetter eastern regions of Canada showing mostly increasing VI trends. These findings indicate that a shift towards warmer and drier growing season conditions may have large negative effects on the health and productivity of boreal forest ecosystems in North America.

5.1 Future Research

The first chapter of this dissertation has already been published (Sulla-Menashe et al., 2014) but there are many potential applications of the MODTrendr algo-

rithm. For example, an application of this algorithm to an entirely different problem, post-classification change detection in Inner Mongolia, has already been published (Yin et al., 2014), and the algorithm has also been tested over a large area of Northern Eurasian boreal forests as part of the Northern Eurasia Land Dynamics Analysis project led by Olga Krankina at Oregon State University. The results of this effort have not yet been published, but are very encouraging (`http://www.fsl.orst.edu/nelda/disturbance/index.html`). In yet another application, a Ph.D. student Yan Li at Peking University in China has applied MODTrendr to specific regions of China with the purpose of assessing their large-scale afforestation programs. Thus, the MODTrendr algorithm provides the means to quickly develop global forest disturbance maps for the period from 2000 to 2015 using MODIS data. The analysis of longer time series relative to that of the original study (2000-2011) will support more accurate predictions of forest changes, but the accuracy of such a product will likely be constrained because small disturbances are difficult to detect from MODIS and the signature of change is affected by noise from co-occurring regrowth and disturbance processes. Further, MODTrendr has only been tested on a limited number of forested ecozones and its internal parameters may need to be adjusted on a biome- or continent-level. The most useful aspect of such large-scale mapping efforts would be to identify hot-spots of recent forest change that could be then further investigated using finer resolution data from Landsat or the new Sentinel program.

The results from the second chapter of this research have already been communicated to the Landsat Science Team (C. Woodcock, personal communication) and are currently in review in the journal *Remote Sensing of Environment* (Sulla-Menashe et al., in review). Most notably, results from this work identify a previously unknown

issue of small, but significant, inter-sensor differences in red band reflectance between the Landsat 5 TM and Landsat 7 ETM+ data. While data from these two sensors are extensively cross-calibrated to remove differences, the bandwidths are slightly different and most of the calibration targets tend to be bright desert targets. If the Landsat calibration targets are expanded to include dark targets, the ETM+ data could be reprocessed by the USGS to correct this effect. If done properly, this would ensure that the TM and ETM+ time series could be combined seamlessly, increasing the available data in the 2000s as well as extending the time series past 2011, which is when Landsat 5 was decommissioned. With new automated methods for atmospheric correction, cloud screening, disturbance detection, and temporal compositing, the time series derived from Landsat data are the best source of information for understanding the impacts of climate change on the biosphere. Hence, accurate cross-calibration of Landsat 5 and Landsat 7 data is essential.

The results from the third chapter are still being prepared for publication but have potential to clarify ongoing questions regarding observed greening and browning of boreal forests in Canada based on coarse resolution AVHRR NDVI data sets (Alcaraz-Segura et al., 2010). The 28-year Landsat 5 TM time series that were carefully compiled for the 46 sites in this work provide a much more nuanced look at the influence of recent climate warming on forest productivity. While the sites we examined do not completely cover the boreal forest zone of Canada, newly developed pre-processing tools should be able to support such an extension in the future. In the meanwhile, analysis of climate factors that have influenced observed VI trends in boreal forests will be completed over the summer months of 2015. Detection of divergent responses of boreal forest productivity to climate warming in Canada is an important result, one that links the impacts of recent climate change to those

of future projections and identifies a potential feedback to the global climate system. That said, the mechanisms behind observed boreal forest browning trends are still poorly understood, and properly characterization of these trends requires more research. Further, additional analyses will be performed to compare the results documented here from Landsat data with previous results based on AVHRR and MODIS time series.

In conclusion, I intend to use the lessons learned from this dissertation to continue research that links climate warming to changes in forest cover and productivity using multi-resolution remote sensing. Specifically, I would like to work on addressing several research questions that are a natural extension from this volume of work: Are boreal forests in Northern Eurasia responding differently to recent climate warming than those of North America? Do trends in Landsat time series correspond to changes in above-ground biomass and tree growth rates in boreal regions? How can we use these remote sensing data sets to reduce uncertainties in global climate models by providing a more accurate history of forest and carbon dynamics for the last three decades?

Bibliography

Alcaraz-Segura, D., Chuvieco, E., Epstein, H. E., Kasischke, E. S., and Trishchenko, A. P. (2010). Debating the greening vs. browning of the North American boreal forest: differences between satellite datasets. *Global Change Biology*, 16(2):760–770.

Allen, C. D., Macalady, A. K., Chenchouni, H., Bachelet, D., McDowell, N., Vennetier, M., Kitzberger, T., Rigling, A., Breshears, D. D., Hogg, E. H. T., Gonzalez, P., Fensham, R., Zhang, Z., Castro, J., Demidova, N., Lim, J.-H., Allard, G., Running, S. W., Semerci, A., and Cobb, N. (2010). A global overview of drought and heat-induced tree mortality reveals emerging climate change risks for forests. *Forest Ecology and Management*, 259(4):660–684.

Amiro, B. D., Stocks, B. J., Alexander, M. E., Flannigan, M. D., and Wotton, B. M. (2001). Fire, climate change, carbon and fuel management in the Canadian boreal forest. *International Journal of Wildland Fire*, 10(4):405.

Anderegg, W. R., Berry, J. A., Smith, D. D., Sperry, J. S., Anderegg, L. D., and Field, C. B. (2012). The roles of hydraulic and carbon stress in a widespread climate-induced forest die-off. *Proceedings of the National Academy of Sciences of the United States of America*, 109(1):233–237.

Angert, A., Biraud, S., Bonfils, C., Henning, C. C., Buermann, W., Pinzon, J., Tucker, C. J., Fung, I., and Field, C. B. (2005). Drier Summers Cancel out the CO_2 Uptake Enhancement Induced by Warmer Springs. *Proceedings of the National Academy of Sciences of the United States of America*, 102(31):10823–10827.

Anisimov, O. (1996). Permafrost distribution in the Northern Hemisphere under scenarios of climatic change. *Global and Planetary Change*, 14:59–72.

Arvidson, T., Goward, S., Gasch, J., and Williams, D. (2006). Landsat-7 Long-Term Acquisition Plan. *Photogrammetric Engineering and Remote Sensing*, 72(10):1137–1146.

Baccini, A., Goetz, S. J., Walker, W. S., Laporte, N. T., Sun, M., Sulla-Menashe, D., Hackler, J., Beck, P. S. A., Dubayah, R., Friedl, M. A., Samanta, S., and Houghton, R. A. (2012). Estimated carbon dioxide emissions from tropical deforestation improved by carbon-density maps. *Nature Climate Change*, 2(1):1–4.

Balshi, M. S., McGuire, A. D., Zhuang, Q., Melillo, J., Kicklighter, D. W., Kasischke, E., Wirth, C., Flannigan, M., Harden, J., Clein, J. S., Burnside, T. J., McAllister, J., Kurz, W. A., Apps, M., and Shvidenko, A. (2007). The role of historical fire disturbance in the carbon dynamics of the pan-boreal region: A process-based analysis. *Journal of Geophysical Research*, 112(G2):G02029.

Baltagi, B. (2008). *Econometric analysis of panel data*, volume 1. John Wiley & Sons.

Barichivich, J., Briffa, K., Myneni, R., Schrier, G., Dorigo, W., Tucker, C., Osborn, T., and Melvin, T. (2014). Temperature and Snow-Mediated Moisture Controls of Summer Photosynthetic Activity in Northern Terrestrial Ecosystems between 1982 and 2011. *Remote Sensing*, 6(2):1390–1431.

Barnett, T. P., Adam, J. C., and Lettenmaier, D. P. (2005). Potential impacts of a warming climate on water availability in snow-dominated regions. *Nature*, 438(7066):303–309.

Beck, H. E., McVicar, T. R., van Dijk, A. I. J. M., Schellekens, J., de Jeu, R. A. M., and Bruijnzeel, L. A. (2011a). Global evaluation of four AVHRR-NDVI data sets: Intercomparison and assessment against Landsat imagery. *Remote Sensing of Environment*, 115(10):2547–2563.

Beck, P. S. A. and Goetz, S. J. (2011). Satellite observations of high northern latitude vegetation productivity changes between 1982 and 2008: ecological variability and regional differences. *Environmental Research Letters*, 6(4).

Beck, P. S. A., Goetz, S. J., Mack, M. M., Alexander, H. D., Jin, Y., Randerson, J. T., and Loranty, M. M. (2011b). The impacts and implications of an intensifying fire regime on Alaskan boreal forest composition and albedo. *Global Change Biology*, 17(9):2853–2866.

Bi, J., Xu, L., Samanta, A., Zhu, Z., and Myneni, R. (2013). Divergent Arctic-Boreal Vegetation Changes between North America and Eurasia over the Past 30 Years. *Remote Sensing*, 5(5):2093–2112.

Bonan, G. B. (2008). Forests and Climate Change: Forcings, Feedbacks, and the Climate Benefits of Forests. *Science*, 320(5882):1444–1449.

Bonan, G. B. and Shugart, H. H. (1989). Environmental factors and ecological processes in boreal forests. *Annual review of ecology and systematics*, 20:1–28.

Bond-Lamberty, B., Peckham, S. D., Ahl, D. E., and Gower, S. T. (2007). Fire as the dominant driver of central Canadian boreal forest carbon balance. *Nature*, 450(7166):89–92.

Bond-Lamberty, B. B., Wang, C. C., Gower, S. T. S., and Norman, J. J. (2002). Leaf area dynamics of a boreal black spruce fire chronosequence. *Tree Physiology*, 22(14):993–1001.

Boschetti, L., Flasse, S. P., and Brivio, P. A. (2004). Analysis of the conflict between omission and commission in low spatial resolution dichotomic thematic products: The Pareto Boundary. *Remote Sensing of Environment*, 91(3-4):280–292.

Brandt, J. P. (2009). The extent of the North American boreal zone. *Environmental Reviews*, 17:101–161.

Bronaugh, D. and Werner, A. (2013). *zyp: Zhang + Yue-Pilon trends package*. R package version 0.9-3.

Brovkin, V., Ganopolski, A., and Svirezhev, Y. (1997). A continuous climate-vegetation classification for use in climate-biosphere studies. *Ecological Modelling*, 101(2):251–261.

Buermann, W., Bikash, P. R., Jung, M., Burn, D. H., and Reichstein, M. (2013). Earlier springs decrease peak summer productivity in North American boreal forests. *Environmental Research Letters*, 8(2):024027.

Bunn, A. G. and Goetz, S. J. (2006). Trends in Satellite-Observed Circumpolar Photosynthetic Activity from 1982 to 2003: The Influence of Seasonality, Cover Type, and Vegetation Density. *Earth Interactions*, 10(12):1–19.

Chander, G., Markham, B. L., and Helder, D. L. (2009). Summary of current radiometric calibration coefficients for Landsat MSS, TM, ETM+, and EO-1 ALI sensors. *Remote Sensing of Environment*, 113(5):893–903.

Cihlar, J., Manak, D., and D'Iorio, M. (1994). Evaluation of Compositing Algorithms for AVHRR Data Over Land. *IEEE Transactions on Geoscience and Remote Sensing*, 32(2):427–437.

Cohen, W. B. and Spies, T. A. (1992). Estimating structural attributes of Douglas-fir/western hemlock forest stands from Landsat and SPOT imagery. *Remote Sensing of Environment*, 41(1):1–17.

Cohen, W. B., Yang, Z., and Kennedy, R. (2010). Detecting trends in forest disturbance and recovery using yearly Landsat time series: 2. TimeSync — Tools for calibration and validation. *Remote Sensing of Environment*, 114(12):2911–2924.

Croissant, Y. and Millo, G. (2008). Panel data econometrics in R: The plm package. *Journal of Statistical Software*, 27(2).

Czerwinski, C. J., King, D. J., and Mitchell, S. W. (2014). Mapping forest growth and decline in a temperate mixed forest using temporal trend analysis of Landsat imagery, 1987-2010. *Remote Sensing of Environment*, 141:188–200.

Dai, A. (2012). Increasing drought under global warming in observations and models. *Nature Climate Change*, 3(1):52–58.

de Groot, W. J., Flannigan, M. D., and Cantin, A. S. (2013). Climate change impacts on future boreal fire regimes. *Forest Ecology and Management*, 294:35–44.

DeBeurs, K. and Townsend, P. (2008). Estimating the effect of gypsy moth defoliation using MODIS. *Remote Sensing of Environment*, 112(10):3983–3990.

DeFries, R. S., Foley, J. A., and Asner, G. P. (2004). Land-use choices: balancing human needs and ecosystem function. *Frontiers in Ecology and the Environment*, 2(5):249–257.

Efron, B. and Tibshirani, R. (1986). Bootstrap methods for standard errors, confidence intervals, and other measures of statistical accuracy. *Statistical science*, 1(1):54–75.

Ellis, E. C. and Ramankutty, N. (2008). Putting people in the map: anthropogenic biomes of the world. *Frontiers in Ecology and the Environment*, 6(8):439–447.

Eugster, W., Rouse, W. R., Pielke, Sr, R. A., Mcfadden, J. P., Baldocchi, D. D., Kittel, T. G., Chapin, F. S., Liston, G. E., Vidale, P. L., and Vaganov, E. (2000). Land–atmosphere energy exchange in Arctic tundra and boreal forest: available data and feedbacks to climate. *Global Change Biology*, 6(S1):84–115.

Euskirchen, E. S. E., McGuire, A. D. A., Chapin, F. S. F., Yi, S. S., and Thompson, C. C. C. (2009). Changes in vegetation in northern Alaska under scenarios of climate change, 2003-2100: implications for climate feedbacks. *Ecological Applications*, 19(4):1022–1043.

Fensham, R. J., Fairfax, R. J., and Ward, A. D. (2009). Drought-induced tree death in savanna. *Global Change Biology*, 15(2):380–387.

Flannigan, M. D., Logan, K. A., Amiro, B. D., Skinner, W. R., and Stocks, B. J. (2005). Future Area Burned in Canada. *Climatic Change*, 72(1-2):1–16.

Fontana, F. M. A., Coops, N. C., Khlopenkov, K. V., Trishchenko, A. P., Riffler, M., and Wulder, M. A. (2012). Generation of a novel 1km NDVI data set over Canada, the northern United States, and Greenland based on historical AVHRR data. *Remote Sensing of Environment*, 121:171–185.

Fraser, R. H., Olthof, I., Carrière, M., Deschamps, A., and Pouliot, D. (2011). Detecting long-term changes to vegetation in northern Canada using the Landsat satellite image archive. *Environmental Research Letters*, 6(4):045502.

French, N. H. F., Kasischke, E. S., Hall, R. J., Murphy, K. A., Verbyla, D. L., Hoy, E. E., and Allen, J. L. (2008). Using Landsat data to assess fire and burn severity in the North American boreal forest region: an overview and summary of results. *International Journal of Wildland Fire*, 17(4):443.

Friedlingstein, P., Cox, P., Betts, R., Bopp, L., Von Bloh, W., Brovkin, V., Cadule, P., Doney, S., Eby, M., Fung, I., Bala, G., John, J., Jones, C., Joos, F., Kato, T., Kawamiya, M., Knorr, W., Lindsay, K., Matthews, H. D., Raddatz, T., Rayner, P., Reick, C., Roeckner, E., Schnitzler, K.-G., Schnur, R., Strassmann, K., Weaver, A. J., Yoshikawa, C., and Zeng, N. (2006). Climate-carbon cycle feedback analysis: Results from the C4MIP model intercomparison. *Journal of Climate*, 19(14):3337–3353.

Frolking, S., Palace, M. W., Clark, D. B., Chambers, J. Q., Shugart, H. H., and Hurtt, G. C. (2009). Forest disturbance and recovery: A general review in the context of spaceborne remote sensing of impacts on aboveground biomass and canopy structure. *Journal of Geophysical Research*, 114:G00E02.

Gao, F., Masek, J., Schwaller, M., and Hall, F. (2006). On the blending of the Landsat and MODIS surface reflectance: predicting daily Landsat surface reflectance. *IEEE Transactions on Geoscience and Remote Sensing*, 44(8):2207–2218.

García, M. J. L. and Caselles, V. (1991). Mapping burns and natural reforestation using thematic Mapper data. *Geocarto International*, 6(1):31–37.

Gibbs, H. K., Brown, S., Niles, J. O., and Foley, J. A. (2007). Monitoring and estimating tropical forest carbon stocks: making REDD a reality. *Environmental Research Letters*, 2(4):045023.

Goetz, S. J., Bunn, A. G., Fiske, G. J., and Houghton, R. A. (2005). Satellite-observed photosynthetic trends across boreal North America associated with climate and fire disturbance. *Proceedings of the National Academy of Sciences of the United States of America*, 102(38):13521–13525.

Gómez, C., White, J. C., and Wulder, M. A. (2011). Characterizing the state and processes of change in a dynamic forest environment using hierarchical spatio-temporal segmentation. *Remote Sensing of Environment*, 115(7):1665–1679.

Guay, K. C., Beck, P. S. A., Berner, L. T., Goetz, S. J., Baccini, A., and Buermann, W. (2014). Vegetation productivity patterns at high northern latitudes: a multi-sensor satellite data assessment. *Global Change Biology*, 20(10):2147–2158.

Hansen, J., Ruedy, R., Sato, M., and Lo, K. (2010a). Global surface temperature change. *Reviews of Geophysics*, 48(4):RG4004.

Hansen, J., Sato, M., Ruedy, R., Lo, K., Lea, D. W., and Medina-Elizade, M. (2006). Global temperature change. *Proceedings of the National Academy of Sciences of the United States of America*, 103(39):14288–14293.

Hansen, M. C., Defries, R. S., Townshend, J., Carroll, M., Dimiceli, C., and Sohlberg, R. A. (2003). Global percent tree cover at a spatial resolution of 500 meters: First results of the MODIS vegetation continuous fields algorithm. *Earth Interactions*, 7(10):1–15.

Hansen, M. C., Potapov, P. V., Moore, R., Hancher, M., Turubanova, S. A., Tyukavina, A., Thau, D., Stehman, S. V., Goetz, S. J., Loveland, T. R., Kommareddy, A., Egorov, A., Chini, L., Justice, C. O., and Townshend, J. R. G. (2013). High-Resolution Global Maps of 21st-Century Forest Cover Change. *Science*, 342(6160):850–853.

Hansen, M. C., Stehman, S. V., and Potapov, P. V. (2010b). From the Cover: Quantification of global gross forest cover loss. *Proceedings of the National Academy of Sciences of the United States of America*, 107(19):8650–8655.

Hardisky, M. A., Klemas, V., and Smart, R. M. (1983). The influence of soil salinity, growth form, and leaf moisture on the spectral radiance of *Spartinia alterniflora* canopies. *Photogrammetric Engineering and Remote Sensing*, 49:77–83.

Haynes, R. W., Bormann, B. T., Lee, D. C., and Martin, J. R. (2006). Northwest Forest Plan, the First 10 Years (1994-2003). Technical Report PNW-GTR-651, Portland, OR.

Healey, S., Cohen, W. B., Zhiqiang, Y., and Krankina, O. N. (2005). Comparison of Tasseled Cap-based Landsat data structures for use in forest disturbance detection. *Remote Sensing of Environment*, 97(3):301–310.

Hicke, J. A., Allen, C. D., Desai, A. R., Dietze, M. C., Hall, R. J., Ted Hogg, E. H., Kashian, D. M., Moore, D., Raffa, K. F., Sturrock, R. N., and Vogelmann, J. (2011). Effects of biotic disturbances on forest carbon cycling in the United States and Canada. *Global Change Biology*, 18(1):7–34.

Hicke, J. A., Logan, J. A., Powell, J., and Ojima, D. S. (2006). Changing temperatures influence suitability for modeled mountain pine beetle (*Dendroctonus ponderosae*) outbreaks in the western United States. *Journal of Geophysical Research*, 111:G02019.

Hilker, T., Wulder, M. A., Coops, N. C., Linke, J., McDermid, G., Masek, J. G., Gao, F., and White, J. C. (2009a). A new data fusion model for high spatial- and temporal-resolution mapping of forest disturbance based on Landsat and MODIS. *Remote Sensing of Environment*, 113(8):1613–1627.

Hilker, T., Wulder, M. A., Coops, N. C., Seitz, N., White, J. C., Gao, F., Masek, J. G., and Stenhouse, G. (2009b). Generation of dense time series synthetic Landsat data through data blending with MODIS using a spatial and temporal adaptive reflectance fusion model. *Remote Sensing of Environment*, 113(9):1988–1999.

Hinzman, L. D., Bettez, N. D., Bolton, W. R., Chapin, F. S., Dyurgerov, M. B., Fastie, C. L., Griffith, B., Hollister, R. D., Hope, A., Huntington, H. P., Jensen, A. M., Jia, G. J., Jorgenson, T., Kane, D. L., Klein, D. R., Kofinas, G., Lynch, A. H., Lloyd, A. H., McGuire, A. D., Nelson, F. E., Oechel, W. C., Osterkamp, T. E., Racine, C. H., Romanovsky, V. E., Stone, R. S., Stow, D. A., Sturm, M., Tweedie, C. E., Vourlitis, G. L., Walker, M. D., Walker, D. A., Webber, P. J., Welker, J. M., Winker, K. S., and Yoshikawa, K. (2005). Evidence and Implications of Recent Climate Change in Northern Alaska and Other Arctic Regions. *Climatic Change*, 72(3):251–298.

Hogg, E. H. T., Brandt, J. P., and Michaelian, M. (2008). Impacts of a regional drought on the productivity, dieback, and biomass of western Canadian aspen forests. *Canadian Journal of Forest Research*, 38(6):1373–1384.

Holden, C. (2015). Yet another time series model (yatsm): v0.4.0.

Huang, C., Goward, S. N., Masek, J. G., Thomas, N., Zhu, Z., and Vogelmann, J. E. (2010). An automated approach for reconstructing recent forest disturbance history using dense Landsat time series stacks. *Remote Sensing of Environment*, 114(1):183–198.

Huang, C., Townshend, J. R., Liang, S., Kalluri, S. N., and DeFries, R. S. (2002). Impact of sensor's point spread function on land cover characterization: assessment and deconvolution. *Remote Sensing of Environment*, 80(2):203–212.

Huete, A., Didan, K., Miura, T., Rodriguez, E. P., Gao, X., and Ferreira, L. G. (2002). Overview of the radiometric and biophysical performance of the MODIS vegetation indices. *Remote Sensing of Environment*, 83(1):195–213.

Irons, J. R., Dwyer, J. L., and Barsi, J. A. (2012). The next Landsat satellite: The Landsat Data Continuity Mission. *Remote Sensing of Environment*, 122:11–21.

Jain, T. B. (2004). Tongue-tied. *Wildfire*, 13(4):22–26.

Jeganathan, C., Dash, J., and Atkinson, P. M. (2014). Remotely sensed trends in the phenology of northern high latitude terrestrial vegetation, controlling for land cover change and vegetation type. *Remote Sensing of Environment*, 143:154–170.

Ji, L., Wylie, B. K., Nossov, D. R., Peterson, B., Waldrop, M. P., McFarland, J. W., Rover, J., and Hollingsworth, T. N. (2012). Estimating aboveground biomass in interior Alaska with Landsat data and field measurements. *International Journal of Applied Earth Observations and Geoinformation*, 18:451–461.

Jin, S. and Sader, S. A. (2005). MODIS time-series imagery for forest disturbance detection and quantification of patch size effects. *Remote Sensing of Environment*, 99(4):462–470.

Jones, E., Oliphant, T., Peterson, P., et al. (2001). SciPy: Open source scientific tools for Python. [Online; accessed 2014-11-21].

Ju, J. and Roy, D. P. (2008). The availability of cloud-free Landsat ETM+ data over the conterminous United States and globally. *Remote Sensing of Environment*, 112(3):1196–1211.

Justice, C. O., Townshend, J., Vermote, E. F., Masuoka, E., Wolfe, R. E., Saleous, N., Roy, D. P., and Morisette, J. T. (2002). An overview of MODIS Land data processing and product status. *Remote Sensing of Environment*, 83(1):3–15.

Kasischke, E. S., Amiro, B. D., Barger, N. N., French, N. H. F., Goetz, S. J., Grosse, G., Harmon, M. E., Hicke, J. A., Liu, S., and Masek, J. G. (2013). Impacts of disturbance on the terrestrial carbon budget of North America. *Journal of Geophysical Research: Biogeosciences*, 118(1):303–316.

Kasischke, E. S., Christensen, Jr, N. L., and Stocks, B. J. (1995). Fire, global warming, and the carbon balance of boreal forests. *Ecological Applications*, 5(2):437–451.

Kasischke, E. S. and Turetsky, M. R. (2006). Recent changes in the fire regime across the North American boreal region—Spatial and temporal patterns of burning across Canada and Alaska. *Geophysical Research Letters*, 33(9):L09703.

Keeley, J. E. (2009). Fire intensity, fire severity and burn severity: a brief review and suggested usage. *International Journal of Wildland Fire*, 18(1):116.

Kennedy, R. E., Yang, Z., and Cohen, W. B. (2010). Detecting trends in forest disturbance and recovery using yearly Landsat time series: 1. LandTrendr — Temporal segmentation algorithms. *Remote Sensing of Environment*, 114(12):2897–2910.

Kennedy, R. E., Yang, Z., Cohen, W. B., Pfaff, E., Braaten, J., and Nelson, P. (2012). Spatial and temporal patterns of forest disturbance and regrowth within the area of the Northwest Forest Plan. *Remote Sensing of Environment*, 122(C):117–133.

Key, C. H. and Benson, N. C. (1999). Measuring and remote sensing of burn severity. In *Proceedings Joint Fire Science Conference and Workshop*, volume 2, page 284, Moscow, ID. University of Idaho and International Association of Wildland Fire.

Keyser, A. R., Kimball, J. S., Nemani, R. R., and Running, S. W. (2002). Simulating the effects of climate change on the carbon balance of North American highlatitude forests. *Global Change Biology*, 6(S1):185–195.

Kim, Y., Kimball, J. S., Zhang, K., and McDonald, K. C. (2012). Satellite detection of increasing Northern Hemisphere non-frozen seasons from 1979 to 2008: Implications for regional vegetation growth. *Remote Sensing of Environment*, 121:472–487.

Lefsky, M. A., Hudak, A. T., Cohen, W. B., and Acker, S. A. (2005). Patterns of covariance between forest stand and canopy structure in the Pacific Northwest. *Remote Sensing of Environment*, 95(4):517–531.

Lenton, T. M., Held, H., Kriegler, E., Hall, J. W., Lucht, W., Rahmstorf, S., and Schellnhuber, H. J. (2008). Tipping elements in the Earth's climate system. *Proceedings of the National Academy of Sciences of the United States of America*, 105(6):1786–1793.

Lepers, E., Lambin, E. F., Janetos, A. C., Defries, R., Achard, F., Ramankutty, N., and Scholes, R. J. (2005). A synthesis of information on rapid land-cover change for the period 1981–2000. *BioScience*, 55(2):115–124.

Li, X. and Strahler, A. H. (1986). Geometric-optical bidirectional reflectance modeling of a conifer forest canopy. *IEEE Transactions on Geoscience and Remote Sensing*, GE-24(6):906–919.

Lloyd, A. H. and Bunn, A. G. (2007). Responses of the circumpolar boreal forest to 20th century climate variability. *Environmental Research Letters*, 2(4):045013.

Loboda, T., O'Neal, K. J., and Csiszar, I. (2007). Regionally adaptable dNBR-based algorithm for burned area mapping from MODIS data. *Remote Sensing of Environment*, 109(4):429–442.

Loboda, T. V., Zhang, Z., O'Neal, K. J., Sun, G., Csiszar, I. A., Shugart, H. H., and Sherman, N. J. (2012). Reconstructing disturbance history using satellite-based assessment of the distribution of land cover in the Russian Far East. *Remote Sensing of Environment*, 118(C):241–248.

Lu, D., Mausel, P., Brondízio, E., and Moran, E. (2004). Change detection techniques. *International Journal of Remote Sensing*, 25(12):2365–2401.

Ma, Z., Peng, C., Zhu, Q., Chen, H., Yu, G., Li, W., Zhou, X., Wang, W., and Zhang, W. (2012). Regional drought-induced reduction in the biomass carbon sink of Canada's boreal forests. *Proceedings of the National Academy of Sciences of the United States of America*, 109(7):2423–2427.

Markham, B. L., Storey, J. C., Williams, D. L., and Irons, J. R. (2004). Landsat sensor performance: history and current status. *IEEE Transactions on Geoscience and Remote Sensing*, 42(12):2691–2694.

Masek, J. G., Honzak, M., Goward, S. N., Liu, P., and Pak, E. (2001). Landsat-7 ETM+ as an observatory for land cover: Initial radiometric and geometric comparisons with Landsat-5 Thematic Mapper. *Remote Sensing of Environment*, 78(1):118–130.

Masek, J. G., Huang, C., Wolfe, R., Cohen, W., Hall, F., Kutler, J., and Nelson, P. (2008). North American forest disturbance mapped from a decadal Landsat record. *Remote Sensing of Environment*, 112(6):2914–2926.

Masek, J. G., Vermote, E. F., Saleous, N. E., Wolfe, R., Hall, F. G., Huemmrich, K. F., Gao, F., Kutler, J., and Lim, T. K. (2006). A Landsat Surface Reflectance Dataset for North America, 1990-2000. *IEEE Geoscience and Remote Sensing Letters*, 3(1):68–72.

McManus, K. M., Morton, D. C., Masek, J. G., Wang, D., Sexton, J. O., Nagol, J. R., Ropars, P., and Boudreau, S. (2012). Satellite-based evidence for shrub and graminoid tundra expansion in northern Quebec from 1986 to 2010. *Global Change Biology*, 18(7):2313–2323.

Meigs, G. W., Kennedy, R. E., and Cohen, W. B. (2011). A Landsat time series approach to characterize bark beetle and defoliator impacts on tree mortality and surface fuels in conifer forests. *Remote Sensing of Environment*, 115(12):3707–3718.

Michaelian, M., Hogg, E. H., Hall, R. J., and Arsenault, E. (2011). Massive mortality of aspen following severe drought along the southern edge of the Canadian boreal forest. *Global Change Biology*, 17(6):2084–2094.

Michels, A., Laird, K. R., Wilson, S. E., Thomson, D., Leavitt, P. R., Oglesby, R. J., and Cumming, B. F. (2007). Multidecadal to millennial-scale shifts in drought conditions on the Canadian prairies over the past six millennia: implications for future drought assessment. *Global Change Biology*, 13(7):1295–1307.

Mildrexler, D. J., Zhao, M., and Running, S. W. (2009). Testing a MODIS Global Disturbance Index across North America. *Remote Sensing of Environment*, 113(10):2103–2117.

Myers-Smith, I. H., Forbes, B. C., Wilmking, M., Hallinger, M., Lantz, T., Blok, D., Tape, K. D., Macias-Fauria, M., Sass-Klaassen, U., Lévesque, E., Boudreau, S., Ropars, P., Hermanutz, L., Trant, A., Collier, L. S., Weijers, S., Rozema, J., Rayback, S. A., Schmidt, N. M., Schaepman-Strub, G., Wipf, S., Rixen, C., Ménard, C. B., Venn, S., Goetz, S., Andreu-Hayles, L., Elmendorf, S., Ravolainen, V., Welker, J., Grogan, P., Epstein, H. E., and Hik, D. S. (2011). Shrub expansion in tundra ecosystems: dynamics, impacts and research priorities. *Environmental Research Letters*, 6(4):045509.

Myneni, R. B., Keeling, C. D., Tucker, C. J., Asrar, G., and Nemani, R. R. (1997). Increased plant growth in the northern high latitudes from 1981 to 1991. *Nature*, 386(6):698–702.

Neigh, C., Tucker, C. J., and Townshend, J. R. G. (2008). North American vegetation dynamics observed with multi-resolution satellite data. *Remote Sensing of Environment*, 112(4):1749–1772.

Neigh, C., Williams, J. J., Diabate, M., and Bolton, D. (2012). A Multi-Decade Vegetation Productivity Decline in Northern Wisconsin and Minnesota Forests Driven by Increased Rates of Disturbance. Technical Report GSFC.JA.6437.2012.

Nemani, R. R., Keeling, C. D., Hashimoto, H., Jolly, W. M., Piper, S. C., Tucker, C. J., Myneni, R. B., and Running, S. W. (2003). Climate-driven increases in global terrestrial net primary production from 1982 to 1999. *Science*, 300(5625):1560–1563.

New, M., Lister, D., Hulme, M., and Makin, I. (2002). A high-resolution data set of surface climate over global land areas. *Climate research*, 21(1):1–25.

Ojima, D. S., Galvin, K. A., and Turner, B. L. (1994). The global impact of land-use change. *BioScience*, 44:300–304.

Olthof, I. and Latifovic, R. (2007). Short-term response of arctic vegetation NDVI to temperature anomalies. *International Journal of Remote Sensing*, 28(21):4823–4840.

Osterkamp, T. E., Viereck, L., Shur, Y., Jorgenson, M. T., Racine, C., Doyle, A., and Boone, R. D. (2000). Observations of thermokarst and its impact on boreal forests in Alaska, USA. *Arctic, antarctic, and alpine research*, 32(3):303–315.

Parida, B. R. and Buermann, W. (2014). Increasing Summer Drying in North American Ecosystems in Response to Longer Non-frozen Periods. *Geophysical Research Letters*, 41:1–8.

Peng, C., Ma, Z., Lei, X., Zhu, Q., Chen, H., Wang, W., Liu, S., Li, W., Fang, X., and Zhou, X. (2011). A drought-induced pervasive increase in tree mortality across Canada's boreal forests. *Nature Climate Change*, 1(12):467–471.

Piao, S., Ciais, P., Friedlingstein, P., Peylin, P., Reichstein, M., Luyssaert, S., Margolis, H., Fang, J., Barr, A., Chen, A., Grelle, A., Hollinger, D. Y., Laurila, T., Lindroth, A., Richardson, A. D., and Vesala, T. (2008). Net carbon dioxide losses of northern ecosystems in response to autumn warming. *Nature*, 451(7174):49–52.

Piao, S., Friedlingstein, P., Ciais, P., Peylin, P., Zhu, B., and Reichstein, M. (2009). Footprint of temperature changes in the temperate and boreal forest carbon balance. *Geophysical Research Letters*, 36(L07404):1–5.

Piao, S., Friedlingstein, P., Ciais, P., Viovy, N., and Demarty, J. (2007). Growing season extension and its impact on terrestrial carbon cycle in the Northern Hemisphere over the past 2 decades. *Global Biogeochemical Cycles*, 21:1–11.

Pinzon, J. and Tucker, C. (2014). A Non-Stationary 1981–2012 AVHRR NDVI3g Time Series. *Remote Sensing*, 6(8):6929–6960.

Pinzon, J. E., Brown, M. E., and Tucker, C. J. (2007). Global Inventory Modeling and Mapping Studies (GIMMS) Satellite Drift Corrected and NOAA-16 incorporated Normalized Difference Vegetation Index (NDVI), Monthly 1981–2006.

Potapov, P., Hansen, M. C., Stehman, S. V., Loveland, T. R., and Pittman, K. (2008). Combining MODIS and Landsat imagery to estimate and map boreal forest cover loss. *Remote Sensing of Environment*, 112(9):3708–3719.

Pouliot, D., Latifovic, R., and Olthof, I. (2009). Trends in vegetation NDVI from 1 km AVHRR data over Canada for the period 1985–2006. *International Journal of Remote Sensing*, 30(1):149–168.

Remmel, T. K., Csillag, F., Mitchell, S., and Wulder, M. A. (2005). Integration of forest inventory and satellite imagery: a Canadian status assessment and research issues. *Forest Ecology and Management*, 207(3):405–428.

Roberts, D. A., Dennison, P. E., Peterson, S., Sweeney, S., and Rechel, J. (2006). Evaluation of Airborne Visible/Infrared Imaging Spectrometer (AVIRIS) and Moderate Resolution Imaging Spectrometer (MODIS) measures of live fuel moisture and fuel condition in a shrubland ecosystem in southern California. *Journal of Geophysical Research*, 111.

Roy, D. P., Jin, Y., Lewis, P. E., and Justice, C. O. (2005). Prototyping a global algorithm for systematic fire-affected area mapping using MODIS time series data. *Remote Sensing of Environment*, 97(2):137–162.

Roy, D. P., Ju, J., Kline, K., Scaramuzza, P. L., Kovalskyy, V., Hansen, M., Loveland, T. R., Vermote, E., and Zhang, C. (2010). Web-enabled Landsat Data (WELD): Landsat ETM+ composited mosaics of the conterminous United States. *Remote Sensing of Environment*, 114(1):35–49.

Ryan, K. C. (2002). Dynamic interactions between forest structure and fire behavior in boreal ecosystems. *Silva Fennica*, 36(1):13–39.

Salomon, J., Hodges, J., Friedl, M., Schaaf, C., Strahler, A., Gao, F., Schneider, A., Zhang, X., El Saleous, N., and Wolfe, R. E. (2004). Global land-water mask derived from MODIS Nadir BRDF-adjusted reflectances (NBAR) and the MODIS land cover algorithm. In *Geoscience and Remote Sensing Symposium (IGARSS), 2004*, pages 239–241. IEEE.

Schaaf, C. B., Gao, F., Strahler, A. H., Lucht, W., Li, X., Tsang, T., Strugnell, N. C., Zhang, X., Jin, Y., and Muller, J.-P. (2002). First operational BRDF, albedo nadir reflectance products from MODIS. *Remote Sensing of Environment*, 83(1):135–148.

Schaefer, K., Zhang, T., Bruhwiler, L., and Barrett, A. P. (2011). Amount and timing of permafrost carbon release in response to climate warming. *Tellus B*, 63(2):165–180.

Scheffer, M., Hirota, M., Holmgren, M., Van Nes, E. H., and Chapin, F. S. (2012). Thresholds for boreal biome transitions. *Proceedings of the National Academy of Sciences of the United States of America*, 109(52):21384–21389.

Schroeder, T. A., Wulder, M. A., Healey, S. P., and Moisen, G. G. (2011). Mapping wildfire and clearcut harvest disturbances in boreal forests with Landsat time series data. *Remote Sensing of Environment*, 115(6):1421–1433.

Schwalm, C. R., Williams, C. A., Schaefer, K., Baldocchi, D., Black, T. A., Goldstein, A. H., Law, B. E., Oechel, W. C., U, K. T. P., and Scott, R. L. (2012). Reduction in carbon uptake during turn of the century drought in western North America. *Nature Geoscience*, 5(8):1–6.

Serbin, S. P., Gower, S. T., and Ahl, D. E. (2009). Canopy dynamics and phenology of a boreal black spruce wildfire chronosequence. *Agricultural and Forest Meteorology*, 149(1):187–204.

Serreze, M. C., Walsh, J. E., Chapin, F. S., Osterkamp, T., Dyurgerov, M., Romanovsky, V., Oechel, W. C., Morison, J., Zhang, T., and Barry, R. G. (2000). Observational evidence of recent change in the northern high-latitude environment. *Climatic Change*, 46(1):159–207.

Sillmann, J., Kharin, V. V., Zwiers, F. W., Zhang, X., and Bronaugh, D. (2013). Climate extremes indices in the CMIP5 multimodel ensemble: Part 2. Future climate projections. *Journal of Geophysical Research: Atmospheres*, 118(6):2473–2493.

Sitch, S. S., McGuire, A. D. A., Kimball, J. J., Gedney, N. N., Gamon, J. J., Engstrom, R. R., Wolf, A. A., Zhuang, Q. Q., Clein, J. J., and McDonald, K. C. K. (2007). Assessing the carbon balance of circumpolar Arctic tundra using remote sensing and process modeling. *Ecological Applications*, 17(1):213–234.

Slayback, D. A., Pinzon, J. E., Los, S. O., and Tucker, C. J. (2003). Northern hemisphere photosynthetic trends 1982–99. *Global Change Biology*, 9(1):1–15.

Smith, S. L., Burgess, M. M., Riseborough, D., and Mark Nixon, F. (2005). Recent trends from Canadian permafrost thermal monitoring network sites. *Permafrost and Periglacial Processes*, 16(1):19–30.

Soja, A. J., Tchebakova, N. M., French, N. H. F., Flannigan, M. D., Shugart, H. H., Stocks, B. J., Sukhinin, A. I., Parfenova, E. I., Chapin, F. S. I., and Stackhouse, Jr., P. W. (2007). Climate-induced boreal forest change: Predictions versus current observations. *Global and Planetary Change*, 56:274–296.

Sokal, R. R. and Rohlf, F. J. (1995). *The principles and practice of statistics in biological research*. Freeman and Company, New York, 3rd edition.

Song, C., Woodcock, C. E., and Li, X. (2002). The spectral/temporal manifestation of forest succession in optical imagery: The potential of multitemporal imagery. *Remote Sensing of Environment*, 82(2-3):285–302.

Spruce, J. P., Sader, S., Ryan, R. E., Smoot, J., Kuper, P., Ross, K., Prados, D., Russell, J., Gasser, G., McKellip, R., and Hargrove, W. (2011). Assessment of MODIS NDVI time series data products for detecting forest defoliation by gypsy moth outbreaks. *Remote Sensing of Environment*, 115(2):427–437.

Stocker, T. F., Qin, D., Plattner, G.-K., Tignor, M., Allen, S. K., Boschung, J., Nauels, A., Xia, Y., Bex, V., and Midgley, P. M. (2013). Climate change 2013: The physical science basis. *Intergovernmental Panel on Climate Change, Working Group I Contribution to the IPCC Fifth Assessment Report (AR5)(Cambridge Univ Press, New York)*.

Stocks, B. J., Mason, J. A., Todd, J. B., Bosch, E. M., Wotton, B. M., Amiro, B. D., Flannigan, M. D., Hirsch, K. G., Logan, K. A., Martell, D. L., and Skinner, W. R. (2002). Large forest fires in Canada, 1959–1997. *Journal of Geophysical Research*, 108(D1):8149.

Stow, D. A., Hope, A., McGuire, D., Verbyla, D., Gamon, J., Huemmrich, F., Houston, S., Racine, C., Sturm, M., Tape, K., Hinzman, L., Yoshikawa, K., Tweedie, C., Noyle, B., Silapaswan, C., Douglas, D., Griffith, B., Jia, G., Epstein, H., Walker, D., Daeschner, S., Petersen, A., Zhou, L., and Myneni, R. (2004). Remote sensing of vegetation and land-cover change in Arctic Tundra Ecosystems. *Remote Sensing of Environment*, 89(3):281–308.

Sturm, M., Racine, C., and Tape, K. (2001). Increasing shrub abundance in the Arctic. *Nature*, 411(6837):546–547.

Sulla-Menashe, D., Friedl, M. A., and Woodcock, C. E. (in review). Sources of bias and variability in long-term Landsat time series over Canadian boreal forests.

Sulla-Menashe, D., Kennedy, R. E., Yang, Z., Braaten, J., Krankina, O. N., and Friedl, M. A. (2014). Detecting forest disturbance in the Pacific Northwest from MODIS time series using temporal segmentation. *Remote Sensing of Environment*, 151(C):114–123.

Tan, B., Woodcock, C. E., Hu, J., Zhang, P., Ozdogan, M., Huang, D., Yang, W., Knyazikhin, Y., and Myneni, R. B. (2006). The impact of gridding artifacts on the local spatial properties of MODIS data: Implications for validation, compositing, and band-to-band registration across resolutions. *Remote Sensing of Environment*, 105(2):98–114.

Tape, K. D., Sturm, M., and Racine, C. (2006). The evidence for shrub expansion in Northern Alaska and the Pan-Arctic. *Global Change Biology*, 12(4):686–702.

Tateishi, R. and Ebata, M. (2004). Analysis of phenological change patterns using 1982–2000 Advanced Very High Resolution Radiometer (AVHRR) data. *International Journal of Remote Sensing*, 25(12):2287–2300.

Teillet, P. M., Barker, J. L., Markham, B. L., Irish, R. R., Fedosejevs, G., and Storey, J. C. (2001). Radiometric cross-calibration of the Landsat-7 ETM+ and Landsat-5 TM sensors based on tandem data sets. *Remote Sensing of Environment*, 78(1):39–54.

Teillet, P. M., Helder, D. L., Ruggles, T. A., Landry, R., Ahern, F. J., Higgs, N. J., Barsi, J., Chander, G., Markham, B. L., and Barker, J. L. (2004). A definitive calibration record for the Landsat-5 thematic mapper anchored to the Landsat-7 radiometric scale. *Canadian Journal of Remote Sensing*, 30(4):631–643.

Townshend, J. R. and Justice, C. O. (2002). Towards operational monitoring of terrestrial systems by moderate-resolution remote sensing. *Remote Sensing of Environment*, 83(1):351–359.

Tucker, C., Pinzon, J., Brown, M., Slayback, D., Pak, E., Mahoney, R., Vermote, E., and El Saleous, N. (2005). An extended AVHRR 8-km NDVI dataset compatible with MODIS and SPOT vegetation NDVI data. *International Journal of Remote Sensing*, 26(20):4485–4498.

Turetsky, M. R., Kane, E. S., Harden, J. W., Ottmar, R. D., Manies, K. L., Hoy, E., and Kasischke, E. S. (2010). Recent acceleration of biomass burning and carbon losses in Alaskan forests and peatlands. *Nature Geoscience*, 4(1):27–31.

Turner, D. P., Ollinger, S. V., and Kimball, J. S. (2004). Integrating Remote Sensing and Ecosystem Process Models for Landscape- to Regional-Scale Analysis of the Carbon Cycle. *BioScience*, 54(6):573–584.

Turner, D. P., Ritts, W. D., Yang, Z., Kennedy, R. E., Cohen, W. B., Duane, M. V., Thornton, P. E., and Law, B. E. (2011). Decadal trends in net ecosystem production and net ecosystem carbon balance for a regional socioecological system. *Forest Ecology and Management*, 262(7):1318–1325.

van Wagtendonk, J. W., Root, R. R., and Key, C. H. (2004). Comparison of AVIRIS and Landsat ETM+ detection capabilities for burn severity. *Remote Sensing of Environment*, 92(3):397–408.

Verbesselt, J., Hyndman, R., Newnham, G., and Culvenor, D. (2010a). Detecting trend and seasonal changes in satellite image time series. *Remote Sensing of Environment*, 114(1):106–115.

Verbesselt, J., Hyndman, R., Zeileis, A., and Culvenor, D. (2010b). Phenological change detection while accounting for abrupt and gradual trends in satellite image time series. *Remote Sensing of Environment*, 114(12):2970–2980.

Vogelmann, J. E., Helder, D., Morfitt, R., Choate, M. J., Merchant, J. W., and Bulley, H. (2001). Effects of Landsat 5 Thematic Mapper and Landsat 7 Enhanced Thematic Mapper Plus radiometric and geometric calibrations and corrections on landscape characterization. *Remote Sensing of Environment*, 78(1):55–70.

Wang, A., Price, D. T., and Arora, V. (2006). Estimating changes in global vegetation cover (1850–2100) for use in climate models. *Global Biogeochemical Cycles*, 20.

Wang, W., Qu, J. J., Hao, X., Liu, Y., and Stanturf, J. A. (2010). Post-hurricane forest damage assessment using satellite remote sensing. *Agricultural and Forest Meteorology*, 150(1):122–132.

Waring, R. H. and Franklin, J. F. (1979). Evergreen coniferous forests of the Pacific Northwest. *Science*, 204:1380–1386.

Westerling, A. L., Hidalgo, H. G., Cayan, D. R., and Swetnam, T. R. (2006). Warming and Earlier Spring Increase Western U.S. Forest Wildfire Activity. *Science*, 313(5789):940–943.

White, J. C. and Wulder, M. A. (2014). The Landsat observation record of Canada: 1972. *Canadian Journal of Remote Sensing*, 39(6):455–467.

Wilmking, M., Juday, G. P., Barber, V. A., and Zald, H. S. J. (2004). Recent climate warming forces contrasting growth responses of white spruce at treeline in Alaska through temperature thresholds. *Global Change Biology*, 10(10):1724–1736.

Wotton, B. M., Nock, C. A., and Flannigan, M. D. (2010). Forest fire occurrence and climate change in Canada. *International Journal of Wildland Fire*, 19:253–271.

Wulder, M. A., Masek, J. G., Cohen, W. B., Loveland, T. R., and Woodcock, C. E. (2012). Opening the archive: How free data has enabled the science and monitoring promise of Landsat. *Remote Sensing of Environment*, 122:2–10.

Wulder, M. A., White, J. C., Cranny, M., Hall, R. J., Luther, J. E., Beaudoin, A., Goodenough, D. G., and Dechka, J. A. (2008a). Monitoring Canada's forests. Part 1: Completion of the EOSD land cover project. *Canadian Journal of Remote Sensing*, 34(6):549–562.

Wulder, M. A., White, J. C., Goward, S. N., Masek, J. G., Irons, J. R., Herold, M., Cohen, W. B., Loveland, T. R., and Woodcock, C. E. (2008b). Landsat continuity: Issues and opportunities for land cover monitoring. *Remote Sensing of Environment*, 112(3):955–969.

Xu, L., Myneni, R. B., Chapin, III, F. S., Callaghan, T. V., Pinzon, J. E., Tucker, C. J., Zhu, Z., Bi, J., Ciais, P., Tømmervik, H., Euskirchen, E. S., Forbes, B. C., Piao, S. L., Anderson, B. T., Ganguly, S., Nemani, R. R., Goetz, S. J., Beck, P. S. A., Bunn, A. G., Cao, C., and Stroeve, J. C. (2013). Temperature and vegetation seasonality diminishment over northern lands. *Nature Climate Change*, 3(5):1–6.

Yin, H., Pflugmacher, D., Kennedy, R. E., Sulla-Menashe, D., and Hostert, P. (2014). Mapping Annual Land Use and Land Cover Changes Using MODIS Time Series. *IEEE Journal of Selected Topics in Applied Earth Observations and Remote Sensing*, 7(8):3421–3427.

Zhan, X., Sohlberg, R. A., Townshend, J., Dimiceli, C., Carroll, M. L., Eastman, J. C., Hansen, M. C., and Defries, R. S. (2002). Detection of land cover changes using MODIS 250 m data. *Remote Sensing of Environment*, 83(1):336–350.

Zhu, Z. and Woodcock, C. E. (2012). Object-based cloud and cloud shadow detection in Landsat imagery. *Remote Sensing of Environment*, 118:83–94.

Zhu, Z. and Woodcock, C. E. (2014). Continuous change detection and classification of land cover using all available Landsat data. *Remote Sensing of Environment*, 144(C):152–171.

Zhu, Z., Woodcock, C. E., and Olofsson, P. (2012). Continuous monitoring of forest disturbance using all available Landsat imagery. *Remote Sensing of Environment*, 122(C):75–91.

Curriculum Vitae